ON COHERENCE EFFECTS IN MAGNETIC AND NON-MAGNETIC NANOSCALE CONDUCTORS

A Dissertation

Presented to the Faculty of the Graduate School

of Cornell University

in Partial Fulfillment of the Requirements for the Degree of

Doctor of Philosophy

by

Joern Niklas Kupferschmidt

May 2010

ON COHERENCE EFFECTS IN MAGNETIC AND NON-MAGNETIC NANOSCALE CONDUCTORS

Joern Niklas Kupferschmidt, Ph.D.

Cornell University 2010

This doctoral dissertation concerns electronic, nanoscale systems exhibiting coherence effects. Two effects are considered in detail: quantum corrections to the ensemble average of the conductance of a network of quantum dots, and superconducting correlations induced in half-metals by a nearby s-wave superconductor. In Chapter 1 the common origin of these two effects is considered and the processes limiting quantum coherence are discussed.

The quantum corrections to the ensemble-averaged conductance of a network of quantum dots are calculated in Chapter 2. All leading quantum corrections to the classical conductance are obtained: weak localization, which reduces the conductance and arises from coherent backscattering of electrons, as well as Altshuler-Aronov corrections, which arise from the Coulomb interaction among the electrons. Employing Random Matrix theory and diagrammatic perturbation theory, we obtain the quantum corrections not only for all magnetic fields strengths but also for all temperatures. Our results are given in terms of contact conductances and capacitances, quantities obtainable directly from experiment for gate-defined quantum dots in semiconductor heterostructures.

From Chapters 3 to 5 we explore superconducting correlations in half-metals, materials in which only one spin species can propagate at the Fermi energy. We investigate two potential "triplet" Andreev reflection mechanisms, which allow superconducting correlations from an s-wave superconductor to extend into magnetic materials, and which involve the rotation of a quasiparticle's spin close to the interface.

In Chapter 3 we assume a thin ferromagnetic spacer layer at the interface between the half-metal and the superconductor, whose magnetization is not collinear with that of the half-metal. We find that here "triplet" Andreev reflection is suppressed close to the Fermi energy. This is shown to be due to unitarity and particle-hole symmetry, which in the single-channel quantum limit lead to the absence of Andreev reflection at the Fermi energy. This absence leads to a suppression of an interface's subgap conductance at low bias voltage, as well as to a suppression of the magnitude of the Josephson current through long half-metallic links.

Chapters 4 and 5 investigate domain walls as an alternative source of "triplet" Andreev reflection. It is shown that orientation of the domain wall with respect to the interface matters: where an interface is invariant under translations as well as half a rotation around the interface normal, the same restrictions as in the single-channel limit apply. If a domain wall is oriented parallel to the interface these invariances are retained; where the domain wall is perpendicular the invariances are broken, allowing for a finite Andreev reflection amplitude at the Fermi energy. We also find that contact geometry affects the magnitude of the Andreev reflection amplitude. If a superconductor is laterally brought into contact with a thin half-metallic film, the Andreev reflection amplitude is enhanced due to multiple reflections occurring in the thin film.

BIOGRAPHICAL SKETCH

The author, Joern Niklas Kupferschmidt, was born in Wuppertal, Germany, on the last day of August in the year 1981. The first son of Marianne and Michael Kupferschmidt, he grew up on the outskirts of this once industrial town, provided with the right amount of trees to never question their existence, yet rarely seeing any larger animals in the wild. He attended school in Germany, taking advantage of its many offerings and most memorably acting in the school's drama group. He developed a taste for barren landscapes, and after obtaining his *Abitur* from the Carl-Fuhlrott-Gymnasium in 2001 he went backpacking beyond the arctic circle in Scandinavia.

He began studying physics and philosophy at the Westfälische Wilhelms Universität in Münster in the fall of 2001. There he was lucky to meet Christian Kappen and Peter Boschan, with whom he explored parts of the wisdom of Landau's course on theoretical physics. He obtained the 'Vordiplom' in Physics in the summer of 2003. In the spring of 2004 he spent two months in the group of Alexander Szalay at Johns Hopkins University, getting to know galaxies, databases, and the United States for the first time. He came to Cornell as a Fulbright scholar in the fall of 2004 and joined the group of Piet Brouwer exploring the physics of the meso- and nanoscales in the fall of 2005. During his Ph.D. work, in the academic year 2006/2007, he had the pleasure to enjoy the hospitality of the group of Jan von Delft at the Ludwig-Maximilians-Universität in Munich, Bavaria. Having returned to Ithaca in the summer of 2007, he again moved with Piet Brouwer in the summer of 2009, this time to the Free University in Berlin, Germany, where he completed his Ph.D. work in the spring of 2010.

für meinen Großvater,

und die nächste Generation

ACKNOWLEDGEMENTS

Despite the latitude encouraged in the American tradition of acknowledgements, there are more people that have directly or indirectly influenced this dissertation than will reasonably fit here. And despite my best efforts, there may be people who I forget to mention who should have been acknowledged. Asking them for forgiveness, I shall nevertheless make an attempt, aiming to minimize omissions.

It is easy to identify my advisor Piet Brouwer as the person who contributed most profoundly to this dissertation. Choosing problems of the right difficulty, which would challenge me and allow myself to learn on my own, and answering almost every question put to him, Piet led me to become an independent researcher. I could not have wished for a more competent advisor. Observing his way of approaching a problem and discerning important aspects amidst unimportant detail, and his way of lucidly interconnecting these aspects to well known principles, has enabled me to eventually stand on my own feet and think for myself.

My other two committee members also helped make my graduate career successful. I am thankful to Erich Mueller for his enthusiasm and curiosity, and for letting me explore aspects of physics which I found interesting, as well as his readiness to go to the blackboard. Dan Ralph has been a source of insight as well as illuminating questions, and got me involved in an interesting research problem that led to my first publication. He also taught an excellent solid state course, which smoothed my transition from aspiring to be a high-energy cosmologist to focussing on the complex and convoluted smaller pieces that constitute condensed matter theory.

Chris Henley taught a wonderfully interactive advanced solid state course that put lots of emphasis on qualitative understanding and analogy. I am grateful to him for having advanced my ability to work associatively, and to always ask questions if they appear to be well thought out and important.

My first committee deserves credit for having advised me well, and I thank Csaba Csaki for his open-mindedness in discussing potential research avenues, and Maxim Perelstein not only for his excellent Quantum Field theory course but also for his non-sanctioning attitude towards alternative occupations during my first summer. David Cassel was an excellent mentor, TA supervisor, and eased the transition from Germany to the United States.

During my undergraduate time in Münster, Peter Boschan got me excited about and engaged with physics. He took the time to answer questions arising from reading Landau and Lifshitz, got me started on a research project, and sent me to the United States. His conviction that physics can be a way of approaching most questions, as well as his work ethic, will stay with me. It has also been a profound pleasure to learn, work and teach together with Christian Kappen during this time. In Münster I also had the good fortune to find in Michael Wilczek, Christian Rehwald, Karsten Dreimann, Christoph Bersch and Cornelia Petrovic a group of people who were passionate about physics as well as cooking. I would also like to acknowledge Tilman Kuhn, for teaching introductory physics courses of excellent clarity, and Klaus Langmann, for understanding that teaching was as much about interacting with his students as covering the material lucidly.

Many Hungarians have influenced my thinking as a physicist. Besides Peter Boschan and Csaba Csaki, I would like to thank Tamas Budavari, Gabor Domokos, Susan Kovesi-Domokos and Alex Szalay for making me feel like a member of their group whenever I visited Baltimore.

A preceeding generation of Physics graduate students was a tremendous help in getting oriented along the path to a successful conclusion of my graduate career. I am particularly grateful to Shaffique Adam, Jens Bardarson, Kirill Bolotin, Stephan Braig, Ferdinand Kuemmeth, Louis Leblond, Ivan Rankenburg, Benjamin Shlaer, Sarah Shandera and Gil Toombes. Shaffique, being a collaborator, group member, friend and mentor,

has influenced much of my outlook on physics, and in particular its role in society. I am glad to find in him someone who thinks on a larger scale—not because it is necessarily within our academic expertise to do so, but because it is necessary for us to do so as members of society. Jens joined our group during my last year in Ithaca, and I have benefited greatly from his presence, in discussing aspects ranging from physics to the world as it has organized itself today. I am happy to share with him an almost identical genealogy in theoretical physics. I am also grateful to the other members of Piet's group in Ithaca: Turan Birol, Manabu Machida, Markus Kindermann, and Saar Rahav. I also thank Gianluigi Catelani for discussions, some of which are reflected in Chapter 2 of this dissertation.

Benjamin Béri and Carlo Beenakker I thank for a fruitful collaboration, as well as the permission to include our joint work in Chapter 3 of this dissertation.

Without experiment, physics were empty, devoid of life and the feedback that makes it different from math. I am grateful to my experimental colleagues and friends who were always willing to discuss the experiments they were doing and inspiring in their approach to it. Ferdinand Kuemmeth, Jack Sankey, Sufei Shi and Kiran Thadani from the Ralph group, as well as Ann Sophie Rittner and Arend van der Zande, deserve particular mention.

Crucial as experiments are to the progress of physics, to me it was crucial to progress in understanding and practicing theoretical physics. That I was able to do so is very much owed to friends sharing a similar path, with whom I discussed problems of all sorts, throughout graduate school, and encompassing all possible topics. To discuss with Sourish Basu, Stefan Baur, Attila Bergou, Kaden Hazzard, Steve Hicks and Simon Gravel—in windowless offices, next to a glass of wine, or late at night in some attic in Fall Creek—is a pleasure that is already missed.

At Cornell I found a community that was excited about physics yet aiming to

not forget about real life, life that is perceived to be occurring outside of a graduate school bubble. I cannot think of my time at Cornell without thinking of Milan Allan, David Bernat, Mohammad Hamidian, Dominik Ho, Nathaniel Gabor, Sharon Gerbode, Praveen Gowtham, John Gregoire, Johannes Heinonen, James Ledoux, Duane Loh, Annita Ngatchou, Vlad Pribiag, Ann Sophie Rittner, Barbara Rojas, Isabelle Smith, Robin Smith, and Xin Shi.

Throughout my time in Ithaca I have been fortunate to share living arrangements with amazing people that have truly become friends. Arend van der Zande, Jonathan Newport, Simon Gravel, Osman Balkan and Shira Adriance will know how much I enjoyed living with them.

One of the opportunities a small university town offers is to engage with students from other departments. At Cornell I have profoundly enjoyed being immersed in a truly interdisciplinary and international community. Amy Arquiza, Amaya Atucha, Cagla Aydin, Henry Berlin, Janelle Burke, Dave Corney, Caroline Ferraris-Besso, Lindsey Glover, Mimmy Gondwe, Elliott Hess, Munira Hyder-Adam, Fatiha Jillali, Kaisa Kaakinen, Pinar Kemerli, Serge Khoudessian, Matthias Kormaksson, Brinda Kumar, Shamoni Maheshwari, Catherine Martel, Boaz Nadav-Manes, Hanh Nguyen, Valentine Petry, John Phan, Mike Reyes, Sezi Seskir, Kavita Singh, Cecily Swanson, Meredith Talusan, Daniel Tonozzi, and Ioana Vartolomei made Ithaca a home and enriched my life for as long as I lived there.

Residing in Ithaca, I was also glad to nevertheless share a certain country of residence, in the INS interpretation of the word, with Sinja Graf, Lena Hipp, Martin Küster and Georgios Markopoulos.

In the course of my Ph.D. I had the unusual opportunity to live in three different cities. In Munich I enjoyed the hospitality of the Arnold Sommerfeld Center for Theoretical Physics, and the opportunity to talk with Jan von Delft, Stefan Kehrein and Florian

Marquardt. Discussions during this time influenced the content of Chapter 2 of this dissertation. I am also glad to have spent the year close to the Pinakotheken with Karen and Murad Alim, Peter Fritsch, Theresa Hecht, Ferdinand Helmer, Andreas Holzner, Wolfram Möbius and Michael Möckel, as well as Kerstin Feurle, Leonie Fresenius and Nina Türk. At the Free University of Berlin the newly founded Dahlem Center for Complex Quantum Physics proved to be an excellent and stimulating environment. It was a pleasure to be here with Niels Bode, Jeroen Danon, Mathias Duckheim, Friedrich Gethmann, Torsten Karzig, Eros Mariani, Dganit Meidan, Tobias Micklitz, Teemu Ojanen, Felix von Oppen, Guillaume Weick and last, but not the least, Francis Wilken.

Moving abroad as well as moving a lot is a two edged sword, even in the era of social networks. I am grateful to friends who have stayed in touch. Peer Haasters, Eva Lieberich, David Richter, Sarah Richter, Birte Rüster and Sophie Witt.

In inevitable times of travel and temporary homelessness, I have been granted generous shelter by Florian Duijsens, Caroline Ferraris-Besso, Kerstin Feurle, Leonie Fresenius, Tatjana Kissing, Eva Lieberich, Sezi Seskir, Kavita Singh, Meredith Talusan and the Telluride House, as well as Gil Toombes.

During my time at Cornell I have been involved in graduate student affairs, serving the Physics Graduate Society as well as the Graduate and Professional Student Assembly. The people I have worked with here have contributed to keeping my life afloat above the details of diagrammatics. I am particularly glad to have met Nighthawk Evensen, Lisa Larrimore, Michelle Leinfelder and Yu Yu. The outreach program of the Cornell Center for Material Research has also provided a meaningful opportunity to leave my desk. I thank in particular Kevin Dilley, Jane Earle and Nev Singhota for the opportunity to teach kids about physics in upstate New York as well as in Harlem. Cornell's policy allowing graduate students to pursue any study made it possible to get tastes of wines as well as economics. I would like to thank in particular Daniel Benjamin, as well as Ori Heffetz

and Benjamin Ho, for enabling me to gain some insight into behavioral economics.

The administrative support I have experienced in Ithaca, as well as in Munich and Berlin, has been excellent. I thank Cindee Ball, Kacey Bray, Gabriele Herrmann, Lynda Keister, Douglas Milton, Stéphane Schoonover, Debbie Sladdich and Connie Wright for their help. From the minute I arrived at Cornell, Lisa Margosian made me feel welcome, and already before had been a great help in navigating the waters of academic exchange commissions.

I thank Sourish Basu for carefully reading parts of this dissertation as well as for helping with the fonts, and Elizabeth Skadden for reading and commenting on the introduction. Naturally, remaining mistakes, idiosyncrasies and obscurities are all mine.

Financial support was crucial in enabling my studies. Besides from my family, I have also benefitted from taxpayers' support in various ways: Through the Studienstiftung des deutschen Volkes, the German-American Fulbright commission as well as via the Universität Münster. I also very much appreciate the continuous support of the Cornell Center for Materials Research, which is funded in large part by the National Science Foundation.

Ohne meine Familie wäre diese Arbeit kaum geschrieben worden. Meiner Mutter bin ich insbesondere dankbar für ihre kontinuierliche Unterstützung, und für die Motivation auch durch tiefere Täler zu schreiten und höhere Berge zu erklimmen. Ich bin dankbar für das kritische Vertrauen das sie immer in meine Arbeit hatte. Meinem Vater danke ich insbesondere für seine Zuversicht und die Ermutigung es auf der anderen Seite des Ozeans—der einmal sehr groß schien—zu versuchen. Ohne seine Offenheit für die Zukunft und für Unbekanntes hätte ich einen solchen Schritt vielleicht nicht gewagt. Meinem Großvater bin ich dankbar, dass er mir zeit seines Lebens die fragende Wissbegierde vermittelt hat, die Welt aufmerksam zu betrachten und wissenschaftliche Erkenntnis zu suchen.

Berlin, May 2010

TABLE OF CONTENTS

LIST OF FIGURES

CHAPTER 1

INTRODUCTION

This thesis concerns electronic systems exhibiting coherence effects in the mesoscopic regime. Physicists have over the last decades explored this intermediate scale, ranging from the nanoscale of individual molecules and carbon nanotubes to microscopic scales of semiconductor heterostructures where aspects of classical properties begin to become apparent while the system still shows distinctively quantum mechanical features. Two effects are considered: the weak localization correction to the conductance and the superconducting proximity effect induced in half- metals.

In Chapter 2 we consider weak localization, a quantum coherent backscattering effect which leads to a reduction of the electrical conductance compared to the classically expected value. We investigate its temperature and magnetic field dependence for a network of quantum dots. Quantum dots are small metallic islands, created by electrostatic confinement with gates in semiconductor heterostructures or defined by the surfaces of metal grains. Electrons on a quantum dot ergodically and coherently explore the available phase space on a very short timescale, so that the conductance through quantum dots is determined primarily by their contacts to leads. For this reason quantum dots are also said to be 'quasi-zero dimensional'. Yet while details of the scattering off boundaries or impurities on the dot do not play a dominant role in determining the conductance, they do give rise to small quantum corrections which are the focus of our investigation.

It was realized almost three decades ago that the phase shift an electron incurs when scattering off impurities in solids need not imply the impossibility of coherent effects. In fact, in an infinite one- or two-dimensional disordered metal quantum interference effects will localize all states and reduce the conductivity to zero. While infinite samples are insulating, finite samples may have a localization length exceeding their size so that

they are effectively metallic. Still, precursor effects to strong localization can already be seen in small samples. These have been dubbed "weak" localization effects, as opposed to "strong" localization effects in larger or more disordered samples.

Weak localization effects are well understood both theoretically and experimentally in three-dimensional as well as in quasi-one and quasi-two dimensional systems. Yet the same cannot be said of the quasi-zero dimensional quantum dots: The observed temperature dependence of the weak localization correction is still inconclusive. Section 1.3 gives a brief overview the current state of the field. Chapter 2 then investigates thoroughly how quantum corrections arise in a network of quantum dots, and, more interestingly, how they are suppressed in the presence of magnetic fields or by interactions.

In Chapters 3–5 we consider the second coherence effect: superconducting pairing correlations induced in half-metals by a nearby *s*-wave superconductor. Andreev reflection—the reflection of electrons into holes and vice versa at the interface of a superconductor—provides such a mechanism. It is well understood for normal metals, yet for half-metals and ferromagnets the situation is more involved. Half-metals in particular are magnetic materials in which only one spin species propagates at the Fermi energy. The macroscopic wavefunction of the superconductor consists of singlet states involving both spin directions and can thus not immediately extend into a half-metal. Ordinary Andreev reflection of an electron incident from the half-metal will result in a hole whose spin is anti-aligned with the majority carrier direction of the half-metal. Such a hole cannot be reflected back into the half-metal.

Instead, to induce superconducting correlations in the half-metal, the spin has to be rotated close to the interface [1]. Josephson currents flowing through a non-superconducting material are a prominent consequence of superconducting correlation. They were in fact observed for a half-metal [2], and in this thesis we investigate poten-

tial mechanisms enabling such a "long range triplet proximity" effect. It is called 'triplet' because it involves pairing of equal spins. In Chapter 3 we consider this problem by employing scattering matrices, an approach with which we show that Andreev reflection into half-metals is absent at the Fermi energy in the single-channel quantum limit. Chapters 4 and 5 investigate domain walls and find that depending on orientation these can give rise to a finite Andreev reflection amplitude at the Fermi energy. The role of contact geometry is also discussed in this context.

The following sections provide some background to the effects considered. In Sec. 1.2 we begin shedding some light on the types of processes limiting coherent effects. Section 1.3 reflects on quantum corrections to the conductance before we motivate in Sec. 1.3.1 the Random Matrix model employed to obtain the ensemble averaged conductance through quantum dot networks. Section 1.4 takes a short look at the role of coherence in superconductivity and links it to the long range triplet proximity effect in ferromagnets and half-metals.

1.1 Coherent effects from classical paths

Quantum Mechanics allows for interference effects. Of these the double slit experiment may be the most paradigmatic, but another equally iconic one is the Aharonov Bohm effect. It is a propagation amplitude's phase that depends sensitively on the path taken and potentials experienced along it. Upon squaring the sum of amplitudes, cross terms–involving relative phase differences–give rise to interference, see Fig. 1.1. The precession of a spin in a magnetic field is also a type of interference effect. The relative phase between the two components of a spinor determines a spin's orientation. Precession in a magnetic field is the accumulation of phase at different rates for the two components of the spinor.

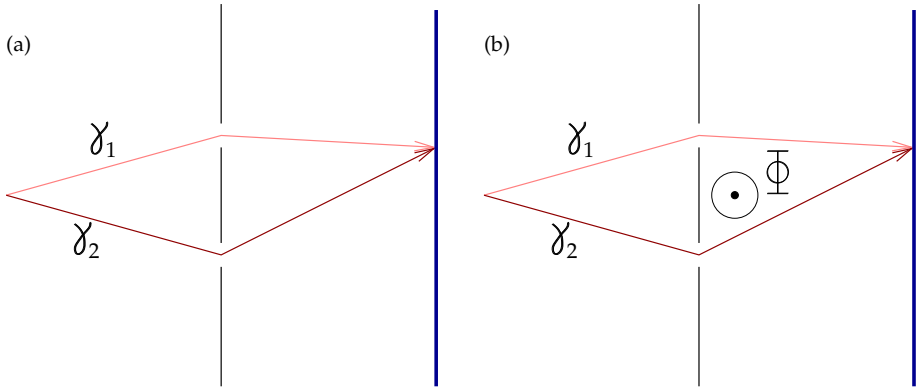

FIGURE 1.1: In the double slit experiment (a), the differing orbital phases along path γ_1 and γ_2 give rise to an interference pattern. This interference pattern's dependence on the magnetic flux Φ encircled by $\gamma_1 \cup \bar{\gamma}_2$ in (b) is the result of the Aharonov Bohm effect.

In these three examples there are only two different probability amplitudes contributing to the final sum. Effects which rely instead on a large number of contributions all contributing with the same phase are often called "coherent". It is worth considering more closely the two coherent effects we are interested in this thesis. Both concern electrons in an interacting Fermi sea. The current-current correlation function from which the conductance is obtained, as well as the superconducting pairing correlations both involve pairs of electron creation or annihilation operators, [1]

$$\langle \psi_\sigma(\mathbf{r}, t)\psi^\dagger_{\sigma'}(\mathbf{r}', t')\rangle \text{ or } \langle \psi^\dagger_\sigma(\mathbf{r}, t)\psi^\dagger_{\sigma'}(\mathbf{r}', t')\rangle \tag{1.1}$$

Such expectation values, taken with respect to the ground state of the system, are interpreted as being related to the propagation of a quasiparticle. $\langle \psi_\sigma(\mathbf{r}, t)\psi^\dagger_{\sigma'}(\mathbf{r}', t')\rangle$, *e.g.*, is the probability amplitude for a quasiparticle created at position $\mathbf{r}'$ at time t' to be found and annihilated at position $\mathbf{r}$ at time t. With Feynman taking seriously the notion that one should sum over all possible paths γ connecting $\mathbf{r}$ to $\mathbf{r}'$ in the given time interval, the

[1] The theory of course also involves quantities of which no average has been taken. Yet a mean field theory, as well as a perturbative treatment by virtue of Wick's theorem, will only involve the pairwise averaged quantities.

propagator is written as

$$\langle \psi_\sigma(\mathbf{r}, t)\psi^\dagger_{\sigma'}(\mathbf{r}', t')\rangle = \sum_\gamma \mathcal{A}_\gamma e^{iS_\gamma/\hbar}, \tag{1.2}$$

where the so called stability amplitude $\mathcal{A}_\gamma$ weighs the contribution of an individual path and S_γ is the action incurred along it.

The dominant contribution to the action arises from the orbital trajectory taken and the potential landscape experienced. The orbital contribution to the phase $S_\gamma/\hbar$, *e.g.*, is $\int_\gamma d\mathbf{l}\cdot\mathbf{k}$. Already changes in the path only of order of the Fermi wavelength λ_F will change the phase entirely. Thus even trajectories differing only by little more than a wavelength cancel each other's contribution in the sum over amplitudes Eq. (1.2). The only trajectories for which such cancellations are absent are those where the action is stationary, so that a small variation of the path does not change the action. These are the paths that contribute to the sum. They correspond to the trajectories of classical particles. One may picture the contributing paths as being contained in tubes of cross-sectional area $\approx (\lambda/2\pi)^2$ fitted around the classical path [3]. The picture of propagation along a classical paths that is herewith established is useful to intuitively understand both effects that will concern us here.

1.1.1 Conductance

The Kubo formula gives the conductance G as an expression involving four fermionic creation and annihilation operators. It is found to be proportional to a double sum

$$G \propto \left|\sum_\gamma \mathcal{A}_\gamma e^{iS_\gamma/\hbar}\right|^2 = \sum_\gamma \sum_\delta \mathcal{A}_\gamma \mathcal{A}^*_\delta e^{i(S_\gamma - S_\delta)/\hbar}. \tag{1.3}$$

At low bias voltage we may picture conductance in mesoscopic systems as an elastic scattering process instead of a dissipative one. The conductance of a device is thus proportional to the probability that an electron entering the device at the source leaves it at the

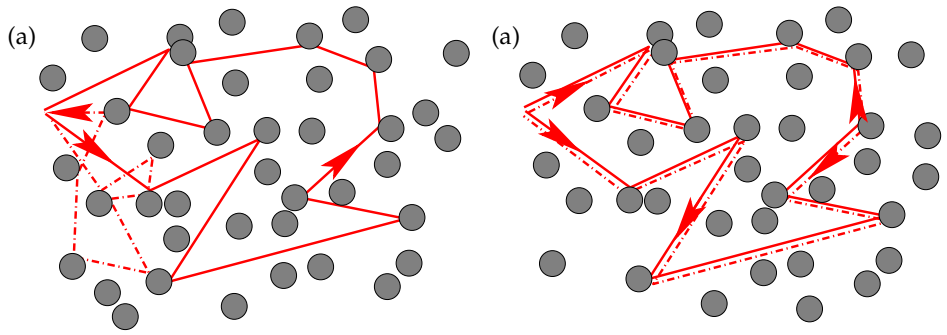

FIGURE 1.2: (a) Generic off-diagonal pairing and (b) time-reversed pairing of two classical paths. The former gives rise to sample to sample variations of the conductance, the latter gives the weak localization correction to the average conductance.

drain. The probability is obtained from a square of amplitudes, thus the above expression (1.3). The classical contribution to the conductance is the diagonal one where $\gamma = \delta$. Quantum corrections appear due to the non-diagonal contributions. In any given phase coherent sample these do not self-average to zero but give rise to a correction to the conductance of universal order of magnitude e^2/h. Sign and size of the correction cannot be predicted for a given sample. Like a speckle pattern in optics the correction depends sensitively on the impurity configuration within the sample.

Taking the average of many samples, it is found that not all non-diagonal contributions reduce to zero. These stem from paired trajectories for which the difference of their actions is stationary, just as it is for the diagonal pairing. Consider a path γ starting and ending at the source contact of a mesoscopic device. Such paths contribute to the probability of an electron to return to the source contact instead of leaving through the drain. One finds that the pairing of γ with its time-reversed $\bar{\gamma}$ gives rise to an additional contribution equal in size to the diagonal, classically expected one. Such a contribution is depicted in Fig. 1.2(b). The difference in action, $\mathcal{S}_\gamma - \mathcal{S}_{\bar{\gamma}}$, is stationary. To see this, note that the sensitive action predominantly depends on the orbital contribution $\int_\gamma d\mathbf{l} \cdot \mathbf{k}$, which simply depends on the length of the trajectory. This is the same for both path and time-

reversed path. Static scalar potentials also contribute equally and so do the phase shifts incurred upon scattering off impurities or boundaries. These time-reversed pairings thus enhance the probability to return to the source contact by a factor of two compared to the classically expected value. By unitarity the probability of transmission through the device must thus be reduced, and so is its conductance. This is the coherent backscattering contribution giving rise to weak localization.

1.1.2 Superconducting correlations

In the case of superconducting correlations, we inquire about $\langle \psi^\dagger_\sigma(\mathbf{r}, t)\psi^\dagger_{\sigma'}(\mathbf{r}', t')\rangle$, the amplitude of an electron initially at position $\mathbf{r}'$ at time t' to be found at $\mathbf{r}$ and t as a hole. We look for a contribution to the sum over amplitudes whose action is stationary as before. A connection to the preceding conductance consideration is established by dividing the path taken into two segments. In the first segment an electron propagates from position $\mathbf{r}$ in the normal or half-metal to $\mathbf{r}''$ on the interface with the superconductor. At the interface it can be converted to a hole, which occurs with some amplitude r_{he}. Ordinary reflection may also occur yet does not contribute to superconducting correlations. The second segment of the path starts at $\mathbf{r}''$ and ends at $\mathbf{r}'$. The hole trajectory $\bar{\delta}{:}\mathbf{r}'' \to \mathbf{r}'$ is the time-reversed of an electron trajectory $\delta{:}\mathbf{r}' \to \mathbf{r}''$. Since under time-reversal $\mathcal{A}_\delta e^{iS_\delta} \to \mathcal{A}^*_\delta e^{-iS_\delta}$ we can write an an expression similar to Eq. (1.3) above

$$\langle \psi^\dagger_\sigma(\mathbf{r}, t)\psi^\dagger_{\sigma'}(\mathbf{r}', t')\rangle = \int_{\mathrm{S|H}} d\mathbf{r}'' \sum_{\delta:\mathbf{r}'\to\mathbf{r}''} \mathcal{A}^*_{\delta,\sigma'} e^{-iS_\delta}\, r^{\mathrm{he}}_{\sigma'\sigma,\delta\gamma}(\mathbf{r}'') \sum_{\gamma:\mathbf{r}\to\mathbf{r}''} \mathcal{A}_{\gamma,\sigma} e^{iS_\gamma}, \tag{1.4}$$

where we explicitly take into account the spin degree of freedom. The integral over $\mathbf{r}''$ is over the interface of the superconductor. Again the relevant contribution arises from pairings whose overall phase is stationary. The expectation is that these are the classical paths as depicted in Fig. 1.3.

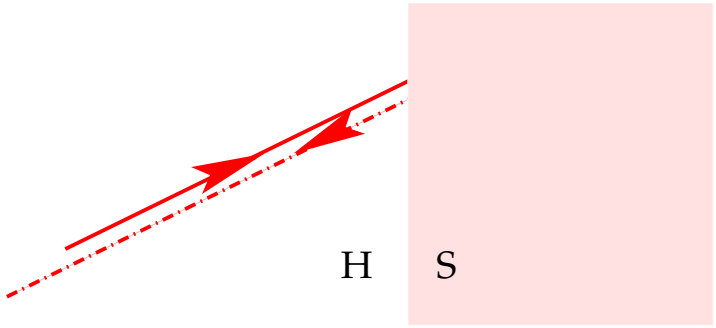

FIGURE 1.3: Classical path γ incident on a superconductor interface, where it is Andreev reflected with amplitude r_{he} and follows the time-reverse of path δ.

1.2 Dephasing

There are two fundamentally different ways in which the coherent contribution to a correlator may be reduced. While both change the relative phase in pairings corresponding to stationary points, one does so in a deterministic manner. The other involves interactions among the quasiparticles in the system or with the environment, interactions which occur with certain transition amplitudes yet cannot be predicted.

1.2.1 Dephasing due to magnetic fields

For time-reversed paths relevant to the conductance the deterministic manner is realized when a magnetic field is applied: The Aharonov-Bohm phase

$$\int_\gamma d\mathbf{l} \cdot e\mathbf{A}/\hbar c = \pi\Phi_\gamma/\Phi_0$$

is proportional to the flux Φ_γ encircled by the path γ, where $\Phi_0 = hc/2e$ is the magnetic flux quantum. The flux encircled depends on orientation. As paths related by time-reversal are traced out in opposite directions, one finds opposite signs, $\Phi_{\bar{\gamma}} = -\Phi_\gamma$. Different paths will generically encircle different amounts of flux. Summing over all pairs

of time-reversed paths will thus reduce the coherent contribution since they contribute with different phase. As Φ_0 is very small, in quantum dots a flux strength of only a few Gauss is sufficient to fully suppress the coherent contribution and thus weak localization.

Similarly, magnetic fields suppress superconducting correlations of singlet type. Ordinary Andreev reflection returns an incoming majority electron as a minority hole. Therefore the two amplitudes in the coherent correlator incur differing orbital phases in the presence of a magnetic field, or generally the exchange interaction in a magnetic material. As the difference in phase accumulated will depend on the length of a path and paths of differing lengths contribute to the correlator, the correlator will generically become short ranged in a magnetic system. The same mechanism limits pairing correlations even in a normal metal adjacent to a superconductor. At a small energy ε away from the Fermi energy the slight difference $\delta k = 2\varepsilon/\hbar v_F$ in the wavenumbers of electrons and holes will limit the range of the pairing correlations. As the Fermi velocity v_F is large, however, this scale is much longer than in the case of even a weak exchange field. In fact, as temperature goes to zero, so does the typical excitation energy, resulting in infinitely long-ranged correlations.

In both these cases the phase along a given path is always affected in the same predictable way. Yet as two paths which initially accrued the same phase now no longer do, the overall phase from the difference in their actions $S_\gamma - S_{\bar{\gamma}}$ no longer cancels. The remaining off-diagonal pairings which initially all contributed with equal phase no longer do and the coherent effect is reduced.

1.2.2 Dephasing due to interactions

Contrast this predictability with the influence of interactions. Similar to an electron accruing a phase shift when scattering off an impurity, electrons accrue phase shifts when they interact and scatter off each other or off lattice excitations, *i.e.* phonons. In addition to the change of phase, their momentum may change and more importantly the environment—the electromagnetic field or the lattice ions—changes its state as well. The propagating electron becomes entangled with the environment. When squaring the sum over propagation amplitudes to obtain the conductance, such entanglement becomes crucial as the scalar product is taken over both the particle's state as well as the state of the environment. Non-diagonal contributions corresponding to pairs of paths along which, *e.g.*, a different number of photons or phonons were emitted then no longer contribute to the coherent effect [4].

At low temperatures, phonons are no longer present and the electron-electron interaction becomes the dominant mechanism reducing coherence. At the low energies of relevance to us we may neglect its effect on the momentum of the propagating particle and the resulting changes of the trajectory and the amplitude $\mathcal{A}_\gamma$. Instead the interaction's effect is well described by a scalar potential, arising from the presence of the other electrons. The interaction thus only affects the action S_γ. Yet where a magnetic field always affects a path predictably in the same way, the electron-electron interaction affects the path only with a certain amplitude. Only the action of those terms in the final expression for which an interaction event actually occurred—involving the emission or absorption of a photon—will be affected. Because the likelihood of such interaction events depends on temperature, this gives rise to a temperature dependence of the coherent correlator.

The phase accumulated by an electron emitting a photon of frequency ω will depend on the time t' that the photon is emitted or absorbed. As this changes the energy of the

particle from ε to $\varepsilon \pm \hbar\omega$, the phase accumulated along a path ending at t is changed by $\pm\omega(t - t')$. One might now be tempted to think that only where photons are emitted or absorbed at the same time along both paths does their pairing continue to contribute to the coherent effect. Yet this is not the case since the emission of photons of the same energy at different times need not result in photon states which are orthogonal to each other. This is apparent in the diagrammatic perturbation theory. While diagrammatic rules stipulate a photon line to have both a beginning and an end—which takes care of the orthogonality of environmental states with different numbers of photons—there are no stipulations on where photon lines may attach. The orthogonality of states with the same number of photons is realized via phases. Long wavelength and low energy photons will generally not give rise to strong dependence of the phase on either position or time and thus they are generally not orthogonal regardless of when and where emission took place in the system [4].

The contribution of a given pair of trajectories to the correlator will thus consist of a sum over the different numbers of photons present in the environment as well as integrals over the different times at which a photon could have been emitted or absorbed. In this final expression one sees that both paths may have accumulated phases due to interactions. What reduces the coherent effect however, is not the variability of the individual phases but only the variability of their relative phase. This implies in particular that a uniform interaction which affects both paths equally does not lead to decoherence.

The effectiveness of the interaction in reducing a coherent effect will depend on the observable calculated. For corrections to the ensemble averaged conductance, which rely on the coherent pairing of time-reversed amplitudes , the reduction will be due to uncertainty of the relative phase of the two paths. Given a probability distribution $P(\varphi)$ for

this relative phase φ the suppression of the contribution is by a factor

$$\langle e^{i\varphi} \rangle = \int d\varphi P(\varphi) e^{i\varphi}. \tag{1.5}$$

For a gaussian distribution Eq. (1.5) can easily be integrated to give a suppression exponential in the variance $\langle \delta\varphi^2 \rangle$ of the relative phase [4]. The variance for a given pair of paths (α, β) is

$$\langle \delta\varphi^2 \rangle = \langle \delta\phi_\alpha^2 \rangle + \langle \delta\phi_\beta^2 \rangle - 2\langle \Delta\phi_\alpha \Delta\phi_\beta \rangle. \tag{1.6}$$

The last term including the covariance ensures that if, *e.g.*, the phases always vary in the same way, the coherent effect is not reduced. A gaussian distribution is expected for a thermal environment, such as a heat bath of phonons or photons at high temperatures. In this case the central limit theorem suggests that the variance grows linearly with the length of the trajectory. The influence of interactions can thus be treated effectively in the form of a dephasing rate.[2] With this time scale, we can associate a length L_φ via the propagation properties of the particles. Coherent effects become relevant when the size of the sample is of the order of L_φ or smaller; larger samples exhibit self-averaging of mesoscopic fluctuations.

Both types of effects—dephasing by interactions and dephasing due to magnetic fields—will be considered more closely in this thesis.

[2]Note that the terminology is inconsistent as regards the use of "dephasing" vs. "decoherence". While the early work by Altshuler and Aronov [23] employs the term "dephasing" for interactions reducing phase coherence, Akkermans and Montambaux [41] suggest to use "decoherence" instead to indicate that a transition in the environment will often have occurred. While we do believe this distinction to be of importance, here we deliberately keep using the term dephasing interchangeably; which type is intended will be apparent from the context.

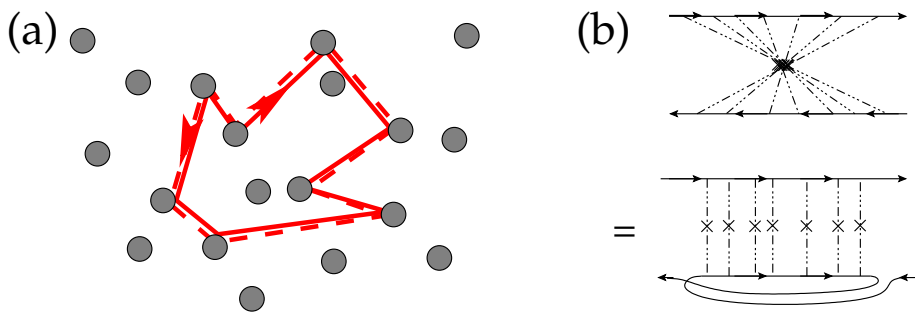

FIGURE 1.4: A path contributing to weak localization. Pictured in (a) as a stretchwise classical path, and (b) as it is encountered in diagrammatic perturbation theory.

1.3 Quantum effects in conductance measurements

Landau's concept of a Fermi liquid allows us to think of electrons as noninteracting particles despite the presence of strong Coulomb interactions. These quasiparticle states are labeled with the same quantum numbers as free electrons. While they do scatter it can be shown through phase space arguments that they decay only slowly in the vicinity of the Fermi surface. Yet Landau's Fermi liquid theory only holds for translationally invariant systems. In the 1980s it was realized that disorder thus changes the picture: Scattering off impurities leads to diffusive rather than ballistic motion of the quasiparticles. Most importantly this allows for self-returning paths. As soon as such paths γ exist the probability of transmission is reduced—weak localization corrections arise through the pairing with time reversed paths $\bar{\gamma}$, as in Fig. 1.2. Writing this off-diagonal contribution explicitly together with the classical diagonal pairing, we find

$$P_{\text{ret}} = \sum_{\gamma} \mathcal{A}_{\gamma}^{*}\mathcal{A}_{\gamma} + \mathcal{A}_{\gamma}^{*}\mathcal{A}_{\bar{\gamma}} e^{-i(S_{\gamma}-S_{\bar{\gamma}})/\hbar}. \tag{1.7}$$

The second term enhances the return probability and thus reduces the conductance. The pictorial analogue of this second term is shown in Fig. 1.4(a).

This contribution crucially relies on the paths remaining coherent with equal actions $S_{\gamma} = S_{\bar{\gamma}}$. The ubiquity of decoherence which upsets this equality, discussed in Sec. 1.2, is

the reason that we need to go to small systems ($L \lesssim \mu m$) and low temperatures ($T \lesssim 4$ K) to find coherent effects.

Assuming an average phase coherence time τ_φ one can obtain the corrections to the conductivity from the fraction of trajectories that will have returned to the origin by this time. Those which do will contribute to quantum corrections, those that don't will not. The resulting integral depends on dimension and gives the quantum correction in terms of the phase coherence time τ_φ.

At the lowest temperatures achievable it is believed that electron-electron interactions are the dominant interaction mechanism causing decoherence. In three dimensional as well as in quasi-two and quasi-one dimensional systems the corresponding dephasing rate can be calculated using diagrammatic perturbation theory. Here it is crucial to take into account the diffusive nature of the particle's propagation both as it directly affects a given particle's path as well as insofar as it changes the screening of the electron-electron interaction. This program has been carried out with great success and can be considered experimentally confirmed.[3] In testing the predictions of the theory it is crucial that the relevant ingredients were well established or accessible in independent experiments. Transport properties rely on the Diffusion constant which is accessible at higher temperatures in a non-coherent experiment. The bare Coulomb interaction in a restricted geometry as well as its screened propagator can be calculated from first principles, taking into account the proper low energy behavior dominated by screening.

Taking seriously the idea that the interaction among electrons is mediated by photons, the fluctuation-dissipation theorem for the photon field predicts the temperature dependence of the dephasing rate. This was first shown by Altshuler, Aronov and Khmelnit-

[3] See *e.g.* the review by Altshuler and Aronov [23] or the recent book by Akkermans and Montambaux [41]. Despite some earlier controversy it is now believed to be the proper explanation for pure systems without magnetic impurities, see *e.g.* [42] and [43, 44]

skii [5], who considered the properly screened photon propagator in various dimensions and thus obtained the temperature dependence of weak localization.

For completeness we mention that phase coherence and diffusive motion of particles are also the ingredients leading to the Altshuler-Aronov interaction corrections to the conductance and the density of states. These are similarly due to an enhanced interaction vertex at small energies [6, 7]. The enhancement arises again because a particle may return to the point of scattering with the same phase if the energy transfer is small enough, thus adding coherently to the original scattering amplitude. Alternatively these effects can be thought of as arising from scattering off Friedel oscillations around impurities [8].

Coherent quantum effects in conductance and their suppression by electron-electron interactions are thus well understood in one and higher dimensions. The situation is less well established in quasi-zero dimensional systems, the quantum dots mentioned earlier. Fig. 1.5 illustrates the different dimensions for the case of a gate-defined quantum dot in semiconductor heterostructures. In all cases the third dimension does not participate in the dynamics, as the wavefunction in this direction factors and relevant states only involve the lowest energy mode. In other directions the sample is either not restricted at all [2D-case, Fig. 1.5(a)] or restricted in only one direction [1D-case, Fig. 1.5(b)]. Diffusion is the dominant reason for a finite resistance in both cases.

In the quasi-zero dimensional case of Fig. 1.5(c) the dominant contribution to the conductance does not arise from the diffusive propagation of the particles. While the motion inside the gate defined region remains diffusive,[4] it is now the low probability to escape—due to the small fraction of the circumference for which this is possible—that

[4]Motion inside the dot may also be ballistically chaotic. This gives rise to a new timescale, the Ehrenfest time τ_E, which is the time it takes the chaotic dynamics to "tear apart" a minimal uncertainty wavepacket until its probability density is distributed evenly across the dot. In the case of diffusive quantum dots $\tau_E \to 0$. Finite Ehrenfest times affect the weak localization correction, see [45–47]. We have considered its effect on the Altshuler-Aronov correction in [48]. Throughout this thesis however we will assume $\tau_E = 0$.

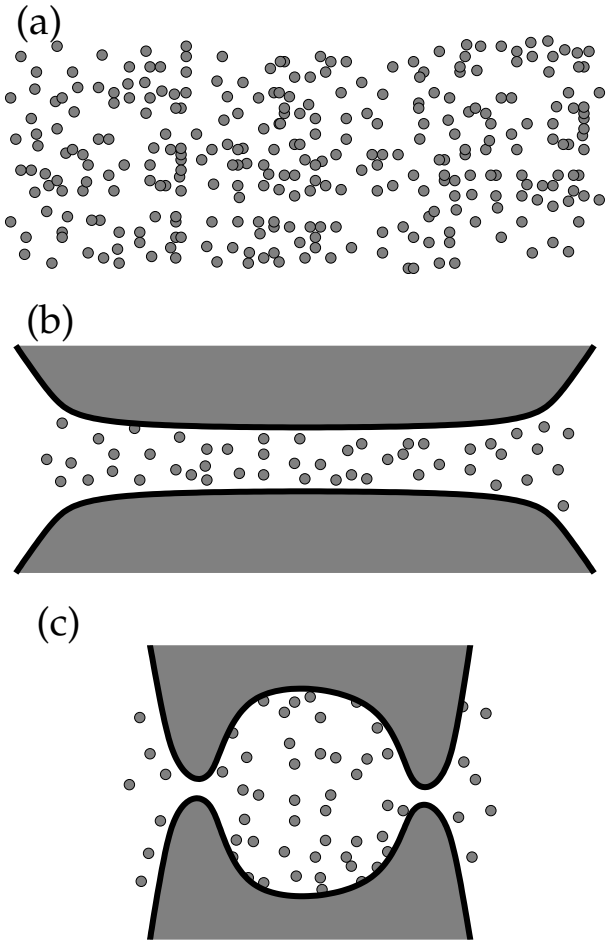

FIGURE 1.5: Illustration of different effective dimensions implemented in a two dimensional electron gas. The third dimension is not shown and forms a quantum well in which only the lowest energy mode is occupied. (a) Quasiparticles propagate in both directions in the plane. (b) Gates constrain the motion to be effectively one dimensional. (c) By forming narrow contact regions a quasi zero dimensional "quantum dot" is formed whose conductance is dominated by the contacts.

dominates the conductance.

Such a quantum dot exhibits a new hierarchy of energy scales. The highest energy scale is the Fermi energy, followed by the Thouless energy $E_{Th} = \hbar\gamma_1$, with γ_1 the smallest nonzero eigenvalue of the diffusion operator for the quantum dot. The smallest energy scale is the single particle level spacing Δ. From the Thouless energy and the mean level spacing a dimensionless quantity, the dimensionless conductance g is formed. In a diffusive dot g is related to $k_F L$ and thus large for the types of quantum dots we are interested in. It is the parameter that justifies the use of Random Matrix theory below, see Sec. 1.3.1. In addition to these single particle energy scales the Coulomb interaction among the electrons on the dot defines an additional scale, the charging energy, which is given in terms of the geometric capacitance C of the dot as $E_c = e^2/C$.

Two different regimes of transport through quantum dots are usually distinguished. 'Closed' dots are connected to leads only by tunnel contacts. Due to interactions among the electrons, closed dots show pronounced level structure, which is why they are sometimes referred to as "artificial atoms". Here we look at the opposite regime, 'open' quantum dots, where the dimensionless contact conductance between lead and dot is large, such that the levels in the dot broaden to form a continuum. One estimates that this occurs when the total of the contacts' conductances $G \approx e^2/h$. Consider the RC-time τ_c of the equivalent resistive circuit in conjunction with Heisenberg's uncertainty principle. As levels will only be well defined as long as $\delta E \ll E_c$ the crossover is in the vicinity of $\tau_c E_c \approx \hbar$, which with $\tau_c = C/G$ gives the condition above [9]. Where the dimensionless contact conductance is large, the energy levels broaden to form a continuum, and perturbation theory in e^2/hG, the inverse of the dimensionless contact conductance, is justified.

The quantum correction to the average conductance at zero temperature can easily be

found for a quantum dot with ballistic contacts. In this case we may think of "channels" forming in the vicinity of the contacts, analogous to the original experiment by van Wees which showed conductance quantization for the first time [10]. Consider then a dot with one contact of N_L and a second of N_R channels. An electron's trajectory entering the dot through one channel will, by the chaotically ergodic nature of transport in the dot, leave through any one of the $N_L + N_R$ channels with equal probability. Weak localization occurs because the pairing of time reversed trajectories doubles the probability to leave the dot through the same channel that it was entered through. This enhancement of backscattering reduces the conductance by

$$\delta G = G - G^{cl} = \left(\frac{N_L N_R}{N_L + N_R + 1} - \frac{N_L N_R}{N_L + N_R} \right) \frac{e^2}{h} \approx - \frac{N_L N_R}{(N_L + N_R)^2} \frac{e^2}{h} + O\left(\frac{e^2}{h G^{cl}} \right). \quad (1.8)$$

The last expression exemplifies the expansion of the quantum corrections in terms of the dimensionless classical conductance $G^{cl}/(e^2/h)$. In our treatment of networks we will be able to treat all corrections of order one.

The magnetic field dependence [11, 12], as well as the effect of nonideal contacts [13], can be included in this description. For the temperature dependence, however, no good agreement between theory and experiment has been found to date. Most unfortunate for a description is that the universal part of the interaction, the uniform charging energy, does not cause dephasing as it always affects both amplitudes in the same way. The non-zero eigenvalues of the diffusion equation are not known and the spatially non-homogenous part of the electromagnetic mode structure which does give rise to dephasing depends both on these as well as on other non-universal details unaccessible in experiment. Assuming a reasonable mode structure theory thus far predicts an intrinsic dephasing rate proportional to T^2 [14, 15], yet experiments tend to not support a pure T^2 law but find regimes intermediate between linear and quadratic dependence on T [16, 17].

In Chapter 2 we investigate quantum dot networks and show that such limitations—

parameters necessary for predictions yet unaccessable to experiments—are absent in this case: The relevant nonhomogenous interaction constants are the capacitances and cross-capacitances among the dots, and the relevant transport parameters are the contact conductances between the individual dots. Both can be measured in gate-defined quantum dots in two dimensional electron gases.

We obtain all quantum corrections to the conductance for such a network of quantum dots. We find that the weak localization correction is reduced as expected in the presence of a magnetic field, and that non-zero temperature dephases part of the weak localization as T^{-1}. In addition we obtain the analogue of the Altshuler-Aronov interaction corrections in such a network.

Our calculation is based on Random Matrix Theory. The following Sec. 1.3.1 gives some background on the description of quantum dots using random matrices and elucidates the analogy to ordinary perturbation theory.

1.3.1 Universal Random Matrix model

Microscopic properties such as the position of each impurity or the precise shape of a quantum dot are not accessible to experiment. To fully model such a system from first principles is thus not only out of the question because of its astounding complexity but also due to our ignorance of the parameters of the model. In higher dimensions effective quantities govern particle propagation and in turn quantum corrections as well as interaction corrections. We do not encounter quite the same advantageous situation in quantum dots.

While it is possible to obtain the relevant information–contact conductances–with which to predict the quantum corrections to the conductance in the zero temperature

noninteracting limit, the dominant universal interaction among the electrons does not give rise to decoherence. Hence the temperature dependence of the quantum corrections cannot be predicted accurately. Considering a network of quantum dots, instead of an individual dot, we regain this ability as the universal interaction modes are no longer uniform across the sample and can thus give rise to dephasing.

At low energies $\boxtimes < E_{Th}$, it is known that the statistics of energy levels of quantum dots is identical to that of ensembles of large random matrices. Using supersymmetric techniques, Efetov [18] has shown this for the case of disordered metal grains. More recently, this identity has also been shown to apply to quantum dots in which the classical motion is ballistically chaotic [19, 20]. Given this equivalence we obtain the average conductance of the quantum dot system considered here using Random Matrix theory.

This allows us to make use of diagrammatic rules developed to calculate ensemble averages. For convenience we choose gaussian ensembles. These can be motivated by the fact that a matrix element in a disordered sample will involve many contributions, hence the central-limit theorem can be thought to apply. The ensembles are named after their invariance properties. They follow from the physical symmetries imposed on the matrix H, which is the analogue of the Hamiltonian matrix for a quantum mechanical system.[5]

1. If the system is believed to obey time reversal symmetry as well as spin rotation symmetry, its Hamiltonian matrix should be real and symmetric: $H = H^* = H^T$.
2. If the system is believed to obey no symmetries, all we ask is that the Hamiltonian matrix be hermitian: $H = H^\dagger$.

[5]For simplicity of presentation we do not include the spin degree of freedom in the following argument. It turns out that the presence of time reversal symmetry with spin rotation symmetry broken gives rise to a new universality class. This class is relevant in the presence of spin-orbit scattering in the absence of magnetic fields. This situation is not considered here. For more on this case and random matrices in quantum transport in general see the review [49].

For the real symmetric matrices the group that leaves the symmetries of the matrices intact is the one of orthogonal matrices O which satisfy $O^T O = \mathbb{1}$. For the hermitian matrices it is the group of unitary matrices U which satisfy $U^\dagger U = \mathbb{1}$. The distribution of the matrix elements of H takes the same gaussian form in both cases,

$$P(H) = \frac{1}{V} \exp\left(-\frac{\beta N}{4\lambda^2} \mathrm{tr} H^2\right), \tag{1.9}$$

where V is a normalization constant, M is the dimension of the matrix and λ determines the width of the distribution. The corresponding ensembles are referred to as the gaussian orthogonal ensemble (GOE) and the gaussian unitary ensemble (GUE), respectively. The parameter $\beta = 1$ for the gaussian orthogonal ensemble whereas $\beta = 2$ for the gaussian unitary one. The resulting spectrum in the limit $M \to \infty$ is the famous Wigner semicircle [21, 22]

$$\nu(\varepsilon) = \frac{M}{\pi\lambda}\sqrt{1 - \frac{\varepsilon}{2\lambda}} = \nu_0 \sqrt{1 - \frac{\pi\varepsilon}{2M\nu_0}} \tag{1.10}$$

Identifying $\nu_0 = M/\lambda\pi$ with the density of states at the Fermi energy in the quantum dot fixes the remaining free parameter λ. The limit $M \to \infty$ is the limit in which the random matrix spectrum is universal, it is the limit considered here.

Being equipped with a Hamiltonian matrix H the "wavefunctions" of the system are vectors ψ of the same dimension. So far we have treated a closed dot. Coupling among different dots, as well as to leads, is included by an approach reminiscent of tight binding Hamiltonians via a transmission matrix t_{ij} between dots i and j. The trace $\mathrm{tr} t_{ij} t_{ij}^\dagger$ determines a contact's conductance g_{ij}, $\mathrm{tr}(t_{ij} t_{ij}^\dagger)^2$ its form factor f_{ij}. Similar matrices are introduced to model coupling to the leads. The leads are assumed to be well coupled to reservoirs such that backscattering is of no concern.

At last we need to consider the Coulomb interactions we intend to include within our model. Given the distribution of Hamiltonian matrices, a corresponding distribution of eigenvectors can be found. With this distribution a hierarchy of the matrix elements

arising from the Coulomb interaction is established [9]. Yet it turns out that the bare Coulomb interaction gives rise to divergent matrix elements and can thus never be treated perturbatively; it needs to be screened [23]. The solution of the resulting exercise for the single quantum dot shows that the largest matrix element couples uniformly all charges in a quantum dot [9]. It is

$$\mathrm{H}_{\mathrm{int}} = \frac{e^2}{2\mathrm{C}}\hat{n}^2 \tag{1.11}$$

where C is the geometric capacitance of the dot and $\hat{n} = \sum_{\alpha=1}^{\mathrm{M}} \hat{\psi}_\alpha^\dagger \hat{\psi}_\alpha$ is the number operator on the dot. In the case of a single dot the resulting Hamiltonian, which also includes an exchange coupling and a Cooper channel, is known as the "universal interaction Hamiltonian" [9].[6] Corrections to this interaction Hamiltonian in turn are expected to be small in the dimensionless conductance as $1/g$ [9].

Using a renormalization group procedure it has also been shown [24] that the addition of a crosscapacitance to the model is the correct limit, in a renormalization group sense, for the particular case of a double quantum dot. Building on these results we postulate that the most relevant interaction Hamiltonian in a network is also the one that includes capacitive couplings of the total charges on the dots

$$\mathrm{H}_{\mathrm{int}} = \sum_{i=1,j}^{\mathcal{N}_\mathrm{D}} \frac{e^2}{2} \hat{n}_i \tilde{\mathrm{C}}_{ij}^{-1} \hat{n}_j, \tag{1.12}$$

where $\hat{n}_i = \sum_{\alpha=1}^{\mathrm{M}_i} \hat{\psi}_{i,\alpha}^\dagger \hat{\psi}_{i\alpha}$ is the number operator on dot i with M_i the dimension of H_i, $\mathcal{N}_\mathrm{D}$ is the number of dots in the network and $\tilde{\mathrm{C}}$ is the capacitance matrix.

Equipped with a random Hamiltonian for the dot, couplings among the different dots, and the interaction matrix elements, the next step is the diagrammatic calculation of the

[6] In this work we do not consider the effect of either the exchange coupling or the Cooper channel. Formally this is justified in the limit where the mean level spacing Δ is smaller than the energy scale related to the dwell time τ_d, the expectation value of the time until a particle escapes from the dot. The charging energy E_c on the other hand is expected to exceed this scale. Relating this to the phase accrued by a particle while on the dot, we see that this implies $\mathrm{E}_\mathrm{c}\tau_\mathrm{d} \gg \hbar \gg \Delta\tau_\mathrm{d}$. As the dwell time is related to the dimensionless conductance of the contacts g_c as $\tau_\mathrm{d} = \hbar g_\mathrm{c}/\Delta$ we see that this requirement can be satisfied in a small dot well coupled to leads.

ensemble average. Techniques for this purpose have been developed, and we have extended them here to treat the case of multiple dots. This case presents some challenges not present in the single dot case. Whereas it is possible to avoid contributions from vertex corrections in single dots by choosing a convenient basis, no such procedure exists for multiple dots. This also complicates the calculation of another ingredient of the theory, the Hikami box, which is essential for the inclusion of self-returning paths contributing to weak localization. Yet these challenges can be overcome; Section 2.4.2 of Chapter 2 proceeds with the calculation, and the appendix to the same Chapter contains exemplarily the calculation of one contribution to the Hikami box.

1.3.2 Connection to perturbation theory

Concluding the introduction to quantum effects in conductance measurements, we establish the connection to diagrammatic perturbation theory with which the reader may be familiar. In the diagrammatic perturbation theory of the disordered electron gas the expansion parameter is $1/k_{\mathrm{F}}\mathrm{L}$, k_{F} the Fermi wavenumber and L a linear size of the system[25]. For the Random Matrix expansion the large parameter is M [9, 22].

White noise disorder $\langle \mathrm{V}(\mathbf{r})\mathrm{V}(\mathbf{r}')\rangle = \mathrm{V}_0^2\delta(\mathbf{r}-\mathbf{r}')$ is the source of scattering among different plane wave states in the electron gas; the matrix elements of H are the "scatterers" in the Random Matrix calculation.

$$\langle \mathrm{H}_{\alpha\beta}\mathrm{H}^*_{\delta\gamma}\rangle = \frac{\lambda}{\mathrm{M}}\delta_{\alpha\delta}\delta_{\beta\gamma} + \frac{\lambda'}{\mathrm{M}}\delta_{\alpha\gamma}\delta_{\beta\delta}, \tag{1.13}$$

where λ is related to the density of states as mentioned above and $\lambda' = \lambda$ nonzero in the orthogonal ensemble only. The crossover due to a weak magnetic field is implemented choosing $\lambda' \in (0, \lambda)$; details are given in Chapter 2 and in Ref. [9]. Given the potential difference in the two correlators, in the RMT calculation it is necessary to keep track of

the order of the indices.

Due to this structural symmetry, the disorder average involves the same ingredients in both cases. One establishes Dyson equations to obtain self energies and the disorder-averaged Green's function. Diffuson ladders describe diffusion across the system [Fig. 1.6(a) and (c)], and the cooperon contribution is the source of the weak localization correction [Fig. 1.6(b) and (d)].

One realizes that the Cooperon contribution vanishes in the unitary ensemble, *e.g.*, when a magnetic field is present, and only contributes in the orthogonal case when time reversal symmetry is not broken. The dependence of weak localization on magnetic field is thus incorporated in the rules for diagrammatic averaging in the random matrix model. In the case of diagrammatic perturbation theory, it arises from the dependence of the free propagator on the vector potential.

To obtain the influence of interactions and thus of temperature on the weak localization correction we perform another diagrammatic expansion, this time in the coupling of electrons to the electromagnetic field, which is appropriate at low temperature when the rate of photon emission or absorption is low. The diagrams contributing in this case are given in Fig. 1.7 as reference.

One important feature of the calculation is that the correction from photons of frequency ω is proportional to $\coth(\omega/2T) + \tanh[(\varepsilon - \omega)/2T]$, where ε is the energy of the electron involved, measured from the Fermi energy. This second term incorporates the Pauli principle, *i.e.* it adjusts for the fact that an electron can only emit a photon of frequency ω if the new state that it would transition to is empty. The corresponding calculation is given in Chapter 2. This "Pauli blocking" ensures that at $T = 0$ no dephasing occurs from interactions. At high temperatures this constraint becomes unimportant.

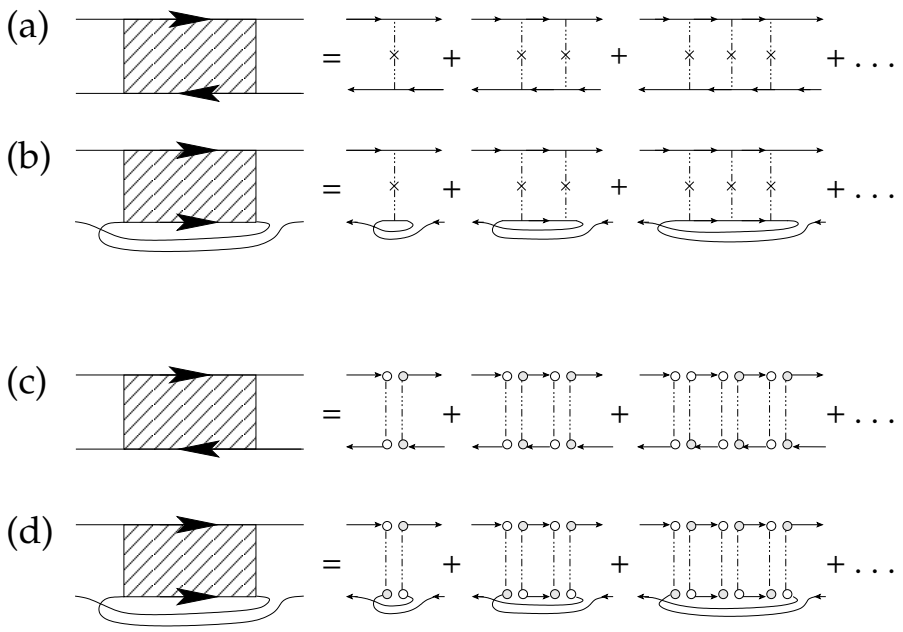

FIGURE 1.6: Diffuson contribution (a) and Cooperon contribution (b) to the diagrammatic averages for the case of disordered metals. Diffuson (c) and Cooperon (d) as encountered for quantum dots modelled with the gaussian ensembles of Random Matrix Theory.

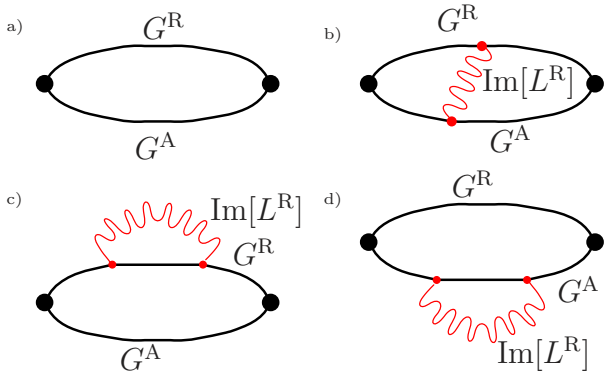

FIGURE 1.7: Diagrams contributing up to first order in the electron-photon coupling. (a) Zeroth order classical result, (b) - (d) first order correction. L^{R} is the photon's retarded interaction propagator, G^{R} (G^{A}) is the retarded (advanced) Green's function of the electron.

Higher order interaction corrections are thus more easily obtained, and with the help of the fluctuation-dissipation theorem one finds that the interaction is effectively instantaneous. The higher temperature regime can then be solved using a Dyson equation. In Chapter 2 we show that the regimes of applicability overlap broadly, enabling us to find the leading quantum corrections for all temperatures.

1.4 Andreev reflection in superconductor–half-metal hybrid systems

Superconductivity was first discovered almost a hundred years ago by Kamerlingh-Onnes in Leiden [26]. The possibility to liquefy helium had made it possible to cool materials to very low temperatures. A simple resistance measurement of mercury revealed an astounding change in its properties below 4.19K; its resistance had dropped to zero. Unbeknownst to the experimenter something dramatic had happened, a new coherent quantum state had been created. The mercury had turned superconducting.

1.4.1 Order parameter

For decades no theory was able to give a comprehensive description. Eventually Ginzburg and Landau [27] posited a complex order parameter and built on the Landau theory of phase transitions to describe this superconducting transition. A microscopic theory was presented somewhat later by Bardeen, Cooper and Schrieffer [28]. BCS theory, as it is now called, gives an explicit form for a grandcanonical ground state of the new system, which at low temperatures is energetically favored over the Fermi liquid due to attractive interactions, even if those interactions are very weak. This ground state is a coherent state of paired electrons, of Cooper pairs. These two pictures are complementary: both intro-

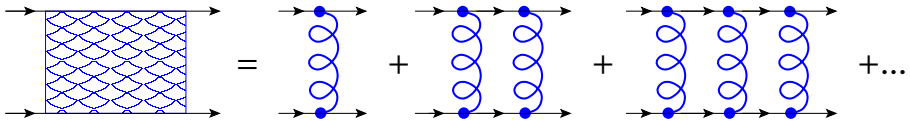

FIGURE 1.8: The cooperon propagator in the context of superconductivity. Here the blue lines connecting retarded and advanced Green functions are those of the phonon mediated attractive interaction.

duce and utilize a new coherent complex order parameter proportional to the pairing amplitude.

Only a few month before positing the new BCS ground state, Cooper had shown that a Fermi liquid develops an instability towards pairing in the presence of weak attractive interactions [29]. Pairs are formed between quasiparticles of the Landau Fermi liquid, related to one another by time reversal symmetry. Once BCS theory was known, it was extended to disordered but time reversal invariant systems by Anderson [30]. Evaluating the pair propagator it was found that arbitrarily weak attractive interactions cause an instability in the Fermi liquid at low temperatures, signalled by a zero energy divergence of the cooperon pair propagator

$$\langle \psi^\dagger_{\mathbf{p}\uparrow} \psi^\dagger_{-\mathbf{p}\downarrow} \psi_{-\mathbf{k}\downarrow} \psi_{\mathbf{k}\uparrow} \rangle. \tag{1.14}$$

The dominant (diverging) contribution to this average arises from the diagram of Fig. 1.8 (see *e.g.* [31]).

The cooperon propagator is identical to the one we encountered before in Fig. 1.4 where it gave rise to weak localization. The difference is in the scattering mechanism. In the case of superconductivity, two electrons scatter off each other via a phonon mediated interaction. In the case of the conductance calculation electrons scatter off the same static impurity. The coherence relies on time reversal symmetry here as it does there. It is then no surprise that superconductivity and magnetism are antagonistic phenomena. A magnetic flux will lead to dephasing of the cooperon propagator here as it does in the

case of the conductance calculation (see Sec. 1.2). But superconductivity is more robust: Due to the attractive interaction, energy is gained by forming pairs, whereas no such gain is present in the conductance problem.

For weak enough fields then, superconductivity may prevail and expel magnetic fluxes so as to be able to form Cooper pairs and let them condense. This is the essence of the Meissner-Ochsenfeld effect, and it makes simultaneous existence of magnetic and superconducting order difficult to achieve in the same region of space. Here we consider instead a magnetic material brought in contact with a superconductor. In this case the regions of different order do not compete to the same extent as they remain spatially separated. We are interested in effects originating at the interface between the two regions.

Despite the fact that Cooper pairs can be said to have a finite extension it has been very fruitful to consider a local pairing amplitude $\langle\psi_\uparrow(\mathbf{r})\psi_\downarrow(\mathbf{r})\rangle$. In a mean field theory, one then finds not only a self-consistent groundstate but is also able to determine fermionic excitations above it. These equations were originally formulated by Bogol'ubov and popularized by de Gennes [32]. Widely known as the Bogoliubov-de Gennes equations, they are the framework within which Chapters 3, 4 and 5 explore superconductivity. The equations read

$$\begin{pmatrix} \mathrm{H} & \Delta \\ \Delta^* & -\mathrm{H}^* \end{pmatrix}\begin{pmatrix} u \\ v \end{pmatrix} = \varepsilon \begin{pmatrix} u \\ v \end{pmatrix} \tag{1.15}$$

where H is the single particle Hamiltonian and u and v can be understood as the electron and hole components of an excitation's wavefunction. One finds that in standard BCS theory the order parameter Δ is related to these components as

$$\begin{aligned} \Delta(\mathbf{r}) &= \lambda_\mathrm{C}\langle\psi_\uparrow(\mathbf{r})\psi_\downarrow(\mathbf{r})\rangle \\ &= \lambda_\mathrm{C}\sum_{\varepsilon>0} v^*(\mathbf{r})u(\mathbf{r})\left[1-2f(\varepsilon)\right], \end{aligned} \tag{1.16}$$

where we sum over all solutions of positive energy and $f(\varepsilon)$ is the Fermi Dirac distribu-

tion function. λ_C is the strength of the attractive phonon mediated interaction. Solving these equations self-consistently reveals a gap in the quasiparticle excitation spectrum of the superconductor [32]. No quasiparticle excitations exist unless their energy exceeds Δ.

1.4.2 Andreev reflection

Normal metals

Having discovered a gap for quasiparticle excitations it is natural to ask what fate is bestowed upon quasiparticles incident on the superconductor from a normal metal. They do not have enough energy to enter the superconductor above the gap, yet at a clean and smooth interface there is also no potential strong enough to allow for backscattering. Yet there is another scattering process that requires very little momentum change and conserves energy. In this process an incident electron is scattered back as a hole. This hole carries almost the same momentum and has the same energy. As it has opposite group velocity it precisely traces out the path of the incoming particle. Andreev [33] first investigated this process and it is now named after him. In a modern way we may write the reflection matrix for this process as

$$\mathcal{R}_A(\varepsilon) = \alpha(\varepsilon) \begin{pmatrix} 0 & e^{i\phi} \\ e^{-i\phi} & 0 \end{pmatrix} \tag{1.17}$$

where the matrix structure is that of electron and hole components as in Eq. (1.15) above. $\alpha(\varepsilon) = \exp[-i \arccos \varepsilon/|\Delta|]$ is a phase shift depending on the energy of the incoming quasiparticle and ϕ is the phase of the superconducting order parameter Δ.

Along the same path, electrons and holes close to the Fermi energy incur phases that are almost identical but of opposite signs. The Andreev reflection mechanism therefore

implies the possibility of extending superconducting correlations into a normal metal, *i.e.*, into a material where there is no attractive interaction that would lead to the formation of Cooper pairs on its own. From the discussion in Sec. 1.1 one realizes that this effect relies on coherence as the phases accumulated along the two paths need to cancel. With the dispersion relation in the vicinity of the Fermi wavenumber k_F

$$k_\mathrm{e}(\varepsilon) = k_\mathrm{h}(-\varepsilon) \approx k_\mathrm{F} + \frac{\varepsilon}{\hbar v_\mathrm{F}}, \tag{1.18}$$

where v_F is the Fermi velocity, we find that the length over which the effect will penetrate the normal metal is limited by the excitation energy ε, as pointed out in 1.2. The scale up to which correlations penetrate the normal metal is given by $\hbar v_\mathrm{F}/|\Delta|$.

Kulik [34] realized that via such correlations the phases of two superconductors adjacent to normal metal could be coupled through this normal metal. The most striking consequence of this is a Josephson current flowing in equilibrium between the two superconductors as soon as the phases of their order parameters differ.

Ferromagnets

In light of the mutually exclusive nature of superconductivity and magnetism it was long thought that pairing correlations originating in ordinary *s*-wave superconductors would not be able to penetrate a ferromagnet. There due to the exchange field two quasiparticles of opposite spin have different dispersion relations, resulting in a short ranged correlator as discussed earlier in Sec. 1.2.

Bergeret, Volkov and Efetov [1] realized that an inhomogeneity in spin space could provide an effective twist to get around this limitation, transforming correlations of singlet symmetry to ones of triplet type: The pair correlator can be presented as the sum of

a singlet and three triplet components.

$$\langle \psi_\sigma \psi_{\sigma'} \rangle = (\Delta_s + \Delta_t \cdot \boldsymbol{\sigma}) i\sigma_2 \tag{1.19}$$

While the singlet component Δ_s, involving spins of both directions, will clearly be affected by the exchange field, parts of the triplet component Δ_t will not be as it involves electrons with spins aligned as well. Thus "long range triplet component" superconducting correlations are induced, which decay on the same long length scale as expected for ordinary singlet correlations in normal metal links.

Treatments of the ferromagnetic problem first considered were restricted to weak exchange fields, see *e.g.* the review [35]. They relied on the quasiclassical method and assumed that the only effect of the exchange field was to change the phase accumulated by carriers of different spin. Results obtained for weak ferromagnets were thus not generalizable to half-metals.

Half metals

In this thesis we focus on the half-metallic case. Motivated by the observation of a Josephson current through the half-metal CrO_2 by Keizer *et al.* [2] we reexamine possible mechanisms of enabling triplet Andreev reflection into half-metals. Previous work has been numerical [36] or based on a phenomenological model of the interface using a scattering matrix combined with quasiclassical Green functions [37–39].

In half-metallic materials only spins of one orientation propagate. The only possible correlator is thus one that involves annihilation of equal spin excitations

$$\langle \psi_\uparrow(\mathbf{r}, t) \psi_\uparrow(\mathbf{r}, t') \rangle \tag{1.20}$$

which are bound by the Pauli principle to vanish at equal time. Considered in Matsubara space one finds the requirement that an equal position correlator be odd in frequency.

This is a surprise, as the normal BCS superconducting correlations are even in frequency. Yet the frequency dependence of the correlator in the half-metal will not only depend on the original symmetry in the superconductor, but also on phases accumulated from propagation in the half-metal. This opens the possibility to find a symmetry different from inside the superconductor in the half-metal.

It has been realized that as in the ferromagnetic case one crucial ingredient to obtain Andreev reflection amplitudes at superconductor–half-metal interfaces is the complete breaking of spin rotational symmetry [37]. The normal state scattering matrix of the interface region may not be diagonal in spin-space.

In Chapter 3 we further investigate the possibility of Andreev reflection into a half-metal using a scattering approach. This approach allows for a quantum-coherent treatment of the system considered. Being thus able to treat the single channel quantum limit, we find that at the Fermi energy Andreev reflection into half-metals is suppressed due to symmetry reasons. If the scattering matrix is block-diagonal with each block containing only one electron and one hole mode, then particle-hole symmetry together with unitarity leads to the condition that the product of the Andreev reflection amplitude r_{he} and the normal reflection amplitude r_{ee} is zero,

$$r_{he}(0)r_{ee}(0) = 0. \tag{1.21}$$

There can thus only either be perfect Andreev reflection or perfect normal reflection. We confirm that perfect normal reflection is the generic case. That Andreev reflection is suppressed has consequences. We find that the subgap conductance of a half-metal–superconductor junction depends quadratically on the bias voltage, vanishing at zero bias. In addition the Josephson current is suppressed by a factor $(E_{Th}/\Delta)^2$ in long junctions where the Thouless energy $E_{Th} = \hbar v_F/L$ is smaller than the gap Δ.

The above argument relies on unitarity. Béri showed that in the presence of dephas-

ing, Andreev reflection may occur at the Fermi energy in a single mode setup [40]. In systems where the scattering matrix takes a block-diagonal form due to additional symmetries, such as at a translationally invariant an inversion symmetric interface, finite Andreev reflection at the Fermi energy can also be obtained by breaking these accidental symmetries. This alternative route to triplet Andreev reflection at the Fermi energy is investigated in Chapter 4. Here a domain wall perpendicular to the interface breaks inversion symmetry. In Chapter 4 we consider the extreme case of a half-metal in which minority carriers are not even evanescently present. We find that such a domain wall can indeed cause triplet Andreev reflection. We also identify the crucial role of geometry for the triplet Andreev reflection into half-metals. The experiments by Keizer *et al.* [2] were done in a lateral geometry with superconducting contacts deposited on top of the half-metallic layer which in turn was evaporated onto an oxide wafer. Yet theorists so far had modelled the contact to the half-metal as a serial geometry, where the two materials are butted against each other, since this was easier to model and did not matter for normal-metal–superconductor hybrid systems. It turns out, however, that the lateral geometry may give rise to multiple reflections at the superconductor interface, resulting in an enhancement of the single Andreev reflection amplitude. It is also intuitive that it has implications for the generic dimension of the blocks of the reflection matrix and thus for the presence or absence of Andreev reflection due to symmetry constraints. In this regard the "serial" geometry is more restrictive. Chapter 5 further investigates domain walls as a source of Andreev reflection. Using a perturbative approach complementary to the one in Chapter 4, we consider arbitrary orientations and allow for the evanescent presence of minority carriers in the half-metal.

BIBLIOGRAPHY

[1] F. S. Bergeret, A. F. Volkov, and K. B. Efetov, Phys. Rev. Lett. **86**, 4096 (2001).

[2] R. S. Keizer, S. T. B. Goennenwein, T. M. Klapwijk, G. X. Miao, G. Xiao, and A. Gupta, Nature **439**, 825 (2006).

[3] B. L. Altshuler and P. A. Lee, Phys. Today **Dec.**, 36 (1988).

[4] Y. Imry, *Introduction to Mesoscopic Physics* (Oxford University Press, 2002).

[5] B. L. Altshuler, A. G. Aronov, and D. E. Khmelnitskii, J. Phys. C **15**, 7367 (1982).

[6] B. L. Altshuler and A. G. Aronov, Solid State Commun. **30**, 115 (1979).

[7] B. L. Altshuler, D. Khmelnitskii, A. I. Larkin, and P. A. Lee, Phys. Rev. B **22**, 5142 (1980).

[8] G. Zala, B. N. Narozhny, and I. L. Aleiner, Phys. Rev. B **64**, 214204 (2001).

[9] I. L. Aleiner, P. W. Brouwer, and L. I. Glazman, Phys. Rep. **358**, 309 (2002).

[10] B. J. van Wees, H. van Houten, C. W. J. Beenakker, J. G. Williamson, L. P. Kouwenhoven, D. van der Marel, and C. T. Foxon, Phys. Rev. Lett. **60**, 848 (1988).

[11] K. B. Efetov, Phys. Rev. Lett. **74**, 2299 (1995).

[12] K. Frahm, Europhys. Lett. **30**, 457 (1995).

[13] M. G. Vavilov and I. L. Aleiner, Phys. Rev. B **60**, R16311 (1999).

[14] U. Sivan, Y. Imry, and A. G. Aronov, Europhys. Lett. **28**, 115 (1994).

[15] Ya. M. Blanter, Phys. Rev. B **54**, 12807 (1996).

[16] A. G. Huibers, S. R. Patel, C. M. Marcus, P. W. Brouwer, C. I. Duruöz, and J. S. Harris, Phys. Rev. Lett. **81**, 1917 (1998).

[17] A. G. Huibers, J. A. Folk, S. R. Patel, C. M. Marcus, C. I. Duruöz, and J. S. Harris, Phys. Rev. Lett. **83**, 5090 (1999).

[18] K. B. Efetov, Adv. Phys. **32**, 53 (1983).

[19] M. Sieber and K. Richter, Phys. Scripta **T90**, 128 (2001).

[20] S. Heusler, S. Müller, A. Altland, P. Braun, and F. Haake, Phys. Rev. Lett. **98**, 044103 (2007).

[21] E. P. Wigner, Phys. Rev. **98**, 145 (1955).

[22] A. Zee, *Quantum Field Theory in a nutshell* (Princeton University Press, 2003).

[23] B. L. Altshuler and A. G. Aronov, in *Electron-Electron Interactions in Disordered Systems*, edited by A. L. Efros and M. Pollak (Elsevier, Amsterdam, 1985).

[24] S. Adam, P. W. Brouwer, and P. Sharma, Phys. Rev. B **68**, 241311 (2003).

[25] A. Abrikosov, L. P. Gorkov, and I. E. Dzyaloshinski, *Methods of Quantum Field Theory in Statistical Physics* (Prentice-Hall, 1963).

[26] H. Kamerlingh Onnes, Commun. Phys. Lab. Univ. Leiden **12**, 120 (1911).

[27] V. L. Ginzburg and L. Landau, Zh. Eksp. Teor. Fiz. **20**, 1064 (1950).

[28] J. Bardeen, L. N. Cooper, and J. R. Schrieffer, Phys. Rev. **108**, 1175 (1957).

[29] L. N. Cooper, Phys. Rev. **104**, 1189 (1956).

[30] P. W. Anderson, J. Phys. Chem. Solids **11**, 26 (1959).

[31] H. Bruus and K. Flensberg, *Many-Body Quantum Theory in Condensed Matter Physics* (Oxford University Press, 2004).

[32] P. G. de Gennes, *Superconductivity of Metals and Alloys* (Benjamin, New York, 1966).

[33] A. F. Andreev, Zh. Eksp. Teor. Fiz. **46**, 1823 (1964), [Sov. Phys. JETP **19**, 1228 (1964)].

[34] I. Kulik, Zh. Eksp. Teor. Fiz. **57**, 1745 (1969), [Sov. Phys. JETP **30**, 944 (1970)].

[35] F. Bergeret, A. Volkov, and K. Efetov, Rev. Mod. Phys. **77**, 1321 (2005).

[36] Y. Asano, Y. Tanaka, and A. A. Golubov, Phys. Rev. Lett. **98**, 107002 (2007).

[37] M. Eschrig, J. Kopu, J. C. Cuevas, and G. Schön, Phys. Rev. Lett. **90**, 137003 (2003).

[38] M. Eschrig and T. Lofwander, Nat. Phys. **4**, 138 (2008).

[39] A. V. Galaktionov, M. S. Kalenkov, and A. D. Zaikin, Phys. Rev. B **77**, 094520 (2008).

[40] B. Beri, Phys. Rev. B **79**, 245315 (2009).

[41] E. Akkermans and G. Montambaux, *Mesoscopic Physics of Electrons and Photons* (Cambridge University Press, 2007).

[42] F. Pierre, A. B. Gougam, A. Anthore, H. Pothier, D. Esteve, and N. O. Birge, Phys. Rev. B **68**, 085413 (2003).

[43] F. Marquardt, J. von Delft, R. A. Smith, and V. Ambegaokar, Phys. Rev. B **76**, 195331 (2007).

[44] J. von Delft, F. Marquardt, R. A. Smith, and V. Ambegaokar, Phys. Rev. B **76**, 195331 (2007).

[45] I. L. Aleiner and A. I. Larkin, Phys. Rev. B **54**, 14423 (1996).

[46] S. Rahav and P. W. Brouwer, Phys. Rev. Lett. **95**, 056806 (2005).

[47] P. W. Brouwer, Phys. Rev. B **76**, 165313 (2007).

[48] P. W. Brouwer and J. N. Kupferschmidt, Phys. Rev. Lett. **100**, 246805 (2008).

[49] C. W. J. Beenakker, Rev. Mod. Phys. **69**, 731 (1997).

CHAPTER 2

TEMPERATURE AND MAGNETIC-FIELD DEPENDENCE OF THE QUANTUM CORRECTIONS TO THE CONDUCTANCE OF A NETWORK OF QUANTUM DOTS

2.1 Introduction

The low temperature conductivity of disordered metals or semiconductors is dominated by the elastic scattering of electrons off impurities and defects. While the conductivity is determined by Drude-Boltzmann theory for not too low temperatures, quantum corrections to the conductivity become important at temperatures low enough that the electronic phase remains well defined over distances large in comparison to the elastic mean free path [1–3]. One usually distinguishes two quantum corrections, the weak localization correction and the interaction correction [4–6]. The former is caused by the constructive interference of electrons traveling along time-reversed paths, whereas the interaction correction can be understood in terms of resonant scattering off Friedel oscillations near impurities [7, 8].

Although they are small in comparison to the Drude conductivity, the quantum corrections are important because they strongly depend on temperature and an applied magnetic field, whereas the Drude conductivity does not (as long as impurity scattering is the dominant source of scattering). Theoretically, the temperature and magnetic-field dependences of the corrections can be expressed in terms of the sample's diffusion constant (or, equivalently, the elastic mean free path), which can be obtained independently from a measurement of the Drude conductivity. The availability of quantitative predictions has made a detailed comparison between theory and experiment possible [9, 10].[1]

[1] Apparent contradictions between theory and experiment [11, 12] have lead to improved understanding

The same quantum corrections also exist for a 'quantum dot', a conductor coupled to electron reservoirs via artificial constrictions (*e.g.,* tunnel barriers or point contacts), such that the conductance of the device is dominated by the contacts and not by scattering off impurities or defects inside the sample. The latter condition is satisfied if the product $E_{Th}\nu$ of the dot's 'Thouless energy' and its density of states is much larger than the dimensionless conductance of the contacts connecting the dot to source and drain reservoirs. (The Thouless energy is the inverse of the time needed for ergodic exploration of the quantum dot.)

In this paper we consider 'open' quantum dots, which have contact conductances larger than the conductance quantum e^2/h. Because transport through a quantum dot is dominated by the contacts, it is described by the sample's conductance, not its conductivity. The quantum corrections then pertain to the conductance after averaging over an ensemble of quantum dots that differ, *e.g.*, in their shape or precise impurity configuration.

While the magnetic-field dependence of quantum corrections to the ensemble averaged conductance is in apparent agreement with the theory [15], the situation regarding the temperature dependence is more complicated and no good agreement has been reported to date. Theoretically, the temperature dependence of the weak localization correction to the conductance of a quantum dot is described by means of a 'dephasing rate' γ_ϕ. For a quantum dot, one expects

$$\gamma_\phi = c\mathrm{T}^2/\mathrm{E}_{\mathrm{Th}}^2\nu, \tag{2.1}$$

where T is the temperature and c is a numerical constant that depends on the dot's size and shape [16, 17].[2] The proportionality constant c can not be measured independently,

of the role of magnetic impurities and of the sample purity required to observe the intrinsic temperature dependence caused by electron-electron interactions alone, see Refs. [10, 13, 14] and references therein.

[2]Equation (2.1) was originally proposed as the dephasing rate in closed quantum dots, see Ref. [16]. It

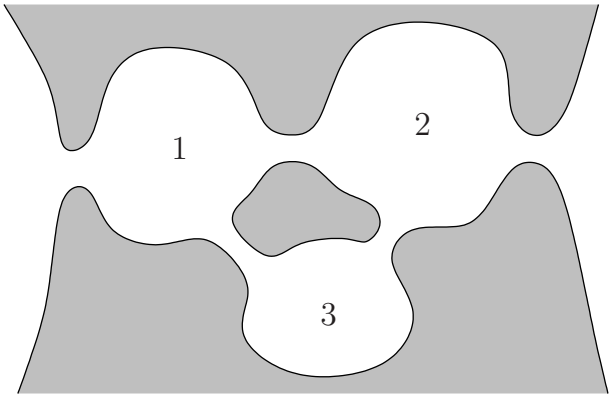

FIGURE 2.1: An example of a quantum dot network with $\mathcal{N}_D = 3$ quantum dots. The conductance of the network is dominated by the conductances of the contacts between the dots. We assume that all dots in the network are 'open', *i.e.*, all contact conductances are much larger than the conductance quantum e^2/h.

however, which is an important difference with the case of a diffusive conductor. The absence of a separate method to determine this constant poses a significant difficulty when comparing theory and experiment. A second difficulty is the lack of a direct theory of the temperature dependence of weak localization. Instead, the available theoretical descriptions employ a phenomenological description [18–23] and match the dephasing rate to Eq. (2.1), from which the temperature dependence of weak localization can be obtained.

In this paper, we study the quantum corrections to the conductance in a network of quantum dots or "quantum circuit" [24]. (See Fig. 2.1 for an example of a quantum dot network with $\mathcal{N}_D = 3$ dots.) Replacing a single quantum dot by a network solves both difficulties mentioned above: A quantum dot network allows a calculation of the complete temperature dependence of the quantum corrections to the conductance without the need of an intermediate step involving a phenomenological dephasing rate and without parameters that can not be measured independently. The relevant parameters

has later been corrected to include effects following from the discrete spectrum. For open quantum dots the spectrum is continuous and the original estimate is expected to be applicable.

in a quantum dot network are the conductances and form factors of the contacts in the network and the capacitances of the quantum dots.[3]

Our main result is an expression for the ensemble average of the dimensionless conductance

$$\mathrm{G} = \frac{d_\mathrm{s} e^2}{h} g, \tag{2.2}$$

where $d_\mathrm{s} = 1$ or 2 in the absence or presence of spin degeneracy, respectively. The result becomes exact in the limit that the contact conductances are much larger than the conductance quantum e^2/h,

$$\langle g \rangle = g^{\mathrm{cl}} + \delta g^{\mathrm{WL}} + \delta g^{\mathrm{int,1}} + \delta g^{\mathrm{int,2}}. \tag{2.3}$$

Here g^{cl} is the 'classical' conductance one obtains from Drude-Boltzmann theory, while δg^{WL}, $\delta g^{\mathrm{int,1}}$, and $\delta g^{\mathrm{int,2}}$ are three quantum corrections to g^{cl}. Explicit expressions for g^{cl} and the three quantum corrections in terms of the contact conductances and the capacitances of the quantum dots in the network, as well as the precise conditions for the validity of Eq. (2.3) will be given in Sec. 2.2 below. The correction δg^{WL} is the weak localization correction. It is the only quantum correction that is affected by the application of a magnetic field. The remaining two corrections arise from electron-electron interactions. The first interaction correction $\delta g^{\mathrm{int,1}}$ represents a non-local correction to the conductance that exists for networks of two or more quantum dots only [26–28]. It is the counterpart of the Altshuler-Aronov correction in the theory of disordered conductors. The second correction, $\delta g^{\mathrm{int,2}}$, describes the renormalization of the contact conductances by the interactions. It is usually referred to as (dynamical) Coulomb blockade, an effect that is well-known from the theory of transport through tunnel junctions in series with

[3] For quantum dots in semiconductor heterostructures that are defined by metal gates, the contact conductances are set independently by gate voltages. Each contact conductance can be measured by choosing gate voltages such that all other contacts are open, whereas the capacitances can be measured by closing off all contacts so that the device is in the Coulomb blockade regime (see *e.g.*, Ref. [25], where this procedure is used for a double quantum dot).

a high impedance or quantum dots with tunneling contacts [29–41]. Its counterpart in the theory of disordered conductors is the Altshuler-Aronov correction to the tunneling density of states [42].

The fact that the temperature dependence of quantum corrections in a quantum dot network does not depend on details of individual dots has its origin in the different form of the relevant electron-electron interaction modes in a quantum dot network and in a single dot. In a single quantum dot, the dominant contribution to the electron-electron interaction is the uniform mode, the strength of which is set by the dot's capacitance. Apart from a possible renormalization of the contact conductances, $\delta g^{\mathrm{int},2}$, the uniform mode has no effect on the quantum correction to the dot's conductance [38, 40, 41, 43]. In particular, the weak localization correction δg^{WL} is unaffected by the interaction and the non-local interaction correction $\delta g^{\mathrm{int},1}$ vanishes. Instead, electron-electron interactions determine δg^{WL} and $\delta g^{\mathrm{int},1}$ in a single quantum dot through sub-dominant non-uniform interaction modes, which are known to depend on the precise sample details [16, 44]. For a quantum dot network, on the other hand, there exist interaction modes that are uniform inside each dot but not across the full network. With such interaction modes, all three interaction corrections δg^{WL}, $\delta g^{\mathrm{int},1}$, and $\delta g^{\mathrm{int},2}$ are generically nonzero and temperature dependent. Moreover, because these modes are uniform inside each quantum dot, their properties depend on the contacts between the dots and on the dot capacitances only, not on the precise geometry of each dot separately. It is this essential feature that makes a quantum dot network an ideal paradigm for studying the effect of electron-electron interactions on quantum transport in finite-size systems.

Separate aspects of the problem we address here have been considered before. Weak localization in single quantum dots without interactions has been studied by various authors [45–54], as well as the effect of the uniform interaction mode on the conductances

of the contacts connecting the dot to the electron reservoirs [29–41]. (See Ref. [43] for a discussion of a comparable effect involving spin-dependent interactions in the quantum dot.) Also, while it is known that the uniform interaction mode has no effect on weak localization because a spatially uniform fluctuating potential affects phases of time-reversed trajectories in the same way [40, 41], the uniform interaction mode can suppress interference contributions to other observables if the quantum dot is part of an interferometer [55, 56].[4]

Weak localization in networks of quantum dots, but without interactions, was considered by Argaman for dots connected by ideal contacts [48, 49], and by Campagnano and Nazarov for dots connected by arbitrary contacts [57]. Golubev and Zaikin calculated the interaction corrections $\delta g^{\mathrm{int},1}$ and $\delta g^{\mathrm{int},2}$ for a linear array of quantum dots [27]. as well as the weak localization correction for non-interacting electrons (but with a phenomenological dephasing rate) [58]. In a recent publication, the same authors also considered the full temperature dependence of weak localization in the special case of a double quantum dot (a network with $\mathcal{N}_{\mathrm{D}} = 2$ quantum dots) with tunneling contacts [59], and reported that electron-electron interactions suppress weak localization even at zero temperature, a conclusion that contradicts the common wisdom that there is no dephasing from electron-electron interactions at zero temperature [1, 3].

Weak localization and interaction corrections have also been considered for networks of diffusive metallic wires [60, 61]. Large arrays of quantum dots connected by tunneling contacts further appear in the study of granular metals [62]. Beloborodov and coworkers considered the interaction corrections $\delta g^{\mathrm{int},1}$ and $\delta g^{\mathrm{int},2}$ for a granular metal [26, 63–66], but accounted for weak localization and its temperature dependence only via a phenomenological dephasing rate and a renormalized diffusion constant. A microscopic

[4] Y. Takane, J. Phys. Soc. Jpn. **67**, 3003 (1998), claims that the uniform mode can suppress weak localization, but his calculation failed to take into account that both trajectories involved in the weak localization correction experience the same phase shift from the uniform interaction mode.

theory of the temperature dependence of weak localization in granular metals was given by Blanter *et al.* in the high temperature limit [67]. Our present analysis (as well as that of Ref. [27]) is for contacts of arbitrary transparency and contains contributions to weak localization and to the interaction correction to the conductance that are absent in a network where all contacts are tunneling contacts. Our results agree with the literature wherever applicable, except for the zero-temperature limit of the weak localization correction δg^{WL}, where we find that weak localization is unaffected by electron-electron interactions, in contrast to Ref. [59].

The remainder of our paper is organized as follows. In Sec. 2.2 we introduce the relevant parameters needed to describe the quantum dot network, formulate our main assumptions, and present our main result, an expression for the ensemble-averaged conductance and its quantum corrections. In Sec. 2.3 we motivate our result for the temperature dependence of the weak localization correction using semiclassical arguments. In Sec. 2.4 we then turn to a fully quantum mechanical calculation of the conductance and its quantum corrections using random matrix theory. We specialize to the simplest network, a double quantum dot, in Sec. 2.5 and discuss the origin of the difference between our result and Ref. [59] for the zero-temperature limit of weak localization. We conclude in Sec. 2.6.

2.2 Definition of the problem and main results

2.2.1 Network of quantum dots

We consider a network of $\mathcal{N}_{\mathrm{D}}$ quantum dots, coupled to two electron reservoirs. A schematic drawing of a network is shown in Fig. 2.1. In this section we introduce the

relevant parameters to describe the quantum dot network and summarize our main results.

The quantum dots are connected to each other and to source and drain electron reservoirs via point contacts. The dots will be labeled by an index $i = 1, \ldots, \mathcal{N}_{\rm D}$; the reservoirs are labeled by the index $a = 1, 2$. The contact between dots i and j is described by its dimensionless conductance g_{ij} (per spin direction) and its form factor f_{ij}. Both g_{ij} and f_{ij} are defined in terms of the transmission matrix t_{ij} of the contact,

$$g_{ij} = \mathrm{tr}\, t_{ij} t_{ij}^\dagger, \quad f_{ij} = \mathrm{tr}\, (t_{ij} t_{ij}^\dagger)^2. \tag{2.4}$$

Form factors are related to Fano factors β often encountered in the literature via $\beta_{ij} = (g_{ij} - f_{ij})/g_{ij}$. The dimensionless conductances and form factors are symmetric, $g_{ij} = g_{ji}$ and $f_{ij} = f_{ji}$, $i, j = 1, \ldots, \mathcal{N}_{\rm D}$. Spin degeneracy will be explicitly taken into account via the parameter $d_{\rm s} = 1, 2$.

Similarly, the contacts between the ith quantum dot and reservoir a, $a = 1, 2$, are described by a dimensionless conductance $g'_{ia} = g'_{ai}$ and a form factor $f'_{ia} = f'_{ai}$, which are related to the transmission matrix t'_{ia} of these contacts as

$$g'_{ia} = \mathrm{tr}\, t'_{ia} t'^\dagger_{ia}, \quad f'_{ia} = \mathrm{tr}\, (t'_{ia} t'^\dagger_{ia})^2. \tag{2.5}$$

For ballistic contacts one has $f = g$; for tunneling contacts one has $f \ll g$. Throughout we assume that all conductances are large,

$$g_{ij},\ g'_{ia}, \gg 1, \quad i, j = 1, \ldots, \mathcal{N}_{\rm D}, \quad a = 1, 2. \tag{2.6}$$

(One may replace this condition by the less strict requirement that each quantum dot be well connected to one of the two reservoirs, such that the regime of strong Coulomb blockade is avoided.) For future use, we arrange the conductances and form factors in

$\mathcal{N}_D \times \mathcal{N}_D$ matrices $\tilde{g}$ and $\tilde{f}$ with elements

$$\tilde{g}_{ij} = \begin{cases} \sum_{a=1}^{2} g'_{aj} + \sum_{k\neq i}^{\mathcal{N}_D} g_{ik} & i = j, \\ -g_{ij} & i \neq j, \end{cases} \tag{2.7}$$

$$\tilde{f}_{ij} = \begin{cases} \sum_{a=1}^{2} f'_{aj} + \sum_{k\neq i}^{\mathcal{N}_D} f_{ik} & i = j, \\ -f_{ij} & i \neq j. \end{cases} \tag{2.8}$$

The quantum dots are assumed to be disordered or ballistic-chaotic, with density of states ν_i per spin degree of freedom and Thouless energy $E_{Th,i}$, $i = 1, \ldots, \mathcal{N}_D$. The Thouless energy $E_{Th,i} = \hbar/\tau_{erg,i}$, where $\tau_{erg,i}$ is the time for ergodic exploration of the ith quantum dot. If the electron motion is diffusive inside each quantum dot with diffusion constant D, $E_{Th,i} \sim D/L_i^2$ where L_i is the linear size of dot i. (Our definition, while common in the literature, differs from some references where $E_{Th,i}$ is the inverse of the dot's dwell time.) We assume

$$E_{Th,i}\nu_i \gg \tilde{g}_{ii}, \quad i = 1, \ldots, \mathcal{N}_D, \tag{2.9}$$

so that random matrix theory can be used to describe the electronic states in the quantum dot network. An external magnetic field is described by means of the dimensionless numbers

$$g_{H,i} = E_{Th,i}\nu_i \frac{\Phi_i^2}{\Phi_0^2}, \quad i = 1, \ldots, \mathcal{N}_D, \tag{2.10}$$

where Φ_i is the magnetic flux through the ith quantum dot and $\Phi_0 = hc/e$ is the flux quantum. In order to simplify the notation, we arrange the densities of states ν_i and the parameters $g_{H,i}$ in diagonal $\mathcal{N}_D$-dimensional matrices $\tilde{\nu}$ and $\tilde{g}_H$,

$$\tilde{\nu}_{ij} = \nu_i \delta_{ij}, \quad (\tilde{g}_H)_{ij} = g_{H,i}\delta_{ij}, \quad i, j = 1, \ldots, \mathcal{N}_D. \tag{2.11}$$

Corrections to the conductance that depend on the magnetic field will only be relevant where $g_{H,i}$ is of order $\tilde{g}_{ii}$ or less, otherwise they will be fully suppressed. In that parameter range, the flux through the insulating regions between the quantum dots is much smaller than Φ_0, so that the corresponding Aharonov-Bohm phases can be neglected.

The inequality (2.9) also implies that the electron-electron interaction in each dot is well screened [44]. Hence, the electron-electron interaction couples to the total charge $q_i = en_i$ of each dot only. Such an interaction is described by means of capacitances C_{ij} for the capacitive coupling between dots (if $i \neq j$) and for each dot's self-capacitance (if $i = j$). Again, we arrange the capacitances into an $\mathcal{N}_\mathrm{D}$-dimensional matrix $\tilde{\mathrm{C}}$,

$$\tilde{\mathrm{C}}_{ij} = \begin{cases} \sum_{k=1}^{\mathcal{N}_\mathrm{D}} \mathrm{C}_{ik} & i = j, \\ -\mathrm{C}_{ij} & i \neq j. \end{cases} \tag{2.12}$$

For metallic dots, one has the inequality

$$\tilde{\mathrm{C}}_{ii}/e^2 \ll \nu_i, \quad i = 1, \ldots, \mathcal{N}_\mathrm{D}. \tag{2.13}$$

2.2.2 Quantum corrections to the conductance

Our main result is a calculation of the ensemble-averaged conductance $\langle \mathrm{G} \rangle = (d_\mathrm{s} e^2/h)\langle g \rangle$ of the quantum dot network as a function of temperature,

$$\langle g \rangle = g^\mathrm{cl} + \delta g^\mathrm{WL} + \delta g^\mathrm{int,1} + \delta g^\mathrm{int,2},$$

where g^cl is the classical conductance of the network and δg^WL, $\delta g^\mathrm{int,1}$, and $\delta g^\mathrm{int,2}$ are corrections. The average conductance is calculated using the following limiting procedure for the parameters of the network:

(1) We first take limit (2.9) needed for the applicability of random matrix theory, while keeping the ratios ν_i/ν_j and T/ν_i, as well as the $g_{\mathrm{H},i}$ fixed, $i, j = 1, \ldots, \mathcal{N}_\mathrm{D}$.

(2) We then take limit (2.6) of large contact conductances, while keeping the ratios g_{ij}/g_{ik}, $g_{ij}/g_{\mathrm{H},i}$, and g_{ij}/g'_{ia} fixed, $i, j, k = 1, \ldots, \mathcal{N}_\mathrm{D}$, $a = 1, 2$.

(3) Finally, we simplify our results using the inequality (2.13), if possible.

In all three limiting steps, the number $\mathcal{N}_\mathrm{D}$ of dots in the network is kept constant. Keeping the ratio T/ν_i fixed in the first limiting step eliminates interaction corrections from non-uniform interaction modes inside the quantum dots, see Eq. (2.1) above. In the second limiting step, we do not make any assumptions about the temperature, thus allowing for the full range of temperature-dependent effects that can be described within random matrix theory. We note that, while the classical conductance g^cl diverges in this limiting procedure, this divergence does not affect the temperature or magnetic-field dependence of $\langle g \rangle$ because g^cl does not depend on temperature or magnetic field. Corrections not included in Eq. (2.3) are either small in the limit (2.6) of large contact conductances or small in the limit (2.9) used to justify the use of random matrix theory.

The leading term g^cl in Eq. (2.3) reads

$$g^\mathrm{cl} = \sum_{i,j=1}^{\mathcal{N}_\mathrm{D}} g'_{1i} (\tilde{g}^{-1})_{ij} g'_{j2} = g'_{1\cdot} \tilde{g}^{-1}_{\cdot\cdot} g'_{\cdot 2}, \tag{2.14}$$

where, in the last expression of Eq. (2.14), we have written "$\cdot$" to denote indices in adjacent factors that are summed over as in matrix multiplication [compare with the second expression of Eq. (2.14)]. This shorthand notation will be employed throughout the text.

The correction δg^WL is the weak localization correction to the ensemble-averaged conductance. It can be distinguished from the remaining two corrections $\delta g^\mathrm{int,1}$ and $\delta g^\mathrm{int,2}$ because δg^WL depends on an applied magnetic field whereas $\delta g^\mathrm{int,1}$ and $\delta g^\mathrm{int,2}$ do not. We find

$$\begin{aligned} \delta g^\mathrm{WL} \;=\; & 2 \sum_{i,j=1}^{\mathcal{N}_\mathrm{D}} \tilde{c}_{ij}\, g'_{1\cdot} (\tilde{g}^{-1}_{\cdot i} - \tilde{g}^{-1}_{\cdot j})(\tilde{g} - \tilde{f})_{ij} \tilde{g}^{-1}_{j\cdot} g'_{\cdot 2} - \sum_{i,j=1}^{\mathcal{N}_\mathrm{D}} \tilde{f}_{ij}\, \tilde{c}_{jj}\, g'_{1\cdot} \tilde{g}^{-1}_{\cdot i} \tilde{g}^{-1}_{i\cdot} g'_{\cdot 2} \\ & + \sum_{i=1}^{\mathcal{N}_\mathrm{D}} \tilde{c}_{ii}\, (g'_{1\cdot} \tilde{g}^{-1}_{\cdot\cdot} \tilde{f}_{\cdot i} - f'_{1i}) \tilde{g}^{-1}_{i\cdot} g'_{\cdot 2} + \sum_{i=1}^{\mathcal{N}_\mathrm{D}} \tilde{c}_{ii}\, g'_{1\cdot} \tilde{g}^{-1}_{\cdot i} (\tilde{f}_{i\cdot} \tilde{g}^{-1}_{\cdot\cdot} g'_{\cdot 2} - f'_{i2}), \end{aligned} \tag{2.15}$$

where the $\mathcal{N}_\mathrm{D} \times \mathcal{N}_\mathrm{D}$ matrix $\tilde{c}$ is the counterpart of the "cooperon" in the theory of weak localization in disordered conductors. For the quantum dot network, $\tilde{c}$ reads

$$\tilde{c}_{ij} = \sum_{k=1}^{\mathcal{N}_\mathrm{D}} \frac{1}{\pi\hbar\nu_k} (\Gamma + \Gamma_\mathrm{H} + \Gamma_\phi)^{-1}_{ik,jk}, \tag{2.16}$$

where Γ, $\Gamma_{\rm H}$, and Γ_ϕ are rank-four tensors,

$$\begin{aligned}
\Gamma_{ik,jl} &= \frac{1}{2\pi\hbar\nu_i}\tilde{g}_{ik}\delta_{jl} + \frac{1}{2\pi\hbar\nu_j}\delta_{ik}\tilde{g}_{jl} \\
(\Gamma_{\rm H})_{ik,jl} &= \frac{1}{2\pi\hbar\nu_i}\tilde{g}_{{\rm H},ik}\delta_{jl} + \frac{1}{2\pi\hbar\nu_j}\delta_{ik}\tilde{g}_{{\rm H},jl}, \\
(\Gamma_\phi)_{ik,jl} &= \frac{4\pi {\rm T}}{d_{\rm s}\hbar}(\tilde{g}_{ii}^{-1} + \tilde{g}_{jj}^{-1} - 2\tilde{g}_{ij}^{-1})\delta_{ik}\delta_{jl}.
\end{aligned} \tag{2.17}$$

The terms $\Gamma_{\rm H}$ and Γ_ϕ describe the suppression of weak localization by a magnetic field and electron-electron interactions, respectively. In the limit of low temperatures $\Gamma_\phi = 0$ and Eq. (2.16) simplifies to

$$\tilde{c}_{ij} = (\tilde{g} + \tilde{g}_{\rm H})^{-1}_{ij}. \tag{2.18}$$

For high temperatures $(\Gamma_\phi)_{ii,jj}$ diverges [other elements are zero because of the Kronecker deltas in Eq. (2.17)], except for the diagonal elements with $i = j$. Hence, one finds

$$\tilde{c}_{ij} \equiv \tilde{c}^{\rm d}_{ij} = (\tilde{g}^{\rm d} + \tilde{g}_{\rm H})^{-1}_{ij}, \tag{2.19}$$

where $\tilde{g}^{\rm d}_{ij}$ is the diagonal part of the matrix $\tilde{g}$, $\tilde{g}^{\rm d}_{ij} = \tilde{g}_{ij}\delta_{ij}$. This is the contribution to the weak localization correction that arises from self-returning electron trajectories that reside inside one quantum dot only and, hence, are unaffected by dephasing from electron-electron interactions [67].

The first interaction correction $\delta g^{\rm int,1}$ is

$$\begin{aligned}
\delta g^{\rm int,1} = &\frac{2\pi}{d_{\rm s}}\int d\omega \left(\frac{\partial}{\partial\omega}\omega\coth\frac{\omega}{2{\rm T}}\right)\sum_{\alpha,\beta=1}^{\mathcal{N}_{\rm D}}\sum_{k,l=1}^{\mathcal{N}_{\rm D}} {\rm Im}\Big[\nu_\alpha(2\pi i\omega\tilde{g}^{-1}_{\alpha\beta} - \tilde{\nu}^{-1}_{\alpha\beta})\nu_\beta \\
&\times(\tilde{g} - 2\pi i\tilde{\nu}\omega)^{-1}_{\alpha k}(\tilde{g} - 2\pi i\tilde{\nu}\omega)_{kl}(\tilde{g} - 2\pi i\tilde{\nu}\omega)^{-1}_{\beta l}\, g_{1\cdot}(\tilde{g}^{-1}_{\cdot\alpha} - \tilde{g}^{-1}_{\cdot k})(\tilde{g}^{-1}_{l\cdot} - \tilde{g}^{-1}_{\beta\cdot})g'_{\cdot 2}\Big].
\end{aligned} \tag{2.20}$$

The second interaction correction $\delta g^{\rm int,2}$ represents the renormalization of the conductances between the quantum dots and between the dots and the reservoirs as a result of the electron-electron interactions,

$$\delta g^{\rm int,2} = \sum_{j=1}^{\mathcal{N}_{\rm D}}\sum_{a=1}^{2}\frac{\partial g_{\rm cl}}{\partial g'_{aj}}\delta g'_{aj} + \sum_{j<k}^{\mathcal{N}_{\rm D}}\frac{\partial g_{\rm cl}}{\partial g_{jk}}\delta g_{jk}. \tag{2.21}$$

The interaction corrections $\delta g'_{ia}$ and δg_{ij} exist for nonideal contacts with $f_{ij} < g_{ij}$ or $f'_{ia} < g'_{ia}$ only, $i, j = 1, \ldots, \mathcal{N}_{\rm D}$, $a = 1, 2$,

$$\begin{aligned} \delta g'_{aj} &= -(g'_{aj} - f'_{aj}) \int \frac{d\omega}{\omega} \left(\frac{\partial}{\partial \omega} \omega \coth \frac{\omega}{2T} \right) \mathrm{Re}\, \delta \tilde{z}_{jj}, \\ \delta g_{jk} &= -(g_{jk} - f_{jk}) \int \frac{d\omega}{\omega} \left(\frac{\partial}{\partial \omega} \omega \coth \frac{\omega}{2T} \right) \mathrm{Re}\, (\delta \tilde{z}_{jj} + \delta \tilde{z}_{kk} - 2\delta \tilde{z}_{jk}), \end{aligned} \tag{2.22}$$

where $\delta\tilde{z}$ is the difference of the network's dimensionless impedance matrices with and without interactions,

$$\delta \tilde{z} = (d_{\rm s} \tilde{g} - 2\pi i \omega \tilde{\rm C}/e^2)^{-1} - (d_{\rm s} \tilde{g} - 2\pi i \omega d_{\rm s} \tilde{\rm v})^{-1}. \tag{2.23}$$

The interaction correction $\delta g^{\rm int,1}$ was obtained previously by Golubev and Zaikin for a linear array of quantum dots [27], and by Beloborodov *et al.* in the context of a granular metal [26]. It is the counterpart of the Altshuler-Aronov correction in disordered metals, where it arises from the diffusive dynamics of the electrons. Although the electron dynamics is not diffusive in a quantum dot network, it is non-ergodic, which is sufficient for this interaction correction to appear. (The exception is a quantum dot network consisting of a single quantum dot only, for which the electron motion is ergodic. Indeed, one verifies that $\delta g^{\rm int,1} = 0$ if $\mathcal{N}_{\rm D} = 1$, in agreement with Refs. [27, 38, 40, 41].) A semiclassical calculation of $\delta g^{\rm int,1}$ for the special case of a double quantum dot with ballistic contacts can be found in Ref. [28].

For the case of a single quantum dot, the renormalization of the contact conductances $\delta g^{\rm int,2}$ or "dynamical Coulomb blockade" was obtained previously in Refs. [35–41]. The renormalization of the contact conductances in the quantum dot network is essentially the same as in the case of a single quantum dot or a single tunnel junction coupled to a high-impedance electrical environment — in both cases the change of the contact conductance is proportional to the factor $(g - f)$ —, the only difference being that the impedance z is replaced by the impedance matrix $\tilde{z}$ in the case of the quantum dot net-

work [27]. The same conclusion was reached for the interaction correction in an array of quantum dots with tunneling contacts in the context of transport through a granular metal [26, 63–66].

Equations (2.3)–(2.23) provide a general solution for the ensemble-averaged conductance and its quantum corrections in an arbitrary quantum dot network for arbitrary temperature. These expressions can be simplified only by specializing to a particular quantum dot network. In Sec. 2.5 we analyze these expressions for the case of a double quantum dot, a network consisting of two quantum dots.

Although it is not possible to proceed quantitatively without specializing to a particular network, we can compare the sizes of these three quantum corrections and their typical temperature dependences. For the limiting procedure taken here — see the discussion following Eq. (2.3) —, the relevant temperature scale for dephasing of the weak localization correction is [67]

$$T_\phi = \hbar d_s \max(g, g_H)/\tau_D, \tag{2.24}$$

where

$$\tau_D \sim \hbar\nu/g \tag{2.25}$$

is the typical dwell time for the network. (Here g and g_H are shorthand notations for typical values of g_{ij} or $g_{H,i}$ in the network, respectively.) For the interaction corrections $\delta g^{int,1}$ and $\delta g^{int,2}$, the relevant temperature scales are $\hbar/\tau_D$ and the inverse charge relaxation time

$$\hbar/\tau_c \sim e^2 g/C. \tag{2.26}$$

(In a more precise analysis one needs to identify $\mathcal{N}_D$ dwell times and $\mathcal{N}_D$ charge relaxation times for a network consisting of $\mathcal{N}_D$ quantum dots, see Sec. 2.5 for an explicit calculation for $\mathcal{N}_D = 2$.) Since, typically, $C/e^2 \ll \nu$, the charge relaxation time and the dwell time

satisfy the inequality

$$\tau_c \ll \tau_D. \tag{2.27}$$

With these definitions, we find the order of magnitude of the weak localization correction δg^{WL} to be

$$\delta g^{\mathrm{WL}} \sim \delta g^{\mathrm{d}}_{\mathrm{WL}} + \frac{\delta g^{\mathrm{od}}_{\mathrm{WL}}}{\max(1, T/T_\phi)}, \tag{2.28}$$

where $\delta g^{\mathrm{d}}_{\mathrm{WL}}$ and $\delta g^{\mathrm{od}}_{\mathrm{WL}}$ are constants of order $\min(1, g/g_{\mathrm{H}})$. Similarly, for interaction corrections we find

$$\delta g^{\mathrm{int,1}} \sim \min(1, \hbar/T\tau_D), \tag{2.29}$$

$$\delta g^{\mathrm{int,2}} \sim \begin{cases} \ln[\max(\tau_c T/\hbar, \tau_c/\tau_D)] & \text{if } T \ll \hbar/\tau_c, \\ \hbar/T\tau_c & \text{if } T \gg \hbar/\tau_c, \end{cases} \tag{2.30}$$

independent of the magnetic field. All three quantum corrections need to be taken into account for a complete description of the temperature and magnetic-field dependence of the conductance of a quantum dot network. In particular, in order to correctly describe the temperature dependence of $\langle g \rangle$ for $T \lesssim \hbar/\tau_D$, $\delta g^{\mathrm{int,1}}$ can not be neglected with respect to $\delta g^{\mathrm{int,2}}$, in spite of the fact that $\delta g^{\mathrm{int,2}}$ is larger than $\delta g^{\mathrm{int,1}}$ by (at least) a large logarithmic factor $\ln(\tau_D/\tau_c)$.

The temperature dependence of Eq. (2.28) implies a dephasing rate that is linear in temperature. A linear temperature dependence of the dephasing rate was obtained previously by Blanter *et al.* in the context of a granular metal [67], and by Seelig and Büttiker for a single quantum dot embedded in one arm of an interferometer [55]. In both cases, the linear temperature dependence of the dephasing rate arose because the fluctuations of the electric potential can be considered classical, similar to the situation encountered in one-dimensional and two-dimensional disordered conductors [68]. As we will discuss in Secs. 2.3 and 2.4, the same mechanism is responsible for the linear temperature dependence of the dephasing rate in the quantum dot network.

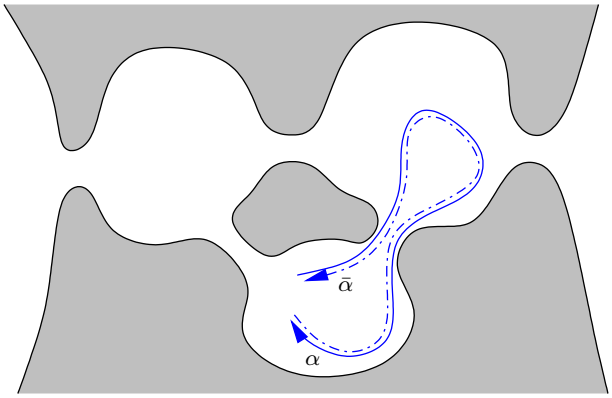

FIGURE 2.2: Schematic drawing of a trajectory α and its time-reversed $\bar{\alpha}$ that contribute to the cooperon propagator $\tilde{c}$.

In Sec. 2.3 we describe a semiclassical derivation of the weak localization correction and its temperature dependence, Eq. (2.15) above. A full quantum mechanical calculation of all three corrections to the conductance is given in Sec. 2.4. We apply the general results presented here to the specific case of a double quantum dot in Sec. 2.5.

2.3 Weak localization: semiclassical considerations

In this section, we give a semiclassical argument for the temperature dependence of the weak localization correction to the conductance of a quantum dot network. These arguments provide a semiclassical interpretation of the fully quantum mechanical calculations of the next section.

Weak localization appears because of constructive interference of time-reversed trajectories. This interference leads to a small increase of the probability P_{ret} that an electron returns to its point of origin. Following the standard arguments [2, 3], P_{ret} is calculated as a square of the return amplitude which, in turn, is written as a sum of amplitudes A_α over all returning paths α. (These paths are classical paths in ballistic conductors [50, 53],

and quantum diffractive paths in conductors with impurity scattering.) The quantum correction to P_{ret} then follows from interference between a path α and its time-reversed $\bar{\alpha}$. Since the length of the self-returning path is arbitrary, the weak localization correction to the dc conductance is proportional to the time integral of the interference correction to the return probability, known as the "cooperon" in the diagrammatic theory of weak localization [2, 3]. The counterpart of the cooperon for the quantum dot network is the quantity

$$\tilde{c}_{ij} \sim \frac{1}{(2\pi\hbar)^2 \nu_i \nu_j} \sum_{\alpha} A_\alpha (A_{\bar{\alpha}})^*, \tag{2.31}$$

where the sum is over all trajectories α that originate in dot j and end in dot i and $\bar{\alpha}$ is the time-reversed of α, see Fig. 2.2. [Note that the return probability involves the diagonal elements $\tilde{c}_{ii}$ of the cooperon matrix only. We have included non-diagonal elements in Eq. (2.31) above in view of the discussion of interaction effects below. Non-diagonal elements $\tilde{c}_{ij}$ with i and j in adjacent dots also appear for the description of weak localization in a network of quantum dots with tunneling contacts, see Eq. (2.15) above.]

At zero temperature and without a magnetic field, $A_{\bar{\alpha}} = A_\alpha$. We may then calculate $\tilde{c}_{ij}$ using that $|A_\alpha|^2$ is the probability that an electron propagates along trajectory α. Hence

$$\tilde{c}_{ij} = \frac{1}{2\pi\hbar\nu_i} \int_0^\infty d\tau P_{ij}(\tau), \tag{2.32}$$

where $P_{ij}(\tau)$ is the probability that an electron in dot j is found in dot i after time τ. In Eq. (2.32) we canceled a factor $2\pi\hbar\nu_j$ in the denominator against the phase space volume of the jth quantum dot. For a quantum dot network, $P_{ij}(\tau)$ can be expressed in terms of a rate matrix $\tilde{\gamma}$,

$$P_{ij}(\tau) = \left(e^{-\tilde{\gamma}\tau}\right)_{ij}, \quad \tilde{\gamma} = \tilde{g}/(2\pi\hbar\tilde{\nu}). \tag{2.33}$$

Integrating over time, we then find

$$\tilde{c}_{ij} = \tilde{g}_{ij}^{-1}. \tag{2.34}$$

The interference between a path α and its time-reversed is suppressed if time-reversal symmetry is broken by a magnetic field, because a magnetic field changes the phases of A_α and $A_{\bar{\alpha}}$ in opposite ways. Interference is also suppressed because of electron-electron interactions at a finite temperature. Interactions cause the electrons to experience a time-dependent potential $\phi(\mathbf{r}, t)$, which modifies the phase of A_α and $A_{\bar{\alpha}}$ in different ways if the trajectories α and $\bar{\alpha}$ are in different dots at the same time t [68]. For a network of quantum dots, the fluctuating potential ϕ is uniform inside each dot, so that we can write $\phi(j, t)$, where $j = 1, \ldots, \mathcal{N}_D$ is the index labeling the quantum dots in the network. For each amplitude A_α one then has [68]

$$A_\alpha[\phi] \to A_\alpha[0] \exp\left\{ i \int_0^{t_\alpha} \phi[j_\alpha(t), t]/\hbar \right\}, \tag{2.35}$$

where t_α is the duration of the path α, $j_\alpha(t)$ the index of the quantum dot corresponding to the position of path α at time t, and $A_\alpha[0]$ the return amplitude in the absence of the potential ϕ.

For a quantum dot network, one may consider ϕ as a classical fluctuating potential. (This will be verified in the exact quantum mechanical calculation of Sec. 2.4.2 below.) Its fluctuations are given by the fluctuation-dissipation relation [69],

$$\langle \phi(i, t)\phi(j, t') \rangle = \int \frac{d\omega}{2\pi} e^{-i\omega(t-t')/\hbar} \frac{2T}{\omega} \mathrm{Im}\left[L^R_{ij}(\omega) \right], \tag{2.36}$$

where the response function $L^R_{ij}(\omega)$ describes the (linear) change $\delta\phi_i/e$ of the electric potential in the ith quantum dot to a change $\delta q_j = e\delta n_j$ of the charge in the jth quantum dot,

$$\delta\phi_i(\omega) = -L^R_{ij}(\omega)\delta n_j(\omega). \tag{2.37}$$

For the quantum dot network, one has

$$L^R_{ij}(\omega) = -\left[\tilde{C}/e^2 + d_s(\tilde{\nu}^{-1} - 2\pi i\omega\tilde{g}^{-1})^{-1} \right]^{-1}_{ij}, \tag{2.38}$$

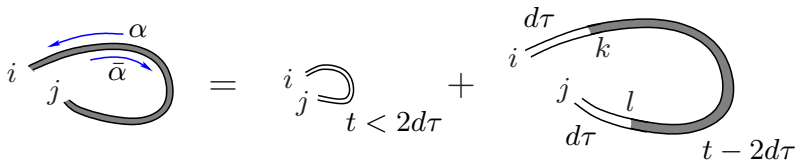

FIGURE 2.3: Calculation of the cooperon propagator for a network of quantum dots. A trajectory α originating in dot j and ending in dot i and duration t is separated into two segments of duration $d\tau$ and a remaining segment of duration $t - 2d\tau$ if $2d\tau < t$. A self-consistent equation for $\tilde{c}_{ij}$ is obtained by considering the combined effect of escape, the magnetic field, and the fluctuating potential to first order in $d\tau$.

where the matrices $\tilde{C}$, $\tilde{\nu}$, and $\tilde{g}$ were defined in Sec. 2.2 above. Typically, $\tilde{C}_{ii}/e^2 \ll \nu_i$, $\tilde{g}_{ii}/|\omega|$, and we can replace Eq. (2.38) by

$$L^R_{ij}(\omega) = \frac{1}{d_s}(2\pi i\omega\tilde{g}^{-1} - \tilde{\nu}^{-1})_{ij}. \tag{2.39}$$

Using this expression for $L^R_{ij}(\omega)$, we find that Eq. (2.36) simplifies to

$$\langle\phi(i,t)\phi(j,t')\rangle = \frac{4\pi\hbar T}{d_s}\,\tilde{g}^{-1}_{ij}\,\delta(t-t'). \tag{2.40}$$

In order to find the effect of the fluctuating potential on the cooperon propagator $\tilde{c}_{ij}$, we separate the contributions from trajectories α of duration t_α smaller and larger than $2d\tau$, where $d\tau$ is a time interval sufficiently short that the net phase shift from the fluctuating potential in the exponent in Eq. (2.35) is small, see Fig. 2.3. We also take $d\tau$ much shorter than the dwell time in a single quantum dot, so that $P_{ij}(d\tau) = \delta_{ij} - \tilde{\gamma}_{ij}d\tau$, see Eq. (2.33) above. For trajectories of duration $t_\alpha > 2d\tau$ we consider the initial and final segment of duration $d\tau$ separately. Recognizing that the contribution from the intermediate segments of duration $t_\alpha - 2d\tau$ can again be expressed in terms of $\tilde{c}$, and

using Eq. (2.40) to average over the fluctuating potentials, we then find

$$\begin{aligned}\tilde{c}_{ij} &= \frac{2d\tau}{2\pi\hbar\nu_i}\delta_{ij} + \sum_{k,l=1}^{\mathcal{N}_\mathrm{D}} (\delta_{ik} - \tilde{\gamma}_{ki}d\tau)(\delta_{jl} - \tilde{\gamma}_{lj}d\tau)\tilde{c}_{kl} \\ &\quad - \sum_{k,l=1}^{\mathcal{N}_\mathrm{D}} (\tilde{\gamma}_{\mathrm{H},ik} + \tilde{\gamma}_{\mathrm{H},jl} + \tilde{\gamma}_{\phi,ij})\delta_{ik}\delta_{jl}\tilde{c}_{kl}d\tau, \\ &= \tilde{c}_{ij} + \frac{d\tau}{\pi\hbar\nu_i}\delta_{ij} - \left(\Gamma + \Gamma_\mathrm{H} + \Gamma_\phi\right)_{ik,jl}\tilde{c}_{kl}d\tau, \end{aligned} \tag{2.41}$$

up to corrections of order $d\tau^2$. Here

$$\begin{aligned}\tilde{\gamma}_{\mathrm{H},ij} &= \frac{g_{\mathrm{H},i}}{2\pi\hbar\nu_i}\delta_{ij}, \\ \tilde{\gamma}_{\phi,ij} &= \frac{4\pi\mathrm{T}}{d_\mathrm{s}\hbar}(\tilde{g}_{ii}^{-1} + \tilde{g}_{jj}^{-1} - 2\tilde{g}_{ij}^{-1}), \end{aligned} \tag{2.42}$$

and $\Gamma_{ik,jl} = \tilde{\gamma}_{ki}\delta_{jl} + \delta_{ik}\tilde{\gamma}_{lj}$, $\left(\Gamma_\mathrm{H}\right)_{ik,jl} = \tilde{\gamma}_{\mathrm{H},ik}\delta_{jl} + \delta_{ik}\tilde{\gamma}_{\mathrm{H},jl}$, $\left(\Gamma_\phi\right)_{ik,jl} = \tilde{\gamma}_{\phi,ij}\delta_{ik}\delta_{jl}$, cf. Eq. (2.17) above. Solving this equation for $\tilde{c}$, we arrive at Eq. (2.16) of the previous section.

It is worth while to point out that the temperature dependence of weak localization is caused by processes that involve the exchange of energy quanta small in comparison to the temperature. Such processes are commonly referred to as "dephasing", in contrast to more general inelastic processes which lead to a broadening of the electronic distribution function [1, 3]. In this sense, interaction effects in the quantum dot network differ from those in a single quantum dot, where weak localization is suppressed by inelastic processes that involve a large energy transfer [16, 17]. Indeed, the characteristic energy exchanged in the electron-electron interactions scales with the inverse of the dwell time $\hbar/\tau_\mathrm{D}$ in each quantum dot — an observation that is closely related to the uniformity of the interaction potential inside a quantum dot. The number of quanta exchanged along a typical trajectory is too small to lead to a significant broadening of the distribution function — in that sense transport in a quantum dot network is always quasi-elastic —, although the exchange of a single quantum is sufficient to suppress the interference from time-reversed trajectories.

The semiclassical arguments of this section relied on the treatment of $\phi(\mathbf{r}, t)$ as a classical fluctuating potential. In this respect, we follow earlier works on quantum dots by Seelig and Büttiker [55] and on granular metals by Blanter *et al.* [67] This approach was taken originally by Altshuler *et al.* for dephasing in quasi one-dimensional and two-dimensional disordered metals [68]. In the next section, we confirm the validity of this approach in the present context by performing a fully quantum mechanical calculation of the weak localization correction to first order in the interaction propagator L. The calculation of Sec. 2.4 shows that the potential fluctuations are essentially classical if $T \gtrsim \hbar/\tau_D$, where τ_D is the (typical) dwell time in a quantum dot in the network. Since $\hbar/\tau_D$ is much smaller than the relevant temperature scale T_ϕ for the suppression of the weak localization correction by electron-electron interactions, cf. Eq. (2.24) of Sec. 2.2, this proves the validity of our approach for all temperatures of interest.

2.4 Quantum mechanical calculation

2.4.1 Random matrix formulation

We consider a network of $\mathcal{N}_D$ chaotic quantum dots coupled to electron reservoirs. The Hamiltonian of the entire system is written as

$$\hat{H} = \hat{H}_0 + \hat{H}_{int}, \tag{2.43}$$

where $\hat{H}_0$ describes the electrons inside the quantum dots or inside leads without taking into account their interactions, and $\hat{H}_{int}$ describes the electron-electron interactions. We write the non-interacting Hamiltonian $\hat{H}_0$ as a sum of three terms,

$$\hat{H}_0 = \hat{H}_D + \hat{H}_{DL} + \hat{H}_L, \tag{2.44}$$

where $\hat{H}_D$ and $\hat{H}_L$ describe the electrons inside the quantum dot network and inside the leads, respectively, whereas $\hat{H}_{DL}$ describes the coupling between the quantum dots and the leads. We now describe each of the three terms contributing to $\hat{H}$ separately.

Linearizing the electronic spectrum around the Fermi energy inside the leads, we have

$$\hat{H}_L = \sum_{a=1,2} \sum_{j=1}^{N_a} \int \frac{dk}{2\pi} v_{a,j} k \hat{\psi}^\dagger_{a,j}(k) \hat{\psi}_{a,j}(k), \tag{2.45}$$

where the index $a = 1, 2$ labels leads connecting to the left and right electron reservoirs. The operators $\hat{\psi}^\dagger_{a,j}(k)$ and $\hat{\psi}_{a,j}(k)$ are for electrons in scattering states at wavenumber k (measured with respect to the Fermi wavenumber) and transverse mode j. The total number of propagating modes in the leads connecting to reservoir a is N_a, $a = 1, 2$. [If a reservoir is coupled to more than one lead, the summation over the index j represents a sum over the transverse modes in all leads connected to the given reservoir.] Finally, $v_{a,j}$ is the Fermi velocity of electrons in mode j. The current operator $\hat{I}_a$ reads

$$\hat{I}_a = e \sum_{j=1}^{N_a} v_{a,j} \left(\hat{\psi}^\dagger_{a,j+} \hat{\psi}_{a,j+} - \hat{\psi}^\dagger_{a,j-} \hat{\psi}_{a,j-} \right), \quad a = 1, 2, \tag{2.46}$$

where

$$\hat{\psi}_{a,j\pm} = \int \frac{dk}{2\pi} e^{\pm ik\delta} \hat{\psi}_{a,j}(k), \quad a = 1, 2, \tag{2.47}$$

and $\delta > 0$ is a positive infinitesimal.

We use random matrix theory to describe the quantum dots. Following standard procedures, the electron operators in each quantum dot are represented by an M_j-component vector $\hat{\psi}_j$, where the index $j = 1, \ldots, \mathcal{N}_D$ labels the quantum dots in the network and M_j is the dimension of the subspace corresponding to the dot with index j. The Hamiltonian $\hat{H}_D$ then reads

$$\hat{H}_D = \sum_{i=1}^{\mathcal{N}_D} \sum_{\alpha,\beta=1}^{M_i} \hat{\psi}^\dagger_{i,\alpha} H_{i,\alpha\beta} \hat{\psi}_{i,\beta} + \sum_{i<j} \sum_{\alpha,\beta} \left(\hat{\psi}^\dagger_{i,\alpha} V_{ij,\alpha\beta} \hat{\psi}_{j,\beta} + \text{h.c.} \right). \tag{2.48}$$

Here the elements $H_{i,\alpha\beta}$ of the M_i-dimensional matrices H_i are random numbers taken from from a Gaussian distribution with zero mean and with variance

$$\langle H_{i,\alpha\beta} H_{i,\gamma\delta} \rangle = \langle H_{i,\alpha\beta} H^*_{i,\delta\gamma} \rangle = \frac{\lambda_i}{M_i} \delta_{\alpha\delta}\delta_{\beta\gamma} + \frac{\lambda'_i}{M_i} \delta_{\alpha\gamma}\delta_{\beta\delta}. \tag{2.49}$$

The parameters λ_i and λ'_i are related to the density of states ν_i and magnetic flux Φ_i in each quantum dot [44], $i = 1, \ldots, \mathcal{N}_D$,

$$\lambda_i = \frac{M_i^2}{\pi^2 \nu_i^2}, \quad \lambda'_i = \frac{M_i^2}{\pi^2 \nu_i^2} \left(1 - \frac{E_{Th,i} \nu_i \Phi_i^2}{4 M_i \Phi_0^2} \right), \tag{2.50}$$

where Φ_0 the flux quantum and $E_{Th,i}$ is the Thouless energy of the ith quantum dot. Further, in Eq. (2.48), the $M_i \times M_j$ matrices V_{ij} are related to the transmission matrices t_{ij} of the contact between dots i and j,

$$t_{ij} = 2\pi V_{ij} (\nu_i \nu_j M_i M_j)^{1/2} (M_i M_j + \pi^2 \nu_i \nu_j V_{ij}^\dagger V_{ij})^{-1}. \tag{2.51}$$

The Hamiltonian H_{DL} describing the coupling between the dots and the leads reads

$$\hat{H}_{DL} = \sum_{a=1}^{2} \sum_{j=1}^{N_a} \sum_{i=1}^{\mathcal{N}_D} \sum_{\alpha=1}^{M_i} \int \frac{dk}{2\pi} \left(\hat{\psi}^\dagger_{i,\alpha} W_{ia,\alpha j} \hat{\psi}_{a,j}(k) + \text{h.c.} \right), \tag{2.52}$$

where the $N_i \times N_a$ matrices $W_{ia} = W_{ai}^\dagger$ are related to the transmission matrices t_{ia} of the contact between the ith quantum dot and reservoir a,

$$t_{ia} = 2\pi W_{ia} (\nu_a \nu_i M_i)^{1/2} (M_i + \pi^2 \nu_i \nu_a^{1/2} W_{ai} W_{ia} \nu_a^{1/2})^{-1}, \tag{2.53}$$

with $a = 1, 2$ and ν_a an N_a-dimensional matrix with elements $(\nu_a)_{ij} = \delta_{ij} (2\pi\hbar\nu_{a,j})^{-1}$. The dimensionless conductance g_{ij} and and form factor f_{ij} of the contact between dots i and j are defined in terms of the transmission matrix t_{ij} as in Eq. (2.4). Similarly, the dimensionless conductance $g'_{ia} = g'_{ai}$ and form factor $f'_{ia} = f'_{ai}$ between the dots and the two electron reservoirs are defined in terms of t'_{ia} as in Eq. (2.5).

For the electron-electron interaction we take density fluctuations inside each dot to be well screened, so that the interaction couples to the total charges of the dots only,

$$\hat{H}_{int} = \sum_{i,j} \frac{e^2}{2} \hat{n}_i \left[\tilde{C}^{-1} \right]_{ij} \hat{n}_j, \quad \hat{n}_i = \sum_{\alpha=1}^{M_i} \hat{\psi}^\dagger_{i,\alpha} \hat{\psi}_{i,\alpha}, \tag{2.54}$$

where the capacitance matrix $\tilde{\mathrm{C}}$ was defined in Eq. (2.12) above. The corresponding interaction Hamiltonian for a single quantum dot is known as 'universal interaction Hamiltonian' [44].

Evaluating the conductance g of the quantum dot network and its leading interaction corrections using the Kubo formula one finds

$$\mathrm{G} = \frac{d_s e^2}{h} g, \quad g = g_0 + \delta g^{\mathrm{deph}} + \delta g^{\mathrm{int}}, \tag{2.55}$$

where g_0 is the conductance in the absence of interactions (*i.e.,* for Hamiltonian $\hat{\mathrm{H}}_0$), and δg^{deph} and δg^{int} are interaction corrections. (The reason for the separation between δg^{deph} and δg^{int} is that these two corrections have different temperature dependences, as will become apparent later.) Denoting with "$\cdot$" adjacent indices to be summed over [as in Eq. (2.14)], the three terms in Eq. (2.55) read

$$g_0 = 4\pi^2 \int d\varepsilon \left[-\partial_\varepsilon f(\varepsilon)\right] \mathrm{tr}\, \nu_1 \mathrm{W}_{1\cdot} \mathrm{G}^{\mathrm{R}}_{\cdot\cdot}(\varepsilon) \mathrm{W}_{\cdot 2} \nu_2 \mathrm{W}_{2\cdot} \mathrm{G}^{\mathrm{A}}_{\cdot\cdot}(\varepsilon) \mathrm{W}_{\cdot 1}, \tag{2.56}$$

and the interaction corrections δg^{deph} and δg^{int} are

$$\begin{aligned}
\delta g^{\mathrm{deph}} =& 4\pi^2 \int d\varepsilon \int \frac{d\omega}{2\pi} \left[-\partial_\varepsilon f(\varepsilon)\right] \{\coth(\omega/2\mathrm{T}) + \tanh[(\varepsilon-\omega)/2\mathrm{T}]\} \sum_{i,j=1}^{\mathcal{N}_{\mathrm{D}}} \mathrm{Im}\left[\mathrm{L}^{\mathrm{R}}_{ij}(\omega)\right] \\
&\times \mathrm{tr}\Big[\nu_1 \mathrm{W}_{1\cdot} \mathrm{G}^{\mathrm{R}}_{\cdot i}(\varepsilon) \mathrm{G}^{\mathrm{R}}_{ij}(\varepsilon-\omega) \mathrm{G}^{\mathrm{R}}_{j\cdot}(\varepsilon) \mathrm{W}_{\cdot 2} \nu_2 \mathrm{W}_{2\cdot} \mathrm{G}^{\mathrm{A}}_{\cdot\cdot}(\varepsilon) \mathrm{W}_{\cdot 1} \\
&\quad + \nu_1 \mathrm{W}_{1\cdot} \mathrm{G}^{\mathrm{R}}_{\cdot\cdot}(\varepsilon) \mathrm{W}_{\cdot 2} \nu_2 \mathrm{W}_{2\cdot} \mathrm{G}^{\mathrm{A}}_{\cdot i}(\varepsilon) \mathrm{G}^{\mathrm{A}}_{ij}(\varepsilon-\omega) \mathrm{G}^{\mathrm{R}}_{j\cdot}(\varepsilon) \mathrm{W}_{\cdot 1} \\
&\quad + \frac{1}{2} \nu_1 \mathrm{W}_{1\cdot} \mathrm{G}^{\mathrm{R}}_{\cdot i}(\varepsilon-\omega) \mathrm{G}^{\mathrm{R}}_{i\cdot}(\varepsilon) \mathrm{W}_{\cdot 2} \nu_2 \mathrm{W}_{2\cdot} \mathrm{G}^{\mathrm{A}}_{\cdot j}(\varepsilon) \mathrm{G}^{\mathrm{A}}_{j\cdot}(\varepsilon-\omega) \mathrm{W}_{\cdot 1} \\
&\quad + \frac{1}{2} \nu_1 \mathrm{W}_{1\cdot} \mathrm{G}^{\mathrm{R}}_{\cdot i}(\varepsilon) \mathrm{G}^{\mathrm{R}}_{i\cdot}(\varepsilon-\omega) \mathrm{W}_{\cdot 2} \nu_2 \mathrm{W}_{2\cdot} \mathrm{G}^{\mathrm{A}}_{\cdot j}(\varepsilon-\omega) \mathrm{G}^{\mathrm{A}}_{j\cdot}(\varepsilon) \mathrm{W}_{\cdot 1}\Big]
\end{aligned} \tag{2.57}$$

$$\begin{aligned}
\delta g^{\mathrm{int}} \;=\; & 4\pi^2 \int d\varepsilon \int \frac{d\omega}{2\pi} \left[-\partial_\varepsilon f(\varepsilon)\right] \tanh[(\varepsilon-\omega)/2\mathrm{T}] \sum_{i,j=1}^{\mathcal{N}_{\mathrm{D}}} \mathrm{Im}\Big\{\mathrm{L}^{\mathrm{A}}_{ij}(\omega) \\
&\times \mathrm{tr}\left[\nu_1 \mathrm{W}_{1\cdot} \mathrm{G}^{\mathrm{R}}_{\cdot i}(\varepsilon) \mathrm{G}^{\mathrm{R}}_{ij}(\varepsilon-\omega) \mathrm{G}^{\mathrm{R}}_{j\cdot}(\varepsilon) \mathrm{W}_{\cdot 2} \nu_2 \mathrm{W}_{2\cdot} \mathrm{G}^{\mathrm{A}}_{\cdot\cdot}(\varepsilon) \mathrm{W}_{\cdot 1}\right. \\
&\quad \left. + \nu_1 \mathrm{W}_{1\cdot} \mathrm{G}^{\mathrm{R}}_{\cdot\cdot}(\varepsilon) \mathrm{W}_{\cdot 2} \nu_2 \mathrm{W}_{2\cdot} \mathrm{G}^{\mathrm{A}}_{\cdot i}(\varepsilon) \mathrm{G}^{\mathrm{R}}_{ij}(\varepsilon-\omega) \mathrm{G}^{\mathrm{A}}_{j\cdot}(\varepsilon) \mathrm{W}_{\cdot 1}\right]\Big\}.
\end{aligned} \tag{2.58}$$

In these equations G^{R}_{ij} and G^{A}_{ij} denote the retarded and advanced Green functions of the network of quantum dots without the electron-electron interaction Hamiltonian $\hat{H}_{int}$. These are matrices of dimension $M_i \times M_j$, which are the solution of

$$\begin{aligned}\left[\varepsilon - H_i + i\pi \sum_{a=1}^{2} W_{ia}\nu_a W_{ai}\right] G^{R}_{ii}(\varepsilon) + V_{i\cdot} G^{R}_{\cdot i}(\varepsilon) &= \mathbf{1}_i, \\ \left[\varepsilon - H_i - i\pi \sum_{a=1}^{2} W_{ia}\nu_a W_{ai}\right] G^{A}_{ii}(\varepsilon) + V_{i\cdot} G^{A}_{\cdot i}(\varepsilon) &= \mathbf{1}_i,\end{aligned} \tag{2.59}$$

with $\mathbf{1}_i$ the $M_i \times M_i$ unit matrix. Finally, $L^{R}_{ij}(\omega)$ and $L^{A}_{ij}(\omega) = L^{R}_{ij}(\omega)^*$ represent the [random-phase-approximation (RPA)] screened interaction propagator [see Eq. (2.38) above].

It remains to calculate the ensemble average of the conductance G for the ensemble of Hamiltonians described by Eq. (2.49) above. This is the subject of Sec. 2.4.2.

2.4.2 Average over random Hamiltonian

The average over the random matrices H_i is performed using a variation of the impurity diagrammatic technique [70]. This technique has been applied for various transport and thermodynamic properties of chaotic quantum dots without electron-electron interactions [52, 71–73]. Below we present its generalization to arbitrary networks.

Average Green function

We first discuss the calculation of the ensemble average of the Green function, $\langle G^{R}_{ij}(\varepsilon)\rangle$ and $\langle G^{A}_{ij}(\varepsilon)\rangle$. Following the diagrammatic rules laid out in Fig. 2.4 and keeping diagrams in the non-crossing approximation only [74], *i.e.* diagrams without crossing double lines,

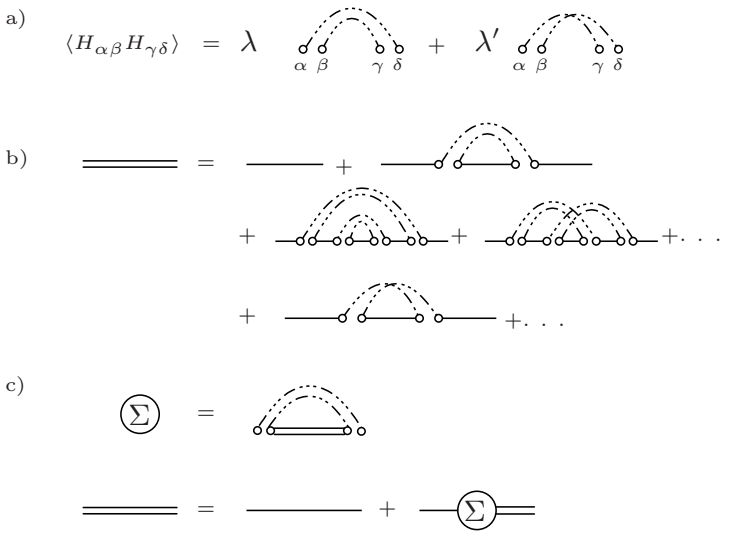

FIGURE 2.4: (a) Diagrammatic rules for the ensemble average using Random Matrix Theory. The weight factors depend on the symmetry present: $\lambda' = \lambda$ in the presence of time reversal symmetry, while λ' is reduced in the presence of a weak magnetic field and $\lambda' = 0$ where time reversal symmetry is fully broken. (b) Expansion of the full matrix propagator in terms of single propagators $1/(\varepsilon + i\pi\nu WW^\dagger)$, depicted by single lines, and the matrix elements $H_{\alpha\beta}$, depicted by two open circles. (c) Dyson equation for the self energy Σ.

one finds that the ensemble averaged Green function $\langle G^R_{ij}(\varepsilon)\rangle$ satisfies the Dyson equation

$$\langle G^R_{ij}(\varepsilon)\rangle = G^R_0(\varepsilon)_{ij} + \sum_k G^R_0(\varepsilon)_{ik}\Sigma_k\langle G^R_{kj}(\varepsilon)\rangle, \tag{2.60}$$

where the self energy Σ_k is

$$\Sigma^R_k(\varepsilon) = \frac{\lambda_k}{M_k}\mathrm{tr}\,\langle G^R_{kk}(\varepsilon)\rangle, \tag{2.61}$$

and $G^R_0(\varepsilon)$ is the solution of Eq. (2.59) with $H_i = 0$. Combining Eqs. (2.60) and (2.61) gives a self-consistent equation for Σ^R. In the limit $M_i \gg g'_{i1} + g'_{i2} + \sum_{j\neq i} g_{ij}$, one finds

$$\langle G^R_{ij}(\varepsilon)\rangle = \langle G^A_{ji}(\varepsilon)\rangle^\dagger = -\frac{i\pi}{M_i + \Delta_i}\tilde{\nu}_{ij} - \sqrt{\frac{\pi^2\nu_i\nu_j}{4M_iM_j}}t_{ij} + \frac{\pi}{2M_i^2}\left(\pi\nu_i\varepsilon - i\mathrm{tr}\,\frac{\Delta_i}{M_i + \Delta_i}\right)\tilde{\nu}_{ij}, \tag{2.62}$$

where $\tilde{\nu}_{ij}$ and t_{ij} are given in Eq. (2.11) and (2.51) above and Δ_i is an hermitian $M_i \times M_i$ matrix,

$$\Delta_i = \pi^2\nu_i\sum_{k\neq i}^{N_D}\frac{1}{M_k}V_{ik}\nu_kV_{ki} + \pi^2\nu_i\sum_{a=1}^{2}W_{ia}\nu_aW_{ai}. \tag{2.63}$$

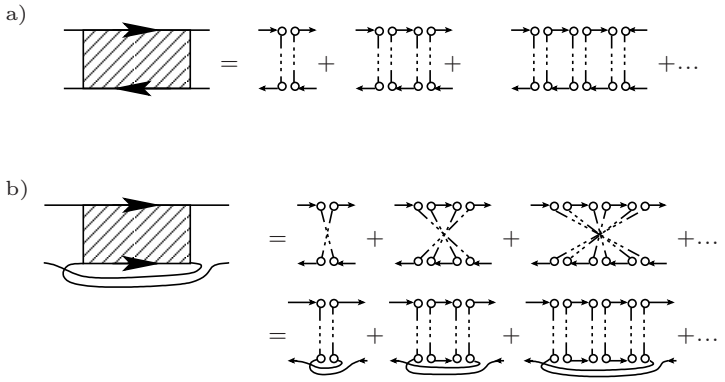

FIGURE 2.5: Diffuson ladder (a) and cooperon ladder (b).

Classical conductance

To leading order in the average number N of transmitting channels per dot, the calculation of the average conductance involves the calculation of geometric series involving the ensemble averaged Green functions. Diagrammatically, these geometric series correspond to "ladder diagrams", as shown in Fig. 2.5. Such ladders are the equivalent of the "diffuson" propagator in diagrammatic perturbation theory. The building block of the geometric series is

$$\mathrm{tr}\langle G^{R}_{ij}(\varepsilon)\rangle\langle G^{A}_{ji}(\varepsilon')\rangle \;=\; \frac{\pi^2\nu_i^2}{M_i}\delta_{ij} - \frac{\pi^2\nu_i\nu_j}{4M_iM_j}\left[\tilde{g} - i2\pi(\varepsilon-\varepsilon')\tilde{\nu}\right]_{ij},$$

where $\tilde{g}_{ij}$ was defined in Eq. (2.7) above. Summing the geometric series in Fig. 2.5(a) then gives the diffuson matrix

$$D_{ij}(\varepsilon,\varepsilon') \;=\; \frac{2M_i}{\pi\nu_i}\left[\tilde{g} - i2\pi(\varepsilon-\varepsilon')\tilde{\nu}\right]^{-1}_{ij}\frac{2M_j}{\pi\nu_j}. \tag{2.64}$$

For the calculation of the mean conductance one also needs a trace that involves the lead indices,

$$D'_{ia} = \pi\nu_a \mathrm{tr}\left[W_{ai}\langle G^{R}_{ii}\rangle\langle G^{A}_{ii}\rangle W_{ia}\right] = \pi\nu_i\frac{g'_{ai}}{4M_i},\; a = 1,2. \tag{2.65}$$

Combining everything as depicted in Fig. 2.6(a), we then find the leading conductance

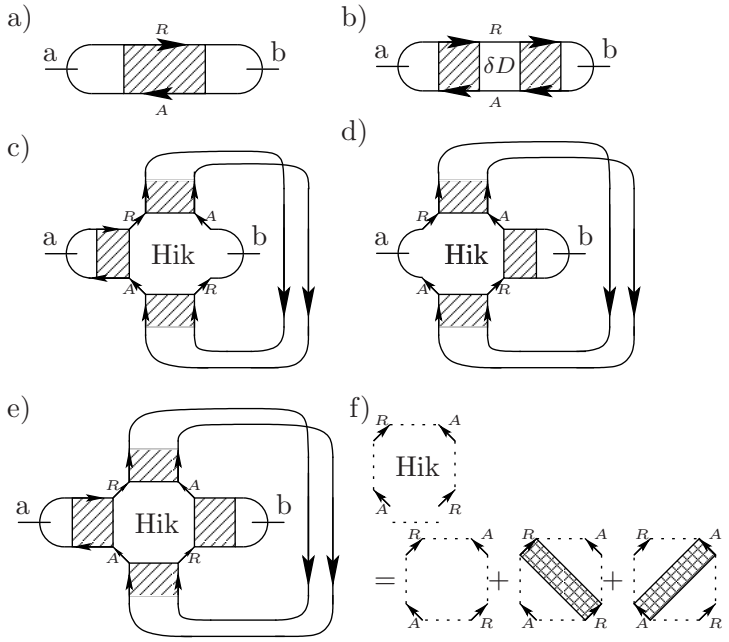

FIGURE 2.6: (a) Diagrammatic representation of the leading contribution g^{cl} to the ensemble-averaged conductance $\langle g \rangle$. (b)–(e) Diagrams contributing to the weak localization correction δg^{WL}. (f) Definition of the Hikami-box used in (c)–(e).

of the system

$$\langle g \rangle = g'_{1\cdot}(\tilde{g}^{-1})_{\cdot\cdot} g'_{\cdot 2},$$

which is Eq. (2.14) of Sec. 2.2.

Weak localization correction

The above calculation gives the conductance to leading order in g. A correction to subleading order in g is given by a class of diagrams that contains a maximally crossed ladder, as shown in Fig. 2.5(b). These contributions are analogous to the "cooperon" contributions in diagrammatic perturbation theory [1]. The summation of the geometric series promotes the contribution to be of order 1/N instead of 1/M, as is the naive expectation for diagrams that contain one crossed line.

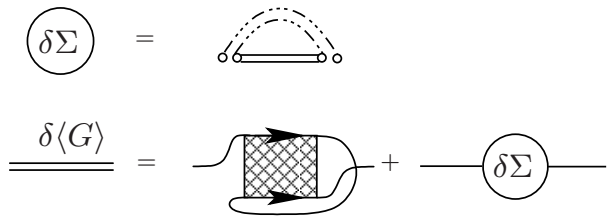

FIGURE 2.7: Dyson equation for corrections to $\langle G_{ii}\rangle$ due to the possibility of cooperon like ladders in the time reversal symmetric case. Double-hatching indicates a retarded-retarded or advanced-advanced pairing. These ladders are parametrically small, and for that reason can also not extend across multiple dots.

In contrast to the diffuson propagator discussed above, the cooperon propagator is sensitive to magnetic flux. Proceeding as before, we find

$$C_{ij}(\varepsilon,\varepsilon') = \frac{2M_i}{\pi\nu_i}\left[\tilde{g}_H + \tilde{g} - 2\pi i\tilde{\nu}(\varepsilon-\varepsilon')\right]^{-1}_{ij}\frac{2M_j}{\pi\nu_j}, \tag{2.66}$$

with g_H defined in Eq. (2.10). For the calculations below, we also need geometric series of Green functions of the same type. These read

$$\begin{aligned} C^{RR}_{ij}(\varepsilon,\varepsilon') =& C^{AA}_{ij}(\varepsilon,\varepsilon')^* \\ =& \frac{1}{16\pi^2\nu_i\nu_j}\{[8M_i + \tilde{g}_{H,ii} + \tilde{g}_{ii} - i2\pi(\varepsilon+\varepsilon')\nu_i]\delta_{ij} - \tilde{g}_{ij}\left(1-\delta_{ij}\right)\}. \end{aligned} \tag{2.67}$$

Cooperon ladders give a correction to the self-energy appearing in the calculation of the average Green function, as depicted in Fig. 2.7. Calculation of the self-energy correction $\delta\Sigma_i$ to leading order in g/M then gives

$$\delta\Sigma_i = \frac{\lambda_i}{M_i}\,\mathrm{tr}\left[\langle G^R_{ii}\rangle(C^{RR}_{ii}\langle G^R_{ii}\rangle + \delta\Sigma_i)\langle G^R_{ii}\rangle\right] = \frac{i}{4\pi\nu_i}. \tag{2.68}$$

As this contribution is already small as $1/M$, one may neglect the effect of a weak magnetic field on this term. The self energy correction $\delta\Sigma$ affects the diffusion ladders as $D \to D + \delta D$, with

$$\delta D_{ij} = -\frac{\pi^2\nu_i^2}{2M_i^2}\delta_{ij}. \tag{2.69}$$

This contribution is depicted in Fig. 2.6(b).

In the diagrams for the weak localization correction to the conductance, the cooperon and diffuson propagators are connected in a so-called "Hikami box" [75]. In our diagrammatic analysis the analogue of a Hikami box is depicted in Fig. 2.6(f). We consider the general case of a Hikami box with four energy arguments. We write ε_1 (ε_1') for the energy argument of the retarded (advanced) matrix propagator on the left side, and ε_2 (ε_2') for the energy argument of the retarded (advanced) propagator on the right. For the calculation of the weak localization correction one only needs the case of equal arguments, $\varepsilon_1 = \varepsilon_1' = \varepsilon_2 = \varepsilon_2'$. For dephasing and interaction corrections, some arguments differ. Explicit calculation shows that the Hikami box depends on the combination $\omega = \varepsilon_1' - \varepsilon_1 + \varepsilon_2' - \varepsilon_2$ only. Hence we write $\mathrm{B}_{ij,kl}(\omega)$, where the indices i and j refer to the left and right (diffuson) ladders and the indices k and l refer to the bottom and top (cooperon) ladders.

The calculation is essential but technical; we outline it in the appendix. The Hikami box $\mathrm{B}_{ij,kl}(\omega)$ is zero except where at most two different indices appear,

$$\begin{aligned}\mathrm{B}_{ij,kl}(\omega) \;=\; & \frac{\pi^4 \nu_i \nu_j \nu_k \nu_l}{16 \mathrm{M}_i \mathrm{M}_j \mathrm{M}_k \mathrm{M}_l}\Big[2\pi i \nu_i \omega \delta_{ij}\delta_{jk}\delta_{kl} - \delta_{ij}\delta_{kl}\tilde{f}_{ik} \\ & +(\delta_{ik}\delta_{il} + \delta_{jk}\delta_{jl})\tilde{f}_{ij} + (\delta_{ij}\delta_{ki} + \delta_{ij}\delta_{li})\tilde{f}_{kl} \\ & +(\delta_{il}\delta_{jk} + \delta_{ik}\delta_{jl})(\tilde{g}_{ij} + \tilde{g}_{\mathrm{H},ij} - \tilde{f}_{ij})\Big]. \end{aligned} \tag{2.70}$$

For the evaluation of the weak localization correction, one also needs to consider Hikami boxes that are connected to the leads, not only to diffuson propagators inside the quantum dot network. The two contributions of this type are depicted in Fig. 2.6(c) and (d). They are

$$\mathrm{B}'_{aj,jj} = \mathrm{B}'_{ja,jj} = -\frac{\pi^3 \nu_j^3}{16 \mathrm{M}_j^3} f'_{aj}. \tag{2.71}$$

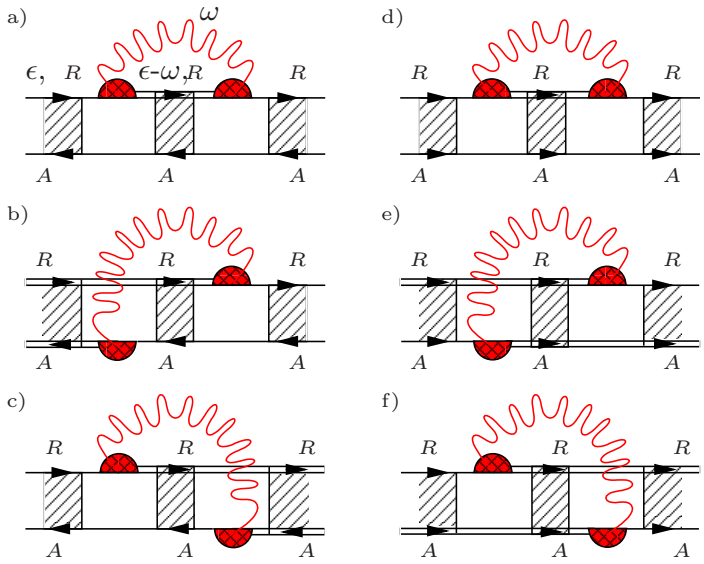

FIGURE 2.8: Diagrams for the first-order dephasing correction. Diagrams depicted in (b), (c) and (e), (f) are weighed with a factor 1/2, in line with Eq. (2.57). Together (a), (b) and (c) constitute the correction to the diffuson propagator, which cancels to leading order. Hence the only relevant contributions are the corrections to the cooperon in (d), (e) and (f). In both cases, complex conjugate contributions exist which are obtained by placing the vertices on the opposite matrix propagation lines.

Combining everything, we have (see Fig. 2.6)

$$\delta g^{\mathrm{WL}} = 4\mathrm{D}'_{1\cdot}\mathrm{D}_{\cdot\cdot}\delta\mathrm{D}_{\cdot\cdot}\mathrm{D}_{\cdot\cdot}\mathrm{D}'_{\cdot 2} + 4\sum_{i,j=1}^{\mathcal{N}_\mathrm{D}} \mathrm{C}_{ij}\left[\mathrm{D}'_{1\cdot}\mathrm{D}_{\cdot\cdot}\mathrm{B}'_{\cdot 2,ji} + \mathrm{B}'_{1\cdot,ji}\mathrm{D}_{\cdot\cdot}\mathrm{D}'_{\cdot 2} + \mathrm{D}'_{1\cdot}\mathrm{D}_{\cdot\cdot}\mathrm{B}_{\cdot\cdot,ji}(0)\mathrm{D}_{\cdot\cdot}\mathrm{D}'_{\cdot 2}\right], \tag{2.72}$$

where $\mathrm{D}'_{ia} = \mathrm{D}'_{ai}$ was defined in Eq. (2.65) above and we have suppressed superscripts as well as inconsequential energy arguments of $\mathrm{D}^{\mathrm{RA}}(\varepsilon,\varepsilon)$, $\mathrm{C}^{\mathrm{RA}}(\varepsilon,\varepsilon)$, cf. Eqs. (2.64), (2.67). The four terms correspond to the four diagrams (b) - (e) of Fig. 2.6. Substituting our results for the Hikami box B, the cooperon and diffuson propagators C and D, and the interaction propagator L, we arrive at Eq. (2.15) of Sec. 2.2, with the zero-temperature cooperon $\tilde{c} = (\tilde{g} + \tilde{g}_{\mathrm{H}})^{-1}$.

So far we have not taken into account electron-electron interactions. To lowest order in perturbation theory in the interaction Hamiltonian $\hat{\mathrm{H}}_{\mathrm{int}}$, the dominant interaction

correction to weak localization comes from $\delta g^{\rm deph}$ in Eq. (2.57). The corresponding diagrams are depicted in Fig. 2.8. We now calculate that correction. This interaction correction is nonzero only if both interaction vertices appear inside the cooperon propagator. (This is why this interaction correction does not affect the leading contribution g_0 to the conductance.)

To calculate the interaction correction, one notices that the interaction vertices are "dressed", as is shown in Fig. 2.9. For this case energy arguments may be neglected, as they lead to corrections small in g/M. Labeling the dot in which the interaction takes place by the index α, the dressed interaction then reads

$$\begin{aligned} I^{R}_{\alpha,ij} = (I^{A}_{\alpha,ij})^{*} &= \delta_{\alpha i}\delta_{\alpha j}\,\mathrm{tr}\left[\langle G^{R}_{ii}\rangle \times \left(1+\ \mathrm{tr}\left[\langle G^{R}_{ii}\rangle\langle G^{R}_{ii}\rangle\right] D^{RR}_{ii}\right)\langle G^{R}_{ii}\rangle\langle G^{A}_{ii}\rangle\right] \\ &= \frac{\pi\nu_i}{2M_i}\left(-i2\pi\tilde{\nu}_{ij}\delta_{\alpha i}\right)\frac{\pi\nu_i}{2M_i} \end{aligned} \tag{2.73}$$

where

$$\begin{aligned} D^{RR}_{ij}(\varepsilon,\varepsilon') &= D^{AA}_{ij}(\varepsilon,\varepsilon')^{*} \\ &= \frac{1}{16\pi^2\nu_i\nu_j}\Big[\left(8M_i+\tilde{g}_{ii}-i2\pi(\varepsilon+\varepsilon')\nu_i\right)\delta_{ij}-\tilde{g}_{ij}\left(1-\delta_{ij}\right)\Big]. \end{aligned} \tag{2.74}$$

The interaction correction δC to the equal-energy cooperon propagator $C(\varepsilon,\varepsilon)$ then becomes

$$\begin{aligned} \delta C_{ij} = &\int d\varepsilon \int \frac{d\omega}{2\pi}\left[-\partial_\varepsilon f(\varepsilon)\right]\left[\coth(\omega/2T)+\tanh((\varepsilon-\omega)/2T)\right]\sum_{\alpha,\beta=1}^{\mathcal{N}_D}\mathrm{Im}\left[L^{R}_{\alpha\beta}(\omega)\right] \\ &\times\Big[C_{i\cdot}(\varepsilon,\varepsilon)I^{R}_{\alpha,\cdot\cdot}C_{\cdot\cdot}(\varepsilon-\omega,\varepsilon)I^{R}_{\beta,\cdot\cdot}C_{\cdot j}(\varepsilon,\varepsilon) \\ &+C_{i\cdot}(\varepsilon-\omega,\varepsilon)I^{A}_{\alpha,\cdot\cdot}C_{\cdot\cdot}(\varepsilon-\omega,\varepsilon-\omega)I^{R}_{\beta,\cdot\cdot}C_{\cdot j}(\varepsilon,\varepsilon-\omega) \\ &+\mathrm{c.c.}\Big]. \end{aligned} \tag{2.75}$$

Performing the energy integration and passing to dimensionless propagators, we then

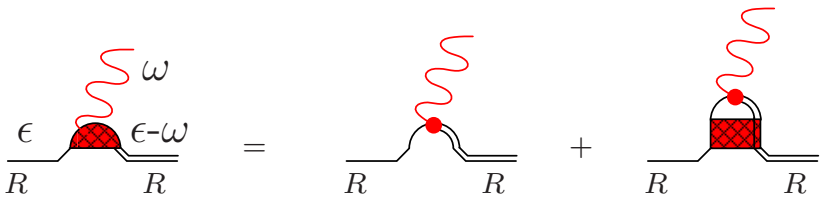

FIGURE 2.9: Renormalization of the interaction vertex by ladder diagrams involving Green's functions of the same type (retarded-retarded or advanced-advanced).

find

$$\begin{aligned}\delta c_{ij} = \int \frac{d\omega}{2\pi} \frac{\omega}{2T\sinh^2(\omega/2T)} \sum_{\alpha,\beta=1}^{\mathcal{N}_D} \mathrm{Im}\left[4\pi^2 \nu_\alpha \nu_\beta L^R_{\alpha\beta}(\omega)\right] \\ \times \Big\{ (\tilde{g} + \tilde{g}_H + i2\pi\omega\tilde{\nu})^{-1}_{i\alpha} (\tilde{g} + \tilde{g}_H)^{-1}_{\alpha\beta} (\tilde{g} + \tilde{g}_H - i2\pi\omega\tilde{\nu})^{-1}_{\beta j} \\ - (\tilde{g} + \tilde{g}_H)^{-1}_{i\alpha} (\tilde{g} + \tilde{g}_H + i2\pi\omega\tilde{\nu})^{-1}_{\alpha\beta} (\tilde{g} + \tilde{g}_H)^{-1}_{\beta j} \\ + (\tilde{g} + \tilde{g}_H - i2\pi\omega\tilde{\nu})^{-1}_{i\alpha} (\tilde{g} + \tilde{g}_H)^{-1}_{\alpha\beta} (\tilde{g} + \tilde{g}_H + i2\pi\omega\tilde{\nu})^{-1}_{\beta j} \\ - (\tilde{g} + \tilde{g}_H)^{-1}_{i\alpha} (\tilde{g} + \tilde{g}_H - i2\pi\omega\tilde{\nu})^{-1}_{\alpha\beta} (\tilde{g} + \tilde{g}_H)^{-1}_{\beta j} \Big\} . \end{aligned} \tag{2.76}$$

Let us now inspect the integral in Eq. (2.76). The term between brackets $\{\ldots\}$ is proportional to ω^{-2} if $\omega \gtrsim \hbar/\tau_D$, where $\hbar/\tau_D \sim g/\nu$ is the inverse dwell time of a dot in the network. Since $\mathrm{Im}\, L^R(\omega) \propto \omega$ for $\omega \sim \hbar/\tau_D$, one thus concludes that the integral in Eq. (2.76) converges at $\omega \sim \min(\hbar/\tau_D, T)$. We focus on the regime $T \gg \hbar/\tau_D$, in which the convergence is at $\omega \sim \hbar/\tau_D$. In this regime the inequality $\omega \ll T$ is obeyed for all frequencies ω contributing to the integral, so that all relevant interaction modes that contribute to dephasing can be described using the classical fluctuation-dissipation theorem. Indeed, one verifies that in this regime the first-order interaction correction (2.76) agrees with the interaction correction to $\tilde{c}$ obtained in the semiclassical framework of Sec. 2.3, taken to first order in the interaction propagator L.

Estimating the magnitude of the first-order correction $\delta\tilde{c}_{ij}$ for $T \gg \hbar/\tau_D$, we find that $\delta\tilde{c}_{ij} \sim \tilde{c}_{ij} T/T_\phi$, where $T_\phi \sim \hbar g/\tau_D$ [see Eq. (2.24) above]. This observation has

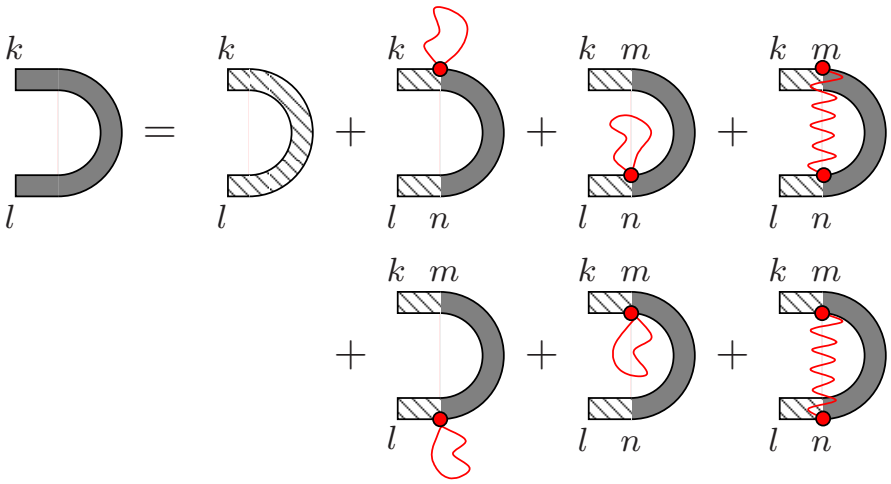

FIGURE 2.10: Dyson equation for the cooperon obtained by perturbation theory in the high temperature limit. The hatched boxes indicate noninteracting cooperon ladders, while gray shading indicates that interactions are taken into account. Wiggly lines indicate the equal time interaction propagator, which can either connect back to the same propagation line, or to the opposite, time reversed one.

two consequences: First, it implies that the regimes of validity of first-order perturbation theory and the semiclassical approach of Sec. 2.3 overlap: Both approaches are valid if $\hbar/\tau_D \ll T \ll T_\phi$. Second, it implies that interactions give no significant correction to the weak localization correction δg^{WL} if $T \lesssim \hbar/\tau_D$, so that we may ignore the difference between the fully quantum-mechanical interaction correction $\delta\tilde{c}_{ij}$ of Eq. (2.76) and the semiclassical result in the low-temperature regime $T \lesssim \hbar/\tau_D$ within the limiting procedure outlined in Sec. 2.2. (Both approaches give essentially no interaction correction to weak localization at these temperatures.) When combined, these two observations justify the semiclassical considerations of Sec. 2.3, as well as the expressions (2.15) – (2.17) for the weak localization correction δg^{WL} that followed from these considerations.

For completeness, we mention that the full temperature dependence of δg^{WL} can also be obtained from diagrammatic perturbation theory. Following the above arguments, in the limit $T \gg \hbar/\tau_D$ all factors $\coth(\omega/2T) + \tanh(\varepsilon - \omega)/2T$ appearing in the calculation may be replaced by $2T/\omega$, irrespective of the value of ε. This considerably simplifies the

calculation, and the m interaction propagators that appear in mth order in perturbation theory may then be placed independently of each other along the cooperon ladder. Using Eq. (2.39) for the interaction propagator and writing the cooperon ladders (without interaction corrections) in an integral form similar to Eq. (2.32),

$$\left(\tilde{g} + \tilde{g}_{\mathrm{H}} + 2\pi i\omega\tilde{\nu}\right)^{-1} = \left(2\pi\hbar\tilde{\nu}\right)^{-1} \int_0^\infty d\tau e^{-\tilde{\gamma}\tau - i\omega\tau}, \tag{2.77}$$

one may perform the frequency integrations. The resulting expression consists solely of time integrations with instantaneous interactions. The remaining combinatorial problem leads to a Dyson equation of the form shown in Fig. 2.10. Here the first term on the right hand side is the noninteracting cooperon $\tilde{c}_{kl} = \left(\tilde{g} + \tilde{g}_{\mathrm{H}}\right)^{-1}_{kl}$ and the six other terms are obtained by different placements of the interaction propagators. [Note that where beginning and end are on the same Green's function line, an additional weight of 1/2 arises from a factor $\int_0^\infty d\tau\delta(\tau) = 1/2$.] Adding the six different contributions gives a vertex proportional to $(4\pi\mathrm{T}/d_{\mathrm{s}}\hbar)(\tilde{g}^{-1}_{mm} + \tilde{g}^{-1}_{nn} - 2\tilde{g}^{-1}_{mn})$, so that one arrives at the Dyson equation

$$\tilde{c}_{kl} = \left(\tilde{g} + \tilde{g}_{\mathrm{H}}\right)^{-1}_{kl} - \sum_{m,n=1}^{\mathcal{N}_{\mathrm{D}}} \left[\left(\Gamma + \Gamma_{\mathrm{H}}\right)^{-1}\Gamma_{\phi}\right]_{km,ln} \tilde{c}_{mn}, \tag{2.78}$$

where Γ, Γ_{H}, and Γ_{ϕ} are rank-four tensors whose definition is given below Eq. (2.17). With a little algebra one verifies that Eq. (2.78) is equivalent to the result (2.16) derived using semiclassical arguments.

Equation (2.76) can also be used to calculate the magnitude of energy quanta ω exchanged with the fluctuating electromagnetic field in the quantum dots. Hereto, we note that the sum of the second and fourth terms between brackets $\{\ldots\}$ in Eq. (2.76) is proportional to (minus) the probability $p_1(\omega)$ for emission or absorption of a photon along

the electron's trajectory, so that

$$\begin{aligned} p_1(\omega) &= \frac{1}{g'_{1\cdot}\tilde{g}^{-1}_{\cdot\cdot}g'_{\cdot 2}} \sum_{\alpha,\beta=1}^{\mathcal{N}_D} \frac{\omega}{2\pi T \sinh^2 \omega/2T} \\ &\quad \times \mathrm{Im}\left[4\pi^2 \nu_\alpha \nu_\beta L^R_{\alpha\beta}(\omega)\right] \mathrm{Re}\left[g'_{1\cdot}\tilde{g}^{-1}_{\cdot\alpha}\left(\tilde{g} + i2\pi\omega\tilde{\nu}\right)^{-1}_{\alpha\beta}\tilde{g}^{-1}_{\beta\cdot}g'_{\cdot 2}\right] \\ &= \frac{16T\pi^2}{g'_{1\cdot}\tilde{g}^{-1}_{\cdot\cdot}g'_{\cdot 2}} \sum_{\alpha,\beta=1}^{\mathcal{N}_D} \nu_\alpha \tilde{g}^{-1}_{\alpha\beta}\nu_\beta \,\mathrm{Re}\left[g'_{1\cdot}\tilde{g}^{-1}_{\cdot\alpha}\left(\tilde{g} + i2\pi\omega\tilde{\nu}\right)^{-1}_{\alpha\beta}\tilde{g}^{-1}_{\beta\cdot}g'_{\cdot 2}\right], \end{aligned} \tag{2.79}$$

where, in the second equality, we took the limit $T \gg \hbar/\tau_D$. The probability that one inelastic scattering event of arbitrary frequency occurs is $P_1 = \int d\omega p_1(\omega)$. Equation (2.79) is valid as long as $P_1 \ll 1$, so that first-order perturbation theory is sufficient.

From Eq. (2.79) we conclude that the energy of photons that are emitted or absorbed is limited by $\min(\hbar/\tau_D, T)$. The temperature T_ϕ at which the interaction correction to weak localization becomes relevant is the temperature at which the probability that at least one energy quantum is exchanged becomes of order unity. However, the typical exchanged energy remains of order $\hbar/\tau_D$ for all temperatures. This implies that the broadening of the distribution function by inelastic processes is parametrically smaller than the temperature T, by a factor $1/g \ll 1$. Transport in the quantum dot network is thus quasielastic for all temperatures. (Inelastic processes become relevant only if $T \gtrsim E_{\mathrm{Th},i} g^{1/2}$, where $E_{\mathrm{Th},i}$ is the Thouless energy of an individual quantum dot.)

Interaction corrections to the conductance

The relevant diagrams for the interaction correction to the conductance δg^{int} are shown in Fig. 2.11. These diagrams do not involve cooperon propagators. The diagram shown in Fig. 2.11(a) is analogous to the ones we have already encountered in calculating the (first-order) dephasing correction to weak localization. It gives an interaction correction to the diffuson propagator $D(\varepsilon, \varepsilon)$ that depends on the frequency ω of the interaction

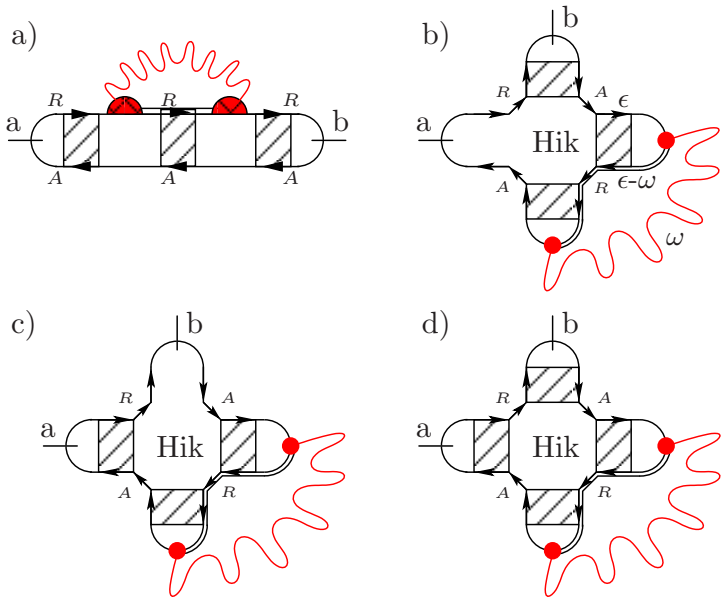

FIGURE 2.11: Diagrams contributing to δg^{int}. The Hikami box is defined in Fig. 2.6.

propagator,

$$\begin{aligned}\delta D_{\beta\alpha,ij}(\omega)^{(a)} &= D_{i\cdot}(\varepsilon,\varepsilon) I^{R}_{\beta,\cdot\cdot} D_{\cdot\cdot}(\varepsilon-\omega,\varepsilon) I^{R}_{\alpha,\cdot\cdot} D_{\cdot j} \\ &= -\frac{4M_i\nu_\beta}{\nu_i}\tilde{g}^{-1}_{i\beta}\left(\tilde{g}+i2\pi\omega\tilde{\nu}\right)^{-1}_{\beta\alpha}\tilde{g}^{-1}_{\alpha j}\frac{4M_j\nu_\alpha}{\nu_j}\end{aligned} \tag{2.80}$$

(The frequency ω will be integrated over in the final expression.) For the remaining diagrams, we need to consider an interaction vertex that connects an advanced and a retarded Green function. Such an interaction vertex is dressed by a diffuson propagator, which allows the interaction vertex to be placed in a dot different from the one that appears at the outer end of the dressed interaction vertex,

$$\begin{aligned}\tilde{I}_{\alpha,i}(\omega) &= \delta_{\alpha i}+\sum_k D_{ik}(\varepsilon-\omega,\varepsilon)\,\mathrm{tr}\,\langle G^{A}_{k\alpha}(\varepsilon)\rangle\langle G^{R}_{\alpha k}(\varepsilon-\omega)\rangle \\ &= \frac{4M_i\nu_\alpha}{\nu_i}\left(\tilde{g}+i2\pi\omega\tilde{\nu}\right)^{-1}_{i\alpha}.\end{aligned} \tag{2.81}$$

With this interaction vertex, the diagrams of Fig. 2.11(b)–(d) (without the outer diffusion ladders) can be represented by Hikami boxes $B_{ij,kl}(\omega)$ and $B'_{aj,kl}$ of Eqs. (2.70) and (2.71),

but with $g_{\rm H} \to 0$ because no cooperon ladders are involved. Combining the contributions to the interaction correction we find

$$\delta g^{\rm int} = -4 \int \frac{d\omega}{2\pi} \left(\frac{\partial}{\partial \omega} \omega \coth \frac{\omega}{2T} \right) \sum_{\alpha\beta}^{N_D} \sum_{k,l=1}^{N_D} {\rm Im} \left\{ L^{A}_{\alpha\beta}(\omega) D'_{1\cdot} \delta D_{\beta\alpha,\cdot\cdot}(\omega)^{(a)} D'_{\cdot 2} \right.$$
$$\left. + L^{A}_{\alpha\beta}(\omega) \tilde{I}_{k\alpha} \tilde{I}_{l\beta} \left[B'_{1l,\cdot k} D_{\cdot\cdot} D'_{\cdot 2} + D'_{1\cdot} D_{\cdot\cdot} B'_{\cdot l,2k} + D'_{1\cdot} D_{\cdot\cdot} B_{\cdot l,\cdot k}(\omega) D_{\cdot\cdot} D'_{\cdot 2} \right] \right\} . \qquad (2.82)$$

Expressing the propagators in terms of the matrices $\tilde{g}$ and $\tilde{f}$, we find that $\delta g^{\rm int}$ naturally separates into two contributions, which are given by Eqs. (2.20)–(2.22) of Sec. 2.2. Both corrections are small for all temperatures, and it is not necessary to consider higher order contributions involving more than one interaction propagator L.

2.5 Application to double quantum dot

We now apply the theory of Secs. 2.3 and 2.4 to the case of a double quantum dot. There are two cases of interest: A linear configuration, in which each dot is coupled to one reservoir, see Fig. 2.12(a), and a side-coupled configuration, in which both reservoirs are connected to the same quantum dot, see Fig. 2.12(b).

2.5.1 Linear configuration

The conductance matrix for the linear double quantum dot reads

$$\tilde{g} = \begin{pmatrix} g'_{11} + g_{12} & -g_{12} \\ -g_{12} & g'_{22} + g_{12} \end{pmatrix}, \qquad (2.83)$$

where g'_{11} and g'_{22} are the dimensionless conductances of the contacts connecting the two dots to the reservoirs, and g_{12} is the dimensionless conductance of the contact between the two dots, see Fig. 2.12. The form factor matrix $\tilde{f}$ has a similar structure, with g'_{11}, g'_{22},

and g_{12} replaced by f'_{11}, f'_{22}, and f_{12}, respectively. The classical conductance of the system is $\mathrm{G_{cl}} = (d_s e^2/h) g_{\mathrm{cl}}$, with

$$g_{\mathrm{cl}}^{-1} = g_{11}'^{-1} + g_{22}'^{-1} + g_{12}^{-1}, \tag{2.84}$$

[see Eq. (2.14) of Sec. 2.2].

Weak localization

The zero temperature weak localization correction to the conductance,

$$\delta \mathrm{G}^{\mathrm{WL}} = (d_s e^2/h) \delta g^{\mathrm{WL}},$$

follows from substitution of the zero-temperature cooperon $\tilde{c}(0)$ of Eq. (2.18) into Eq. (2.15),

$$\begin{aligned} \frac{\delta g^{\mathrm{WL}}}{g_{\mathrm{cl}}^2} = & -\frac{f'_{11}/g'^2_{11} + f_{12}/g_{12}^2}{g'_{11} + g_{\mathrm{H},1} + g_{12} - g_{12}^2/(g'_{22} + g_{\mathrm{H},2} + g_{12})} \\ & - \frac{f'_{22}/g'^2_{22} + f_{12}/g_{12}^2}{g'_{22} + g_{\mathrm{H},2} + g_{12} - g_{12}^2/(g'_{11} + g_{\mathrm{H},1} + g_{12})} \\ & - \frac{2(g_{12} - f_{12})/g_{12}}{(g'_{11} + g_{\mathrm{H},1} + g_{12})(g'_{22} + g_{\mathrm{H},2} + g_{12}) - g_{12}^2}. \end{aligned} \tag{2.85}$$

Here $g_{\mathrm{H},2}$ and $g_{\mathrm{H},1}$ are dimensionless numbers describing the effect of an applied magnetic field, see Eq. (2.10). The limit of zero magnetic field $g_{\mathrm{H},2} = g_{\mathrm{H},1} = 0$ agrees with the result obtained previously by Golubev and Zaikin [58]. The high-temperature limit of $\delta g^{\mathrm{WL,d}}$ of the weak localization correction is found by taking the diagonal contribution $\tilde{c}^{\mathrm{d}}$ of Eq. (2.19) for the cooperon propagator,

$$\frac{\delta g^{\mathrm{WL,d}}}{g_{\mathrm{cl}}^2} = -\frac{f'_{11}/g'^2_{11} + f_{12}/g_{12}^2}{g'_{11} + g_{\mathrm{H},1} + g_{12}} - \frac{f_{12}/g_{12}^2 + f'_{22}/g'^2_{22}}{g'_{22} + g_{\mathrm{H},2} + g_{12}}. \tag{2.86}$$

Note that $|\delta g^{\mathrm{WL,d}}| < |\delta g^{\mathrm{WL}}|$. The remainder of the weak localization correction, $\delta g^{\mathrm{WL}} - \delta g^{\mathrm{WL,d}}$, is temperature dependent because of dephasing from electron-electron interac-

tions. Taking the temperature-dependent cooperon from Eq. (2.16), we find that the temperature dependence of the full matrix $\tilde{c}(\mathrm{T})$ is encoded in a single scalar function $f(\mathrm{T})$,

$$\tilde{c}(\mathrm{T}) = \tilde{c}(0) - [\tilde{c}(0) - \tilde{c}^{\mathrm{d}}] f(\mathrm{T}). \tag{2.87}$$

Equation (2.87) immediately implies that

$$\delta g^{\mathrm{WL}}(\mathrm{T}) = \delta g^{\mathrm{WL,d}} + [\delta g^{\mathrm{WL}}(0) - \delta g^{\mathrm{WL,d}}][1 - f(\mathrm{T})], \tag{2.88}$$

where $\delta g^{\mathrm{WL}}(0)$ and $\delta g^{\mathrm{WL,d}}$ are given in Eqs. (2.85) and (2.86), respectively. In the regime where temperature is large enough for dephasing effects to give a sizeable correction to the weak localization correction to the conductance, we obtain $f(\mathrm{T})$ from Eq. (2.16),

$$f(\mathrm{T}) = \frac{\mathrm{T}}{\mathrm{T}_\phi + \mathrm{T}}, \tag{2.89}$$

with

$$\frac{\mathrm{T}_\phi}{d_{\mathrm{s}}} = \frac{\hbar(\tau_1 + \tau_2)(g'_{11}g'_{22} + g'_{11}g_{12} + g'_{22}g_{12})}{4\pi\tau_+\tau_-(g'_{11} + g'_{22})}. \tag{2.90}$$

Here τ_1 and τ_2 are the (classical) dwell times of the two dots, modified for the presence of a magnetic field,

$$\tau_1 = \frac{2\pi\hbar\nu_1}{g'_{11} + g_{\mathrm{H},1} + g_{12}},\ \tau_2 = \frac{2\pi\hbar\nu_2}{g'_{22} + g_{\mathrm{H},2} + g_{12}}, \tag{2.91}$$

whereas $\tau_\pm$ are time scales representing the relaxation of symmetric (+) or antisymmetric (−) charge configurations in the double dot,

$$\frac{1}{\tau_\pm} = \frac{1}{2\tau_1} + \frac{1}{2\tau_2} \mp \frac{1}{2}\sqrt{\left(\frac{1}{\tau_1} - \frac{1}{\tau_2}\right)^2 + \frac{g_{12}^2}{\pi^2\hbar^2\nu_1\nu_2}}. \tag{2.92}$$

It is instructive to compare Eq. (2.89) with the expression for $f(\mathrm{T})$ obtained in first-order perturbation theory,

$$\begin{aligned} f(\mathrm{T}) = & \int \frac{d\omega}{2\pi} \frac{\omega/2\mathrm{T}}{\sinh^2(\omega/2\mathrm{T})} \mathrm{Im}\left[\mathrm{L}^{\mathrm{R}}_{11}(\omega) + \mathrm{L}^{\mathrm{R}}_{22}(\omega) - 2\mathrm{L}^{\mathrm{R}}_{12}(\omega)\right] \\ & \times \frac{2\omega^2}{(1 + \omega^2\tau_+^2/\hbar^2)(1 + \omega^2\tau_-^2/\hbar^2)} \frac{\tau_+^3\tau_-^3}{\hbar^4\tau_1\tau_2}. \end{aligned} \tag{2.93}$$

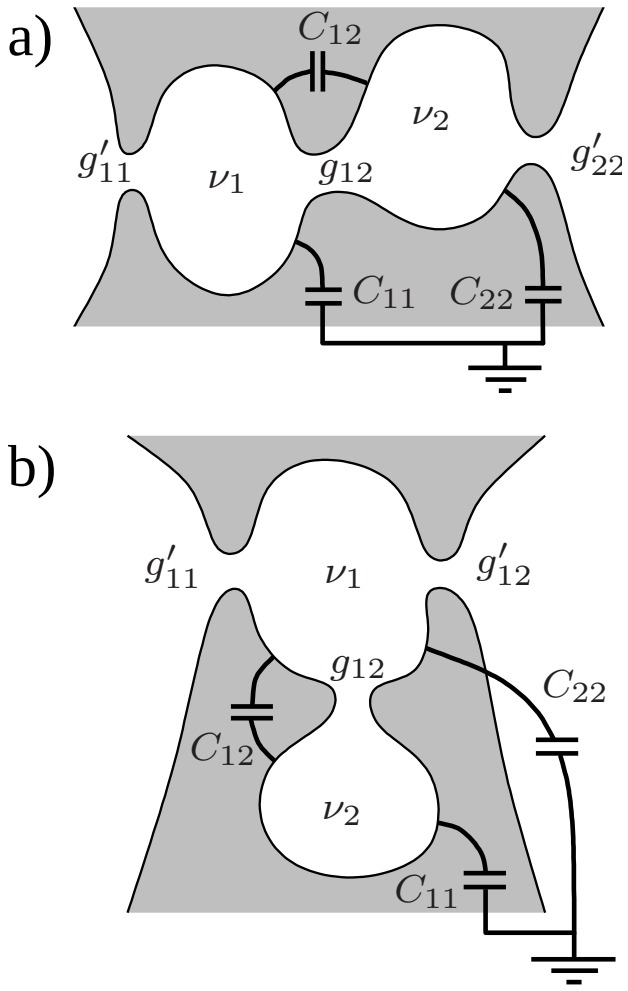

FIGURE 2.12: Schematic drawings of two double quantum dots. Panel (a) shows a linear configuration; Panel (b) shows a side-coupled configuration.

The integral in Eq. (2.93) converges for frequencies $\omega/\hbar$ of order $\tau_{\pm}^{-1}$. For these frequencies, we may neglect the capacitance C in the expression for the interaction propagator L since $C/e^2 \ll \nu$. The resulting frequency integration yields

$$f(T) = \frac{2\pi T\tau_+\tau_-}{3\hbar(\tau_+ - \tau_-)}\frac{T}{T_\phi}\left[\mathcal{F}_1(2\pi T\tau_-/\hbar) - \mathcal{F}_1(2\pi T\tau_+/\hbar)\right], \tag{2.94}$$

where

$$\mathcal{F}_1(x) = \frac{3}{x^2}\left\{\frac{1}{x}\left[2\psi'\left(\frac{1}{x}\right) - x^2\right] - 2\right\}, \tag{2.95}$$

and ψ' is the derivative of the digamma function. With the asymptotic behavior of $\mathcal{F}_1(x)$,

$$\mathcal{F}_1(x) = \begin{cases} 1 - \frac{1}{5}x^2 + \frac{1}{7}x^4 + \ldots, & x \ll 1, \\ \frac{3}{x} - \frac{6}{x^2} + \frac{\pi^2}{x^3} + \ldots, & x \gg 1, \end{cases} \tag{2.96}$$

we identify three different regimes for the temperature dependence of the dephasing correction:

$$f(T) = \frac{1}{15}\tau_+\tau_-(\tau_+ + \tau_-)\left(\frac{2\pi T}{\hbar}\right)^3\frac{T}{T_\phi} \tag{2.97}$$

if $T \ll \hbar/\tau_+$,

$$f(T) = \frac{2\pi T\tau_-}{3\hbar}\frac{T}{T_\phi} \tag{2.98}$$

if $\hbar/\tau_+ \ll T \ll \hbar/\tau_-$, and

$$f(T) = T/T_\phi \tag{2.99}$$

if $\hbar/\tau_- \ll T$, where T_ϕ is given by Eq. (2.90) above. The intermediate temperature regime exists only if $\tau_+ \gg \tau_-$. A comparison of Eq. (2.99) with Eqs. (2.89) shows that the two expressions for $f(T)$ agree in the temperature regime $\hbar/\tau_- \ll T \ll T_\phi$ where both expressions are valid. It is in this temperature regime that the factor $(\omega/2T)/\sinh^2(\omega/2T)$ in Eq. (2.93) can be approximated by $2T/\omega$, which is the appropriate weight appearing in the classical fluctuation-dissipation theorem.

It should be noted that the low temperature corrections, Eqs. (2.97) and (2.98), result in contributions to the conductance of order $O(1/g)$. Such contributions are beyond the

accuracy achieved in the limiting procedure outlined in Sec. 2.2. Further contributions of the same order might be obtained by calculating, *e.g.*, weak localization corrections to the interaction corrections $\delta g^{\mathrm{int},1}$ and $\delta g^{\mathrm{int},2}$. For disordered metals such contributions have been considered explicitly in Ref. [7].

The above equations take a simpler form in the limiting cases of large and small interdot coupling g_{12} and of a large magnetic field. For small interdot coupling $g_{12} \ll \min(g'_{11}, g'_{22})$, one has

$$\delta g^{\mathrm{WL}} = -\frac{f'_{11}g_{12}^2 + f_{12}g_{11}'^2}{g_{11}'^2(g'_{11}+g_{\mathrm{H},1})} - \frac{f'_{22}g_{12}^2 + f_{12}g_{22}'^2}{g_{22}'^2(g'_{22}+g_{\mathrm{H},2})} \tag{2.100}$$

$$- \frac{2(g_{12}-f_{12})g_{12}}{(g'_{11}+g_{\mathrm{H},1})(g'_{22}+g_{\mathrm{H},2})}\frac{\mathrm{T}_\phi}{\mathrm{T}_\phi+\mathrm{T}}, \tag{2.101}$$

$$\frac{\mathrm{T}_\phi}{d_{\mathrm{s}}} = g'_{11}g'_{22}\frac{(g'_{11}+g_{\mathrm{H},1})\nu_1^{-1} + (g'_{22}+g_{\mathrm{H},2})\nu_2^{-1}}{8\pi^2(g'_{11}+g'_{22})}, \tag{2.102}$$

so that only a small part of the total weak localization correction is temperature dependent. In the limit of a large interdot conductance, $g_{12} \gg \max(g'_{11}, g'_{22}, g_{\mathrm{H},1}, g_{\mathrm{H},2})$, the full weak localization correction acquires a temperature dependence,

$$\delta g^{\mathrm{WL}} = -\frac{g_{22}'^2 f'_{11} + g_{11}'^2 f'_{22}}{(g'_{11}+g'_{22})^2(g'_{11}+g_{\mathrm{H},1}+g'_{22}+g_{\mathrm{H},2})}\frac{\mathrm{T}_\phi}{\mathrm{T}_\phi+\mathrm{T}},$$
$$\frac{\mathrm{T}_\phi}{d_{\mathrm{s}}} = g_{12}\frac{(g'_{11}+g_{\mathrm{H},1}+g'_{22}+g_{\mathrm{H},2})(\nu_1^{-1}+\nu_2^{-1})}{8\pi^2}. \tag{2.103}$$

Finally, in the limit of large magnetic field, $g_{\mathrm{H},1}, g_{\mathrm{H},2} \gg \max(g'_{11}, g'_{22}, g_{12})$, we have

$$\delta g^{\mathrm{WL}} = -g_{\mathrm{cl}}^2\frac{f'_{11}/g_{11}'^2 + f_{12}/g_{12}^2}{g_{\mathrm{H},1}} - g_{\mathrm{cl}}^2\frac{f'_{22}/g_{22}'^2 + f_{12}/g_{12}^2}{g_{\mathrm{H},2}}$$

$$- g_{\mathrm{cl}}^2\frac{g_{12}-f_{12}}{g_{12}g_{\mathrm{H},1}g_{\mathrm{H},2}}\frac{\mathrm{T}_\phi}{\mathrm{T}_\phi+\mathrm{T}}, \tag{2.104}$$

$$\frac{\mathrm{T}_\phi}{d_{\mathrm{s}}} = \frac{g_{12}}{8\pi^2}\left(g_{\mathrm{H},1}\nu_1^{-1} + g_{\mathrm{H},2}\nu_2^{-1}\right). \tag{2.105}$$

A special case of two weakly coupled quantum dots ($g_{12} \ll g'_{11}, g'_{22}$) with tunneling contacts ($f'_{11} \ll g'_{11}$, $f'_{22} \ll g'_{22}$, $f_{12} \ll g_{12}$) has been considered recently by Golubev and Zaikin [59]. While our calculation agrees with that of Ref. [59] in the high temperature regime $T \gg T_\phi$, significant differences appear in the low temperature limit. In particular, Golubev and Zaikin find a finite dephasing correction to weak localization at zero temperature, whereas we find no such effect. A similar discrepancy has been found previously in the context of dephasing from the electron-electron interaction in disordered metals [7, 76]. In this case the neglect of recoil effects in the influence functional approach used by Golubev and Zaikin has been identified as the cause of the problem [77]. This causes an ultraviolet divergence, which does not appear in the perturbation theory, where it is avoided by the tanh-term in the factor $\coth(\omega/2T) + \tanh((\varepsilon - \omega)/2T)$ that sets the magnitude of the dephasing correction at low temperatures, see, *e.g.*, Eq. (2.57) and Refs. [7, 77]. (Neglect of recoil amounts to neglecting the ω-dependence of the argument of the tanh, which causes this factor to no longer approach zero at large frequencies ω.) We believe that the discrepancy between our result and that of Ref. [59] has the same origin.

Interaction corrections

The interaction corrections $\delta g^{\mathrm{int},1}$ and $\delta g^{\mathrm{int},2}$ do not depend on the magnetic field. Hence, the relevant time scales do not involve $g_{\mathrm{H},1}$ and $g_{\mathrm{H},2}$, and we define

$$\tau_i = \frac{2\pi\hbar\nu_i}{g'_{ii} + g_{12}}, \quad i = 1, 2. \tag{2.106}$$

Again, we introduce time scales $\tau_\pm$ related to τ_1 and τ_2 as in Eq. (2.92) above. For the first interaction correction $\delta g^{\mathrm{int},1}$ we then find

$$\delta g^{\mathrm{int},1} = \frac{g_{\mathrm{cl}}^3}{d_s g'_{11} g_{12} g'_{22}} \int d\omega \left(\frac{\partial}{\partial\omega}\omega\coth\frac{\omega}{2T}\right) \mathrm{Im}\frac{(\tau_+ + \tau_-)/\hbar}{(1 + i\omega\tau_+/\hbar)(1 + i\omega\tau_-/\hbar)}. \tag{2.107}$$

This result was obtained previously in Ref. [28] for the symmetric case $g'_{11} = g'_{22}$, $\nu_1 = \nu_2$ and in Ref. [27] for the case $g'_{11} = g'_{22} = g_{12}$, $\nu_1 = \nu_2$. The frequency integral in Eq. (2.107)

can be evaluated in terms of digamma functions. We have

$$\int d\omega \left(\frac{\partial}{\partial\omega}\omega\coth\frac{\omega}{2T}\right)\mathrm{Im}\left[\frac{1}{(1+i\omega\tau_\alpha/\hbar)(1+i\omega\tau_\beta/\hbar)}\right] = \frac{2\hbar}{\tau_\alpha-\tau_\beta}\left[\mathcal{F}_2\left(\frac{\hbar}{2\pi T\tau_\alpha}\right)-\mathcal{F}_2\left(\frac{\hbar}{2\pi T\tau_\beta}\right)\right], \tag{2.108}$$

where

$$\mathcal{F}_2(x) = \psi(1+x)+x\psi'(1+x) \tag{2.109}$$

and $\psi(x)$ is the digamma function [27]. From the asymptotic behavior of $\mathcal{F}_2$,

$$\mathcal{F}_2(x) = \begin{cases} -\gamma+\frac{\pi^2}{3}x-3\zeta(3)x^2+\ldots, & x\ll 1,\\ 1+\ln x+\frac{1}{12x^2}+\ldots, & x\gg 1,\end{cases} \tag{2.110}$$

with γ the Euler-Mascheroni constant, we obtain the high and low temperature limit of the interaction correction $\delta g^{\mathrm{int,1}}$

$$\delta g^{\mathrm{int,1}} = -\frac{2g_{\mathrm{cl}}^3}{d_s g_{11}' g_{12} g_{22}'}\times\begin{cases}\dfrac{\tau_++\tau_-}{\tau_+-\tau_-}\ln\dfrac{\tau_+}{\tau_-}, & T\ll\hbar/\tau_\pm,\\ \dfrac{\pi\hbar(\tau_++\tau_-)}{6T\tau_+\tau_-}, & T\gg\hbar/\tau_\pm.\end{cases} \tag{2.111}$$

The second interaction correction $\delta g^{\mathrm{int,2}}$ is expressed in terms of interaction-induced shifts $\delta g_{11}'$, $\delta g_{22}'$, and δg_{12} to the conductances g_{11}', g_{22}', and g_{12}, respectively, see Eq. (2.21). In contrast to the interaction correction $\delta g^{\mathrm{int,1}}$ considered above, the frequency integrations needed to calculate $\delta g_{11}'$, $\delta g_{22}'$, and δg_{12} converge only if we account for the finite (nonzero) capacitances of the quantum dots, see Eq. (2.22). [The integration in Eq. (2.22) diverges logarithmically if the limit $C_{ii}/e^2\nu_i\to 0$ is taken.]

Below we give explicit expressions for the case of a symmetric double dot only, $g_{11}' = g_{22}' = g'$, $f_{11}' = f_{22}' = f'$, $\nu_1=\nu_2$, and $C = C_{11} = C_{22}$. In this case, the logarithmic divergence of the integration in Eq. (2.22) is cut off at the inverse of the charge-relaxation times,

$$\tau_{c+} = \frac{\tau_+}{d_s e^2\nu/C},\quad \tau_{c-} = \frac{\tau_-}{d_s e^2\nu/(C+2C_{12})}, \tag{2.112}$$

and the corrections $\delta g'_{11} = \delta g'_{22} = \delta g'$ and δg_{12} are found to be

$$\delta g' = \frac{g' - f'}{d_s g'} \sum_{\sigma=\pm} \frac{\tau_\sigma}{\tau_+} \left[\mathcal{F}_2\left(\frac{\hbar}{2\pi T \tau_\sigma}\right) - \mathcal{F}_2\left(\frac{\hbar}{2\pi T \tau_{c\sigma}}\right)\right], \tag{2.113}$$

$$\delta g_{12} = \frac{2(g_{12} - f_{12})}{d_s g_{12}} \frac{\tau_+ - \tau_-}{\tau_+} \left[\mathcal{F}_2\left(\frac{1}{2\pi T \tau_- /\hbar}\right) - \mathcal{F}_2\left(\frac{1}{2\pi T \tau_{c-} /\hbar}\right)\right]. \tag{2.114}$$

For the case $g' = g_{12}$, $f' = f_{12}$ and $C_{12} = 0$, Eqs. (2.113) and (2.114) agree with results obtained previously in Ref. [27]. [The result of Ref. [27] differs from Eqs. (2.113) and (2.114) if $C_{12} > 0$ because Ref. [27] includes cross capacitances between each dot and adjacent reservoir of the same magnitude as the cross capacitance C_{12} between the two dots.] Equation (2.113) simplifies to the renormalization of the contact conductance for a single quantum dot in the limit $g_{12} \to \infty$ [38, 40, 41]. Again making use of the asymptotic behavior of the digamma function, we find that the above expressions simplify to

$$\delta g' = -\frac{g' - f'}{d_s g'} \begin{cases} \ln\dfrac{\tau_+}{\tau_{c+}} + \dfrac{\tau_-}{\tau_+}\ln\dfrac{\tau_-}{\tau_{c-}}, & T \ll \hbar/\tau_\pm, \\ \ln\dfrac{e^{1+\gamma}}{2\pi T\tau_{c+}} + \dfrac{\tau_-}{\tau_+}\ln\dfrac{e^{1+\gamma}}{2\pi T\tau_{c-}}, & \hbar/\tau_\pm \ll T \ll \hbar/\tau_{c\pm}, \\ \dfrac{\pi\hbar}{6T\tau_+}\left(\dfrac{\tau_+}{\tau_{c+}} + \dfrac{\tau_-}{\tau_{c-}}\right), & \hbar/\tau_{c\pm} \ll T, \end{cases} \tag{2.115}$$

$$\delta g_{12} = -\frac{4(g_{12} - f_{12})}{d_s g_{12}} \frac{\tau_+ - \tau_-}{\tau_+} \begin{cases} \ln\dfrac{\tau_-}{\tau_{c-}}, & T \ll \hbar/\tau_\pm, \\ \ln\dfrac{e^{1+\gamma}}{2\pi T\tau_{c-}}, & \hbar/\tau_- \ll T \ll \hbar/\tau_{c-}, \\ \dfrac{\pi\hbar}{6T\tau_{c-}}, & \hbar/\tau_{c\pm} \ll T. \end{cases} \tag{2.116}$$

2.5.2 Side-coupled quantum dot

For the side-coupled double dot configuration of Fig. 2.12 the structure of the weak localization correction and the interaction corrections is essentially the same as for the linear configurations. The classical conductance is

$$g_{cl}^{-1} = g_{11}'^{-1} + g_{12}'^{-1}. \tag{2.117}$$

The weak localization correction to the conductance is

$$\delta g^{\rm WL} = -\frac{f'_{22}g'^2_{11} + f'_{11}g'^2_{12}}{(g'_{11}+g'_{12})^2(g'_{11}+g'_{12}+g_{12}+g_{\rm H,1})} \times \left\{1 + \frac{g_{12}^2[1-f(\mathrm{T})]}{(g'_{11}+g'_{12}+g_{\rm H,1})(g_{12}+g_{\rm H,2})+g_{12}g_{\rm H,2}}\right\},$$

where $f(\mathrm{T}) = \mathrm{T}/(\mathrm{T}_\phi + \mathrm{T})$,

$$\frac{\mathrm{T}_\phi}{d_{\rm s}} = \frac{1}{4\pi}\frac{\tau_1+\tau_2}{\tau_+\tau_-}g_{12}, \tag{2.118}$$

and

$$\tau_1 = \frac{2\pi\hbar\nu_1}{g'_{11}+g'_{12}+g_{\rm H,1}+g_{12}},\ \tau_2 = \frac{2\pi\hbar\nu_2}{g_{12}+g_{\rm H,2}}, \tag{2.119}$$

with $\tau_\pm$ given in terms of τ_1 and τ_2 as in Eq. (2.92).

Again, it is instructive to compare to what one finds to lowest order in perturbation theory. The result is identical to Eq. (2.94), where τ_1, τ_2 and T_ϕ are those of the side-coupled system, Eqs. (2.118) and (2.119). Simplified expressions for the function $f(\mathrm{T})$ in the regimes $\mathrm{T} \ll \hbar/\tau_+$, $\hbar/\tau_+ \ll \mathrm{T} \ll \hbar/\tau_-$, and $\hbar/\tau_- \ll \mathrm{T}$ are as in Eqs. (2.97)–(2.99).

In the limit of small interdot coupling $g_{12} \to 0$ only a very small fraction of the weak localization correction is temperature dependent,

$$\begin{aligned}\delta g^{\rm WL} &= -\frac{f'_{22}g'^2_{11}+f'_{11}g'^2_{12}}{(g'_{11}+g'_{12})^2(g'_{11}+g'_{12}+g_{\rm H,1})}\left[1+\frac{g_{12}^2}{(g'_{11}+g'_{12}+g_{\rm H,1})g_{\rm H,2}}\frac{\mathrm{T}_\phi}{\mathrm{T}_\phi+\mathrm{T}}\right],\\ \frac{\mathrm{T}_\phi}{d_{\rm s}} &= \frac{g_{12}}{8\pi^2}\left[(g'_{11}+g'_{12}+g_{\rm H,1})\nu_1^{-1}+g_{\rm H,2}\nu_2^{-1}\right].\end{aligned} \tag{2.120}$$

In the opposite limit of a large interdot conductance the entire weak localization correction is temperature dependent. In this limit there is no difference between the linear and side-coupled configurations, and one finds that $\delta g^{\rm WL}$ is given by Eq. (2.103) above, with g'_{22} replaced by g'_{12}. Finally, in the limit of large magnetic fields we find

$$\begin{aligned}\delta g_{\rm WL} &= -\frac{g'^2_{12}f'_{11}+g'^2_{11}f'_{22}}{(g'_{11}+g'_{12})^2 g_{\rm H,1}}\left(1+\frac{g_{12}^2}{g_{\rm H,1}g_{\rm H,2}}\frac{\mathrm{T}_\phi}{\mathrm{T}_\phi+\mathrm{T}}\right),\\ \frac{\mathrm{T}_\phi}{d_{\rm s}} &= \frac{g_{12}}{8\pi^2}\left(g_{\rm H,1}\nu_1^{-1}+g_{\rm H,2}\nu_2^{-1}\right).\end{aligned} \tag{2.121}$$

With a side coupled quantum dot, the interaction correction $\delta g^{\mathrm{int},1}$ to the conductance vanishes. The interaction correction $\delta g^{\mathrm{int},2}$ coming from the renormalization of the contact conductances remains. The detailed expressions are rather lengthy and will not be reported here.

2.6 Conclusion

We have calculated the quantum corrections to the conductance of a network of quantum dots, including the full dependence on temperature and magnetic field. Our results are valid in the limit that the quantum dot network has conductance g much larger than the conductance quantum, so that the quantum corrections are small in comparison to the classical conductance, and in the limit that the electron dynamics inside each quantum dot is ergodic. Following the literature, we separated the quantum corrections into the weak localization correction δg^{WL} and two interaction corrections $\delta g^{\mathrm{int},1}$, $\delta g^{\mathrm{int},2}$. Our results for the interaction corrections agree with previous calculations of $\delta g^{\mathrm{int},1}$ and $\delta g^{\mathrm{int},2}$ by Golubev and Zaikin [27] for a linear array of quantum dots, and are closely related to similar interaction corrections in a granular metal, see Ref. [26]. Our result for δg^{WL} agrees with the literature in the limit of zero temperature [57, 58] and in the high temperature limit [67], but we are not aware of a calculation of the full temperature dependence of δg^{WL} in the literature. (The exception is a calculation of δg^{WL} for a double quantum dot by Golubev and Zaikin which, however, gives an unphysical result in the limit of zero temperature [59]).

All quantum corrections to the conductance can be expressed in terms of the inter-dot conductances, form factors, and the capacitances only. (Capacitances and form factors play a role only if the dots are connected via non-ideal contacts in which one or

more transmission eigenvalues are smaller than one. For lateral quantum dot networks defined in semiconductor heterostructures, contacts can be ballistic, and the only relevant parameters are the quantized conductances of the contacts between the quantum dots.) This makes a small quantum dot network an ideal model system to compare theory and experiment, as, in principle, these parameters–conductances, form factors and capacitances–can be measured independently. Agreement between our results and experiments would unambiguously identify the electron-electron interaction as the sole important source of dephasing at very low, if not the lowest, temperatures. It would add an experimental result to the discussion about low temperature dephasing, see, *e.g.*, in Ref. [77]. In this context, agreement between our results and experiments would vindicate the orthodox theory, which predicts the absence of dephasing at zero temperature.

We have formulated our final results in such a way that the evaluation of quantum corrections for a network of a relatively small number $\mathcal{N}_{\rm D}$ of quantum dots does not require more than the inversion of an $\mathcal{N}_{\rm D}$-dimensional matrix. The simplest example of a small quantum dot network is a 'double quantum dot', which consists of two quantum dots coupled to each other and to electron reservoirs via point contacts. Several groups have reported transport measurements on such double dots [25, 78–80], or even on triple dots [78]. (Double quantum dots also play a prominent role in recent attempts to achieve quantum computation [81]. However, the dots used in these experiments typically hold only one or two electrons each and can not be described by random matrix theory.) The experiments of Refs. [25, 78–80] were performed for quantum dots weakly coupled to source or drain reservoirs. In that limit, transport is dominated by the Coulomb blockade. Our theory applies to the opposite regime in which all dots in the network are open, *i.e.*, well coupled to source or drain reservoirs. In principle, the contact conductances in lateral double and triple quantum dot networks are fully tunable, such that the open regime considered here can be realized. A double dot system with large interdot con-

ductance is particularly well suited to the comparison of theory to experiment. Equation (2.103) predicts the weak localization correction's dependence on temperature to be of the form $T_\phi/(T_\phi + T)$ and quantifies the dependence of the temperature T_ϕ on the dots' contact conductances. This functional form, and more saliently the dependence of T_ϕ on the contact conductance, can directly be compared to what is found in experiment. We hope that the availability of such quantitative predictions will lead to renewed experimental interest in quantum transport through open quantum dots.

APPENDIX

Hikami Box calculation

In this appendix we provide details on the derivation of Eqs. (2.70) and (2.71) of Sec. 2.4. The explicit expression for the Hikami box is an essential part of the calculation of the quantum corrections to the conductance, but we have not found the explicit expression of Eq. (2.70), nor its derivation, in the literature.

We refer to the text surrounding Eq. (2.70) for the notations used in this appendix. In general, the Hikami box $\mathrm{B}_{ij,kl}(\omega)$ will be nonzero only if the four indices span at most two adjacent quantum dots. We here show the calculation of $\mathrm{B}_{ii,ii}(\omega)$. There are three contributions to $\mathrm{B}_{ii,ii}(\omega)$, which are shown in Figs. 2.13ii,ii (a)–(c). They read

$$\begin{aligned}\mathrm{B}^{(a)}_{ii,ii}(\varepsilon_1,\varepsilon_1',\varepsilon_2,\varepsilon_2') &= \mathrm{tr}\left[\langle \mathrm{G}^{\mathrm{R}}_{ii}(\varepsilon_1)\rangle\langle \mathrm{G}^{\mathrm{A}}_{ii}(\varepsilon_2')\rangle\langle \mathrm{G}^{\mathrm{R}}_{ii}(\varepsilon_2)\rangle\langle \mathrm{G}^{\mathrm{A}}_{ii}(\varepsilon_1')\rangle\right] \\ &= \frac{\pi^4\nu_i^4}{\mathrm{M}_i^3}\left(1+\frac{i\pi\nu_i(\varepsilon_1-\varepsilon_1'+\varepsilon_2-\varepsilon_2')}{2\mathrm{M}_i}+\mathrm{tr}\left[\frac{-2\Delta_i(\mathrm{M}_i-\Delta_i)}{(\mathrm{M}_i+\Delta_i)^3}+\frac{\Delta_i^4}{\mathrm{M}_i(\mathrm{M}_i+\Delta_i)^4}\right]\right),\end{aligned} \tag{2.122}$$

$$\begin{aligned}&\mathrm{B}^{(b)}_{ii,ii}(\varepsilon_1,\varepsilon_1',\varepsilon_2,\varepsilon_2') \\ &\quad= \left(\mathrm{tr}\left[\langle \mathrm{G}^{\mathrm{R}}_{ii}(\varepsilon_1)\rangle\langle \mathrm{G}^{\mathrm{A}}_{ii}(\varepsilon_2')\rangle\langle \mathrm{G}^{\mathrm{R}}_{ii}(\varepsilon_2)\right]\right)\mathrm{C}^{\mathrm{RR}}_{ii}(\varepsilon_1,\varepsilon_2)\left(\mathrm{tr}\left[\langle \mathrm{G}^{\mathrm{R}}_{ii}(\varepsilon_1)\rangle\langle \mathrm{G}^{\mathrm{R}}_{ii}(\varepsilon_2)\langle \mathrm{G}^{\mathrm{A}}_{ii}(\varepsilon_1')\rangle\right]\right) \\ &\quad= -\frac{\pi^4\nu_i^4}{2\mathrm{M}_i^3}\left(1+\frac{\tilde{g}_{ii}-\tilde{g}_{\mathrm{H},ii}+i2\pi(3\varepsilon_1-2\varepsilon_1'+3\varepsilon_2-2\varepsilon_2')}{8\mathrm{M}_i}+\frac{1}{\mathrm{M}_i}\,\mathrm{tr}\left[\frac{\Delta_i^3-3\mathrm{M}_i^2\Delta_i}{(\mathrm{M}_i+\Delta_i)^3}\right]\right),\end{aligned} \tag{2.123}$$

$$\begin{aligned}&\mathrm{B}^{(c)}_{ii,ii}(\varepsilon_1,\varepsilon_1',\varepsilon_2,\varepsilon_2') \\ &\quad= \left(\mathrm{tr}\left[\langle \mathrm{G}^{\mathrm{R}}_{ii}(\varepsilon_1)\rangle\langle \mathrm{G}^{\mathrm{A}}_{ii}(\varepsilon_2')\rangle\langle \mathrm{G}^{\mathrm{A}}_{ii}(\varepsilon_1')\right]\right)\mathrm{C}^{\mathrm{AA}}_{ii}(\varepsilon_2',\varepsilon_1')\left(\mathrm{tr}\left[\langle \mathrm{G}^{\mathrm{A}}_{ii}(\varepsilon_2')\rangle\langle \mathrm{G}^{\mathrm{R}}_{ii}(\varepsilon_2)\rangle\langle \mathrm{G}^{\mathrm{A}}_{ii}(\varepsilon_1')\right]\right) \\ &\quad= -\frac{\pi^4\nu_i^4}{2\mathrm{M}_i^3}\left(1+\frac{\tilde{g}_{ii}-\tilde{g}_{\mathrm{H},ii}+i2\pi(2\varepsilon_1-3\varepsilon_1'+2\varepsilon_2-3\varepsilon_2')}{8\mathrm{M}_i}+\frac{1}{\mathrm{M}_i}\,\mathrm{tr}\left[\frac{\Delta_i^3-3\mathrm{M}_i^2\Delta_i}{(\mathrm{M}_i+\Delta_i)^3}\right]\right),\end{aligned} \tag{2.124}$$

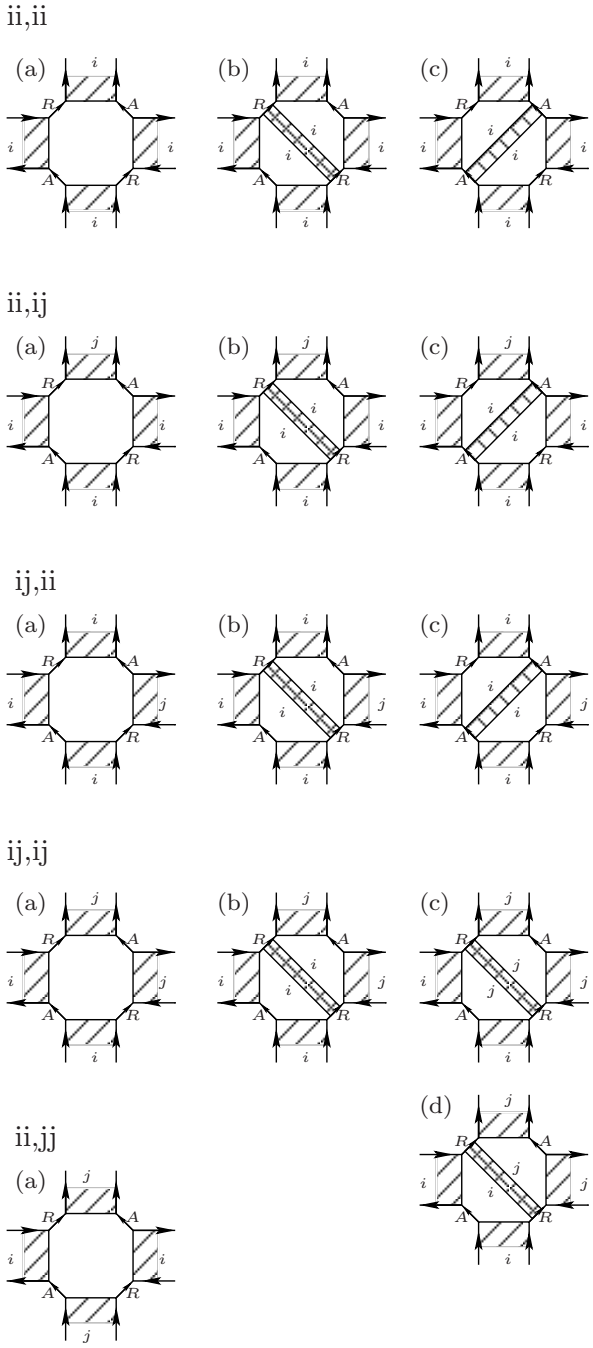

FIGURE 2.13: Diagrammatic depiction of Hikami boxes. Different diagrams contribute depending on where the cooperon and diffuson like ladders end and begin.

where the $M_i \times M_i$ matrix Δ_i was defined in Eq. (2.63) above. Traces involving the matrices Δ_i can be calculated using the identities

$$\mathrm{tr}\left[\frac{\Delta_i}{(M_i+\Delta_i)^2}\right] = \sum_k \frac{g_{ik}}{4M_i}, \tag{2.125}$$

$$\mathrm{tr}\left[\frac{\Delta_i^2}{(M_i+\Delta_i)^4}\right] = \sum_k \frac{f_{ik}}{16M_i^2}. \tag{2.126}$$

Addition of Eqs. (2.122)–(2.124) gives

$$B_{ii,ii}(\omega) = \frac{\pi^4 \nu_i^4}{16M_i^4}\left[2\pi i \nu_i \omega + 2(\tilde{g}_{\mathrm{H},ii} + \tilde{g}_{ii}) + \tilde{f}_{ii}\right], \tag{2.127}$$

where $\omega = \varepsilon_1' - \varepsilon_1 + \varepsilon_2' - \varepsilon_2$.

The diagrams for the relevant contributions to $B_{ij,kl}(\omega)$ in which the indices differ are shown in the other panels of Fig. 2.13. Expressing these contributions in terms of the matrices Δ_i and performing the traces with the help of Eqs. (2.125) and (2.126), we find

$$B_{ij,ij}(\omega) = \frac{\pi^4 \nu_i^2 \nu_j^2}{16M_i^2 M_j^2}\left(f_{ij} - g_{ij}\right), \tag{2.128}$$

$$B_{ii,ij}(\omega) = \frac{\pi^4 \nu_i^3 \nu_j}{16M_i^3 M_j}\left(-f_{ij}\right), \tag{2.129}$$

$$B_{ii,jj}(\omega) = \frac{\pi^4 \nu_i^2 \nu_j^2}{16M_i^2 M_j^2} f_{ij}, \tag{2.130}$$

for $i \neq j$. Other contributions are related by symmetry. Rewriting the general case $B_{ij,kl}(\omega)$ in terms of the matrices $\tilde{g}$ and $\tilde{f}$ for contact conductances and form factors, we obtain the result given in Eq. (2.70) of Sec. 2.4.

If a Hikami box is placed adjacent to a lead, one finds the three contributions shown in Fig. 2.14. Adding these we find, with the help of Eq. (2.126),

$$B'_{aj,jj} = \frac{\pi^5 \nu_a \nu_j^4}{M_j^4}\,\mathrm{tr}\left[W_{ja} W_{aj} \frac{-M_j^3 \Delta_j}{(M_j+\Delta_j)^4}\right] = -\frac{\pi^3 \nu_j^3}{16M_j^3} f'_{aj}. \tag{2.131}$$

This is the result reported in Eq. (2.71) of the main text.

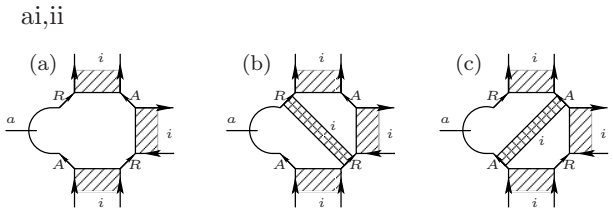

FIGURE 2.14: Diagrammatic depiction of contribution from Hikami boxes placed adjacent to leads.

BIBLIOGRAPHY

[1] B. L. Altshuler and A. G. Aronov, in *Electron-Electron Interactions in Disordered Systems*, edited by A. L. Efros and M. Pollak (Elsevier, Amsterdam, 1985).

[2] B. L. Altshuler and B. D. Simons, in *Mesoscopic Quantum Physics*, edited by E. Akkermans, G. Montambaux, J.-L. Pichard, and J. Zinn-Justin (North-Holland, 1995).

[3] Y. Imry, *Introduction to mesoscopic physics* (Oxford University Press, 2002).

[4] P. W. Anderson, E. Abrahams, and T. V. Ramakrishnan, Phys. Rev. Lett. **43**, 718 (1979).

[5] L. P. Gorkov, A. I. Larkin, and D. E. Khmelnitskii, Pis'ma Zh. Eksp. Teor. Fiz. **30**, 248 (1979) [JETP Lett. **30**, 228 (1979)].

[6] B. L. Altshuler and A. G. Aronov, Zh. Eksp. Teor. Fiz. **77**, 2028 (1979).

[7] I. L. Aleiner, B. L. Altshuler, and M. E. Gershenson, Waves in Random Media **9**, 201 (1999).

[8] G. Zala, B. N. Narozhny, and I. L. Aleiner, Phys. Rev. B **64**, 214204 (2001).

[9] H. Bouchiat, in *Mesoscopic Quantum Physics*, edited by E. Akkermans, G. Montambaux, J.-L. Pichard, and J. Zinn-Justin (North-Holland, 1995).

[10] F. Pierre, A. B. Gougam, A. Anthore, H. Pothier, D. Esteve, and N. O. Birge, Phys. Rev. B **68**, 085413 (2003).

[11] H. Pothier, S. Guéron, N. O. Birge, D. Esteve, and M. H. Devoret, Phys. Rev. Lett. **79**, 3490 (1997).

[12] P. Mohanty, E. M. Q. Jariwala, and R. A. Webb, Phys. Rev. Lett. **78**, 3366 (1997).

[13] F. Pierre and N. O. Birge, Phys. Rev. Lett. **89**, 206804 (2002).

[14] B. Huard, A. Anthore, N. O. Birge, H. Pothier, and D. Esteve, Phys. Rev. Lett. **95**, 036802 (2005).

[15] C. M. Marcus, S. R. Patel, A. G. Huibers, S. M. Cronenwett, M. Switkes, I. H. Chan, R. M. Clarke, J. A. Folk, S. F. Godijn, K. Campman *et al.*, Chaos, Solitons & Fractals **8**, 1261 (1997).

[16] U. Sivan, Y. Imry, and A. G. Aronov, Europhys. Lett. **28**, 115 (1994).

[17] Ya. M. Blanter, Phys. Rev. B **54**, 12807 (1996).

[18] C. M. Marcus, R. M. Westervelt, P. F. Hopkins, and A. C. Gossard, Phys. Rev. B **48**, 2460 (1993).

[19] R. M. Clarke, I. H. Chan, C. M. Marcus, C. I. Duruöz, J. S. Harris, K. Campman, and A. C. Gossard, Phys. Rev. B **52**, 2656 (1995).

[20] H. U. Baranger and P. A. Mello, Phys. Rev. B **51**, 4703 (1995).

[21] P. W. Brouwer, Phys. Rev. B **51**, 16878 (1995).

[22] C. W. J. Beenakker and B. Michaelis, J. Phys. A: Math. Gen. **38**, 10639 (2005).

[23] H. Forster, P. Samuelsson, S. Pilgram, and M. Büttiker, Phys. Rev. B **75**, 035340 (2007).

[24] Yu. V. Nazarov, Physical Review Letters **73**, 1420 (1994).

[25] C. Livermore, C. H. Crouch, R. M. Westervelt, K. L. Campman, and A. C. Gossard, Science **274**, 1332 (1996).

[26] I. S. Beloborodov, K. B. Efetov, A. V. Lopatin, and V. M. Vinokur, Phys. Rev. Lett. **91**, 246801 (2003).

[27] D. S. Golubev and A. D. Zaikin, Phys. Rev. B **70**, 165423 (2004).

[28] P. W. Brouwer and J. N. Kupferschmidt, Phys. Rev. Lett. **100**, 246805 (2008).

[29] M. H. Devoret, D. Esteve, H. Grabert, G.-L. Ingold, H. Pothier, and C. Urbina, Phys. Rev. Lett. **64**, 1824 (1990).

[30] S. M. Girvin, L. I. Glazman, M. Jonson, D. R. Penn, and M. D. Stiles, Phys. Rev. Lett. **64**, 3183 (1990).

[31] Yu. V. Nazarov, Pis'ma Zh. Eksp. Teor. Fiz. **49**, 105 (1989) [JETP Lett. **49**, 126 (1989)].

[32] K. Flensberg, Phys. Rev. B **48**, 11156 (1993).

[33] A. Furusaki and K. A. Matveev, Phys. Rev. Lett. **75**, 709 (1995).

[34] A. Furusaki and K. A. Matveev, Phys. Rev. B **52**, 16676 (1995).

[35] D. S. Golubev and A. D. Zaikin, Phys. Rev. Lett. **86**, 4887 (2001).

[36] A. Levy Yeyati, A. Martin-Rodero, D. Esteve, and C. Urbina, Phys. Rev. Lett. **87**, 046802 (2001).

[37] M. Kindermann and Yu. V. Nazarov, Phys. Rev. Lett. **91**, 136802 (2003).

[38] D. S. Golubev and A. D. Zaikin, Phys. Rev. B **69**, 075318 (2004).

[39] D. A. Bagrets and Yu. V. Nazarov, Phys. Rev. Lett. **94**, 056801 (2005).

[40] P. W. Brouwer, A. Lamacraft, and K. Flensberg, Phys. Rev. Lett. **94**, 136801 (2005).

[41] P. W. Brouwer, A. Lamacraft, and K. Flensberg, Phys. Rev. B **72**, 075316 (2005).

[42] B. L. Altshuler and A. G. Aronov, Solid State Commun. **30**, 115 (1979).

[43] Y. Ahmadian, G. Catelani, and I. L. Aleiner, Phys. Rev. B **72**, 245315 (2005).

[44] I. L. Aleiner, P. W. Brouwer, and L. I. Glazman, Phys. Rep. **358**, 309 (2002).

[45] H. U. Baranger and P. A. Mello, Phys. Rev. Lett. **73**, 142 (1994).

[46] R. A. Jalabert, J.-L. Pichard, and C. W. J. Beenakker, Europhys. Lett **27**, 255 (1994).

[47] K. B. Efetov, Phys. Rev. Lett. **74**, 2299 (1995).

[48] N. Argaman, Phys. Rev. Lett. **75**, 2750 (1995).

[49] N. Argaman, Phys. Rev. B **53**, 7035 (1996).

[50] I. L. Aleiner and A. I. Larkin, Phys. Rev. B **54**, 14423 (1996).

[51] P. W. Brouwer and C. W. J. Beenakker, J. Math. Phys. **37**, 4904 (1996).

[52] M. G. Vavilov and I. L. Aleiner, Phys. Rev. B **60**, R16311 (1999).

[53] K. Richter and M. Sieber, Phys. Rev. Lett. **89**, 206801 (2002).

[54] R. S. Whitney, Phys. Rev. B **75**, 235404 (2007).

[55] G. Seelig and M. Büttiker, Phys. Rev. B **64**, 245313 (2001).

[56] G. Seelig, S. Pilgram, and M. Büttiker, Turk. J. Phys. **27**, 331 (2003).

[57] G. Campagnano and Yu. V. Nazarov, Phys. Rev. B **74**, 125307 (2006).

[58] D. S. Golubev and A. D. Zaikin, Phys. Rev. B **74**, 245329 (2006).

[59] D. S. Golubev and A. D. Zaikin, New J. Phys. **10**, 063027 (2008).

[60] C. Texier and G. Montambaux, Phys. Rev. Lett. **92**, 186801 (2004).

[61] C. Texier and G. Montambaux, Phys. Rev. B **76**, 094202 (2007).

[62] I. S. Beloborodov, A. V. Lopatin, V. M. Vinokur, and K. B. Efetov, Rev. Mod. Phys. **79**, 469 (2007).

[63] I. S. Beloborodov, K. B. Efetov, A. Altland, and F. W. J. Hekking, Physical Review B **63**, 115109 (2001).

[64] I. S. Beloborodov, A. V. Andreev, and A. I. Larkin, Phys. Rev. B **68**, 024204 (2003).

[65] K. B. Efetov and A. Tschersich, Phys. Rev. B **67**, 174205 (2003).

[66] I. S. Beloborodov, A. V. Lopatin, and V. M. Vinokur, Phys. Rev. B **70** 205120 (2004).

[67] Y. M. Blanter, V. M. Vinokur, and L. I. Glazman, Phys. Rev. B **73**, 165322 (2006).

[68] B. L. Altshuler, A. G. Aronov, and D. E. Khmelnitskii, J. Phys. C **15**, 7367 (1982).

[69] L. D. Landau and E. M. Lifshitz, *Statistical Physics*, vol. 5 of *Course of Theoretical Physics* (Pergamon, London, 1958).

[70] A. Zee, *Quantum Field Theory in a nutshell* (Princeton University Press, 2003).

[71] J. A. Melsen, P. W. Brouwer, K. M. Frahm, and C. W. J. Beenakker, Europhys. Lett. **35**, 7 (1996).

[72] A. A. Clerk and V. Ambegaokar, Phys. Rev. B **61**, 9109 (2000).

[73] M. G. Vavilov, V. Ambegaokar, and I. L. Aleiner, Phys. Rev. B **63**, 195313 (2001).

[74] A. Abrikosov, L. P. Gorkov, and I. E. Dzyaloshinski, *Methods of quantum field theory in statistical physics* (Prentice-Hall, 1963).

[75] S. Hikami, Physical Review B **24**, 2671 (1981).

[76] D. S. Golubev and A. D. Zaikin, Phys. Rev. Lett. **81**, 1074 (1998).

[77] J. von Delft, Int. J. Mod. Phys. B **22**, 727 (2008); arXiv:cond-mat/0510563 (2005).

[78] F. R. Waugh, M. J. Berry, D. J. Mar, R. M. Westervelt, K. L. Campman, and A. C. Gossard, Phys. Rev. Lett. **75**, 705 (1995).

[79] T. H. Oosterkamp, S. F. Godijn, M. J. Uilenreef, Yu. V. Nazarov, N. C. van der Vaart, and L. P. Kouwenhoven, Phys. Rev. Lett. **80**, 4951 (1998).

[80] A. W. Holleitner, C. R. Decker, H. Qin, K. Eberl, and R. H. Blick, Phys. Rev. Lett. **87**, 256802 (2001).

[81] W. G. van der Wiel, S. De Franceschi, J. M. Elzerman, T. Fujisawa, S. Tarucha, and L. P. Kouwenhoven, Rev. Mod. Phys. **75**, 1 (2003).

CHAPTER 3

QUANTUM LIMIT OF THE TRIPLET PROXIMITY EFFECT IN HALF-METAL - SUPERCONDUCTOR JUNCTIONS

3.1 Introduction

The recent experimental observation of the Josephson effect in a half-metallic junction between two superconducting reservoirs [1] has renewed interest in superconductor–ferromagnet hybrid devices. The observation of a supercurrent in a half metal is remarkable, because Cooper pairs in spin-singlet superconductors consist of a pair of electrons with opposite spin, whereas a half metal conducts electrons of one spin direction only [2–4]. The resolution of this apparent paradox is the so-called "triplet proximity effect", first predicted theoretically by Bergeret, Volkov, and Efetov [5]. (See also Refs. [6–8], as well as Ref. [9] for a review.) The triplet proximity effect relies on the conversion of spin-singlet Cooper pairs of electrons with opposite spin into pairs of electrons of equal spin at a spin-active interface between the superconductor and the half metal [5, 6, 8]. Since pairs of equal-spin electrons can be transmitted coherently through a half metal, the triplet proximity effect can indeed explain the observation of a Josephson current in the experiment.

Most theoretical studies of the triplet proximity effect were done using the quasiclassical Green's function method [5–8, 10–15]. This method is appropriate for systems in which transport takes place through many conducting channels [16, 17]. For systems with few channels only, the Green's function technique should be applied without the quasiclassical approximation. This, albeit doable [12, 13, 15], can lead to calculations of significant complexity. Another method that is particularly well suited for few channel structures is the scattering matrix approach. This method has been frequently used in the context of transport problems involving superconductors (for a review, see [18]). How-

ever, it has not yet been applied to the triplet proximity effect. It is the goal of the present article to fill this gap.

In the language of the scattering approach, the triplet proximity effect relies on the coherent Andreev reflection of electron-like excitations into hole-like excitations with the same spin [19]. Conventional Andreev reflection, as it takes place at the interface between a normal metal and a superconductor, consists of the reflection of an electron into a hole with opposite spin. "Same spin" and "opposite spin" here refers to the spin band from which the electron and hole are taken. Since electron and hole from the same spin band have opposite angular momentum, conservation of angular momentum implies that electron and hole are from opposite spin bands. Hence, Andreev reflection of electrons into holes from the same spin band requires that the interface between the half metal and the superconductor is spin active. Examples of appropriate spin active interfaces are a thin ferromagnetic or half-metallic layer with a polarization that is non-collinear with the half metal's polarization or a normal-metal spacer layer with strong spin-orbit scattering.

Our focus is on systems with the fewest number of channels possible, a single conducting channel at the Fermi level. This limit can be achieved by having single channel contacts between the superconductor(s) and the half metal. As an example of this limit, we use the scattering theory to address the simplest single channel half-metal–superconductor (HS) junction that can display triplet proximity effect: a single channel ferromagnetic or half-metallic ballistic point contact between H and S electrodes. Béri *et al.* [20] extended this treatment to cover the more complex situation of HS and superconductor–half-metal–superconductor (SHS) junctions where the half metal is a chaotic quantum dot with single-channel point contacts. Here we also study the case of ballistic devices which have translation invariance along the interfaces. This situation allows for a single channel description as well, since the translation symmetry ensures

that different transverse modes do not mix. While the latter system can in principle be addressed by the quasiclassical Green's function method, the former, physically single channel setups are fully quantum mechanical, hence falling outside of the scope of quasiclassics.

We use the scattering matrix approach to calculate the differential conductance of an HS junction, and the (zero-bias) supercurrent in an SHS junction. We find that there is a remarkable difference between these two observables in the single-channel limit. For a single-channel half-metal–superconductor junction at zero temperature, the linear conductance vanishes at the Fermi level. The conductance becomes appreciable only if the applied voltage is comparable to the superconducting gap Δ or to the Thouless energy of the junction, whichever is smaller. The Josephson current, on the other hand, proves to be nonzero at zero temperature. The origin of this different behavior is that the Josephson effect contains information about the entire excitation spectrum of an SHS junction, whereas the linear conductance is a property that requires knowledge of excitations at the Fermi-level only.

The remainder of this article is organized as follows. In Sec. 3.2 we outline the key elements of the scattering approach and its application to HS junctions with a spin-active superconductor interface. In Secs. 3.3 and 3.4 we then apply the scattering theory to transport through an HS junction and to the Josephson effect in an SHS junction, respectively. We conclude in Sec. 3.5.

3.2 Scattering approach

For a scattering description of the triplet proximity effect, we consider half-metal–superconductor (HS) junctions that consist of a half metal "end", a spin-active intermedi-

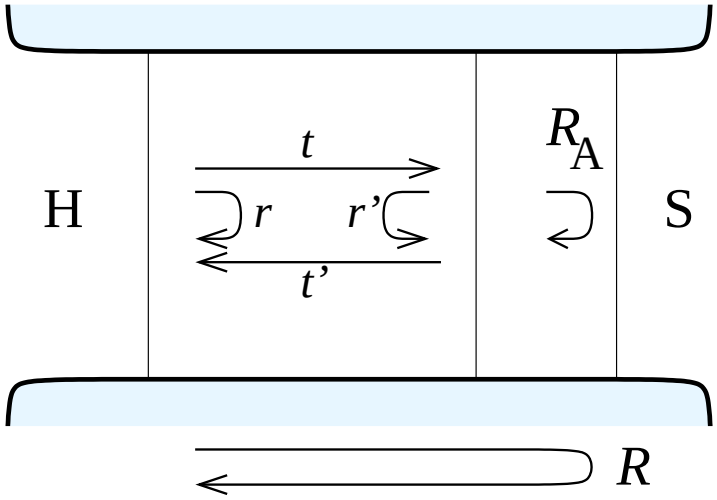

FIGURE 3.1: Composite HS junction consisting of a half-metallic contact (left), a superconducting contact (right), and a spin-active intermediate layer (center). In most of our considerations, the intermediate layer is taken to be ferromagnetic with a magnetization direction not collinear with the polarization of the half metal. Transport through the HS junction is described by the scattering matrix $\mathcal{R}$, which is calculated in terms of the Andreev reflection matrix $\mathcal{R}_\mathrm{A}$ of an ideal normal-metal–superconductor interface and the reflection and transmission matrices r, r', t, and t' of the non-superconducting region.

ate layer, and a superconductor. The intermediate layer may be half-metallic, ferromagnetic, or normal metallic.

The central object in the scattering approach is the scattering matrix $\mathcal{R}(\varepsilon)$ of the HS junction. It relates the amplitudes of excitations at energy $\varepsilon > 0$ propagating towards the superconductor and excitations propagating away from the superconductor at the half-metal end of the junction, see Fig. 3.1. If ε is below the superconducting gap Δ, all excitations must be reflected at the interface with the superconductor. This reflection can be of normal type (electron-like excitations are reflected as electrons, and hole-like excitations are reflected as holes), or of Andreev type (electron-like excitations are reflected as holes and vice versa). Both reflection types are contained in the matrix $\mathcal{R}$, which is made explicit by the decomposition

$$\mathcal{R}(\varepsilon) = \begin{pmatrix} r_{ee}(\varepsilon) & r_{eh}(\varepsilon) \\ r_{he}(\varepsilon) & r_{hh}(\varepsilon) \end{pmatrix}, \tag{3.1}$$

where r_{ee} and r_{hh} are matrices that describe normal reflection, whereas r_{eh} and r_{he} describe Andreev reflection. All four matrices have dimension N, the number of propagating modes at the Fermi level in H. Note that the propagating modes in H are not spin degenerate. Below, we will use the polarization direction of H as the spin quantization axis and refer to the electrons with spin parallel to the polarization direction of H as "spin up".

Knowledge of the scattering matrix $\mathcal{R}$ is sufficient to calculate the conductance of an HS junction, as well as the Josephson current in an SHS junction. The zero temperature differential conductance of an HS junction reads [21, 22]

$$\mathrm{G}(e\mathrm{V}) = \frac{2e^2}{h} \mathrm{Tr}\, r_{he}^{\dagger}(e\mathrm{V}) r_{he}(e\mathrm{V}). \tag{3.2}$$

(The factor of 2 accounts for the doubling of the current by the conversion of an electron into a hole.) An SHS junction can be viewed as two HS junctions opposed to each other,

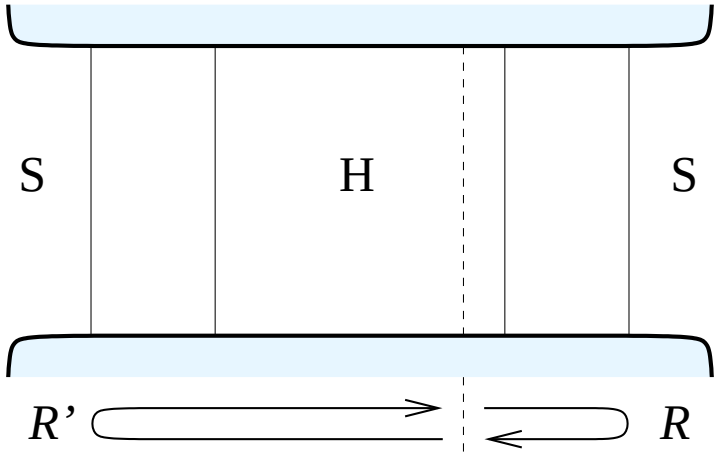

FIGURE 3.2: Schematic drawing of an SHS junction. In the scattering approach, an SHS junction is seen as two opposing (composite) HS junctions, with scattering matrices $\mathcal{R}'$ and $\mathcal{R}$, respectively. In the calculations of Sec. 3.4.1, scattering phase shifts from the central half-metallic part are included into $\mathcal{R}'$.

see Fig. 3.2. Denoting the scattering matrix corresponding to the second junction as $\mathcal{R}'$, the Josephson current reads [23]

$$\mathrm{I} = -\frac{2ek_\mathrm{B}\mathrm{T}}{\hbar}\frac{d}{d\delta\phi}\sum_{n=0}^{\infty}\ln\det[1-\mathcal{R}'(i\omega_n)\mathcal{R}(i\omega_n)], \tag{3.3}$$

where $\omega_n = (2n+1)\pi k_\mathrm{B}\mathrm{T}$ are the Matsubara frequencies, and $\delta\phi$ is the phase difference between the two superconductors.

In principle, the explicit calculation of $\mathcal{R}$ requires a solution of the Bogoliubov-de Gennes equation for the full HS junction. Here, we take a different approach [24], and express $\mathcal{R}$ in terms of the scattering matrix $\mathcal{S}$ of the non-superconducting region – that is, the intermediate layer and the half metallic region combined – and the reflection matrix $\mathcal{R}_\mathrm{A}$ for Andreev reflection off an ideal normal-metal–superconductor interface. Using the same block structure as in Eq. (3.1), it reads

$$\mathcal{R}_\mathrm{A} = \alpha(\varepsilon)\begin{pmatrix} 0 & i\sigma_2 e^{i\phi}\mathbb{1}_{\mathrm{N_S}} \\ -i\sigma_2 e^{-i\phi}\mathbb{1}_{\mathrm{N_S}} & 0 \end{pmatrix}, \tag{3.4}$$

where $\mathrm{N_S}$ is the number of propagating spin-degenerate orbital modes at the Fermi level at the superconductor interface and σ_2 is the Pauli matrix acting in spin space, ϕ is the phase of the superconducting order parameter, and

$$\alpha(\varepsilon) = e^{-i\arccos(\varepsilon/\Delta)}. \tag{3.5}$$

The scattering matrix $\mathcal{S}$ has the structure

$$\mathcal{S} = \begin{pmatrix} \mathrm{S}(\varepsilon) & 0 \\ 0 & \mathrm{S}(-\varepsilon)^* \end{pmatrix}, \tag{3.6}$$

where $\mathrm{S}(\varepsilon)$ is the scattering matrix describing the scattering of electron-like excitations off the non-superconducting region. The scattering matrix $\mathrm{S}(\varepsilon)$ can be further divided into transmission and reflection blocks,

$$\mathrm{S} = \begin{pmatrix} r & t' \\ t & r' \end{pmatrix}, \tag{3.7}$$

where r describes reflection for electrons coming from H, r' describes reflection for electrons coming from the superconductor interface, and t and t' describe transmission from and to H. The matrices r and r' have dimension N and $2N_S$, respectively. Solving for the total scattering matrix $\mathcal{R}$ in terms of $\mathcal{R}_A$ and $\mathcal{S}$, one then finds

$$r_{ee} = r + \alpha^2 t' \sigma_2 r'^* \sigma_2 (1 - \alpha^2 r' \sigma_2 r'^* \sigma_2)^{-1} t \,, \tag{3.8a}$$

$$r_{eh} = i e^{i\phi} \alpha t' \sigma_2 (1 - \alpha^2 r'^* \sigma_2 r' \sigma_2)^{-1} t^* \,, \tag{3.8b}$$

$$r_{he} = -i e^{-i\phi} \alpha t'^* \sigma_2 (1 - \alpha^2 r' \sigma_2 r'^* \sigma_2)^{-1} t \,, \tag{3.8c}$$

$$r_{hh} = r^* + \alpha^2 t'^* \sigma_2 r' \sigma_2 (1 - \alpha^2 r'^* \sigma_2 r' \sigma_2)^{-1} t^* . \tag{3.8d}$$

Here we suppressed the energy arguments; the complex conjugate matrices in Eq. (3.8) should be taken at energy $-\varepsilon$.

In the scattering matrix approach, a necessary condition for the superconducting proximity effect is to have a nonvanishing r_{he}. For an HS junction, having a nonzero r_{he} is not automatic: In the absence of spin-flip scattering in the intermediate layer, an electron coming from H is Andreev reflected as a spin-down hole. This cannot re-enter the half metallic contact; it is reflected from the half metal instead, upon which it is Andreev reflected once more to return as a spin-up electron. Andreev reflection can occur only if the intermediate layer is spin active, that is, its scattering matrix is *not* diagonal in the spin up/down basis of the half-metallic contact. Such anomalous Andreev reflection, in which a spin-up electron coming from the half-metallic contact is reflected as a spin-up hole, is the key to the triplet proximity effect. Examples of spin active layers that make this possible are a ferromagnet with a magnetization direction not collinear with the polarization of the half metal, a normal metal with strong spin-orbit coupling, or a half-metallic spacer layer with a different polarization direction and thin enough that there is nonzero transmission of minority electrons through evanescent modes.

In the next two sections we use the scattering theory to calculate the conductance of

an HS junction and the Josephson current in an SHS junction.

3.3 HS junctions

3.3.1 General considerations

The scattering matrix $\mathcal{R}(\varepsilon)$ obeys particle-hole symmetry,

$$\mathcal{R}(\varepsilon) = \Sigma_1 \mathcal{R}(-\varepsilon)^* \Sigma_1, \tag{3.9}$$

where Σ_1 is the first Pauli matrix acting in electron-hole space. For the special case N = 1, this symmetry, in combination with the condition that $\mathcal{R}(\varepsilon)$ is unitary, leads to the condition that either $r_{ee} = 0$ or $r_{eh} = 0$ at the Fermi level $\varepsilon = 0$. As we show in the appendix to this chapter generically one has $r_{eh}(0) = 0$, although the possibility $r_{ee}(0) = 0$ does occur for certain special choices of the spacer layer. The case N = 1 is relevant for the case that the contact to the half metal has only one propagating mode at the Fermi level or, alternatively, for the case that there is perfect translation symmetry in the transverse direction so that different orbital modes do not mix. To the best of our knowledge, the observation that Andreev reflection at the Fermi level is absent for single-mode HS junctions has not been made before. It presents a qualitative difference compared to FS junctions in which both spin directions can propagate.

In the general theory of Sec. 3.2 the spin quantization axis is taken to be the polarization direction of the half metal. Fixing the spin polarization axis still allows for rotations around that axis. For the scattering matrices appearing in the theory, such a rotation is

represented by the transformation

$$S \to \begin{pmatrix} e^{i\psi/2} & 0 \\ 0 & e^{i\psi\sigma_3/2} \end{pmatrix} S \begin{pmatrix} e^{-i\psi/2} & 0 \\ 0 & e^{-i\psi\sigma_3/2} \end{pmatrix}, \tag{3.10}$$

where S is the scattering matrix of the non-superconducting region, see Eq. (3.6), the block structure is that of Eq. (3.7), and ψ is the (azimuthal) angle of the rotation. Substituting this transformation into the expression (3.8) for $\mathcal{R}$, one concludes that such a rotation has the same effect on $\mathcal{R}$ as a change of the superconducting order parameter ϕ as

$$\phi \to \phi + \psi. \tag{3.11}$$

A consequence of this observation is that, if the intermediate layer is ferromagnetic or half metallic with a polarization along the unit vector

$$\mathbf{m} = (\sin\theta\cos\psi, \sin\theta\sin\psi, \cos\theta)^{\mathrm{T}}, \tag{3.12}$$

which makes an angle θ with the polarization direction of the half-metallic contact, $\mathcal{R}$ is a function of the difference $\phi - \psi$ only. (Here, and in what follows, the polarization of the half metal is taken to be along the z axis.) This observation, which will be important in our discussion of the Josephson effect in SHS junctions below, was first made by Braude and Nazarov, using the quasiclassical approach [10]. Here, it appears as a natural consequence of the transformation rules of the scattering matrix under rotations.

3.3.2 HS junction with ferromagnetic spacer

As a first and simplest application of the theory, we consider an HS junction for which the intermediate layer is a ferromagnet. The ferromagnet's magnetization points along the unit vector given in Eq. (3.12). We take the interfaces on both sides of the ferromagnetic spacer layer F to be ideal and assume that the electron motion in F is ballistic. In that

case, different orbital modes decouple, and one can use an effective single-mode description for each orbital mode μ separately. We also assume that the thickness of F is short in comparison to the superconducting coherence length $\xi_S = \hbar v_F/\Delta$ (v_F is the Fermi velocity), so that the energy-dependence of the scattering matrix S can be neglected, and we assume that the magnetic flux through F is small in comparison to the flux quantum, so that the orbital motion is time-reversal symmetric.

For this system, the calculation of S requires the composition of the 4×4 scattering matrix of the ballistic ferromagnetic spacer layer,

$$S_F = \begin{pmatrix} 0 & U \\ U & 0 \end{pmatrix}, \quad U = e^{i(\eta+\rho\mathbf{m}\cdot\boldsymbol{\sigma})/2}, \tag{3.13}$$

and the 3×3 scattering matrix S_H of the ideal interface between the half-metallic contact and the ferromagnetic spacer layer,

$$S_H = \begin{pmatrix} 0 & 1 & 0 \\ 1 & 0 & 0 \\ 0 & 0 & e^{i\beta} \end{pmatrix}. \tag{3.14}$$

In the above expressions, $\boldsymbol{\sigma}$ is the vector of Pauli matrices (acting in spin space), $\rho = \nu_\uparrow - \nu_\downarrow$ is the difference of the phase shifts of majority and minority electrons in F upon propagation through the spacer layer, and $\eta = \nu_\uparrow + \nu_\downarrow$. In Eq. (3.14), β is the phase shift spin-down electrons experience upon reflection from the half metallic contact. The three phases ρ, η, and β depend on the orbital mode μ. We have suppressed the mode dependence here, but will restore it in the final expression, Eq. (3.16) below. The block structure of S_F is as in Eq. (3.7). The same is true for S_H, where the lower right 2×2 submatrix corresponds to the lower right block in Eq. (3.7).

Combining Eqs. (3.13) and (3.14) to calculate S, and then using Eq. (3.8) to find $\mathcal{R}$, we

obtain

$$\mathcal{R}(\varepsilon) = \frac{\alpha^2}{1+\alpha^2\sin^2\rho\sin^2\theta}\begin{pmatrix} e^{-i\beta}(\cos\rho + i\sin\rho\cos\theta)^2 & -2i(\varepsilon/\Delta)e^{i(\phi-\psi)}\sin\theta\sin\rho \\ -2i(\varepsilon/\Delta)e^{i(\psi-\phi)}\sin\theta\sin\rho & e^{i\beta}(\cos\rho - i\sin\rho\cos\theta)^2 \end{pmatrix}. \tag{3.15}$$

Substituting Eq. (3.5) for α and summing over all orbital modes μ, we conclude that the differential conductance of a short ballistic HFS junction is

$$G(\varepsilon) = \frac{2e^2}{h}\sum_\mu \frac{4\varepsilon^2\sin^2\theta\sin^2\rho_\mu}{\Delta^2(1-\sin^2\theta\sin^2\rho_\mu)^2 + 4\varepsilon^2\sin^2\theta\sin^2\rho_\mu}, \tag{3.16}$$

where the summation is over the orbital modes in the HS junction.

This simple result illustrates the two main properties of the triplet proximity effect in HS junctions: First, Andreev reflection is possible as soon as there is a spacer layer that breaks spin-rotation symmetry around the half-metal's polarization direction, provided the electron's spin precesses by an angle different from 0 or π. [In Eq. (3.16) this translates to the requirement that $\sin\theta \neq 0$ and $\sin\rho_\mu \neq 0$.] And, second, in the absence of orbital mode mixing, $G = 0$ at the Fermi level, except for very special choices of the thickness (proportional to ρ_μ) and magnetization direction of the spacer layer. In the present case, these special choices are angles θ and ρ_μ for which $\sin^2\theta = \sin^2\rho_\mu = 1$. In that case, one finds $G = (2e^2/h)M$, where M is the number of modes with $\sin^2\rho_\mu = 1$.

Unlike the quasiclassical approach, the scattering approach can also deal with systems in which the number of orbital modes is small. The simplest way to illustrate this is to consider the contribution of one orbital mode; in this case, the result in Eq. (3.15) and the corresponding term in Eq. (3.16) describe a single mode ballistic ferromagnetic quantum point contact between the half-metal and the superconductor. In Fig. 3.3 we show the differential conductance of such an HS quantum point contact for a few representative values of the ferromagnet parameters ρ and θ. Both features mentioned are clearly seen: the conductance decreases with $\sin^2\theta$ and $\sin^2\rho$, and it vanishes at the Fermi energy.

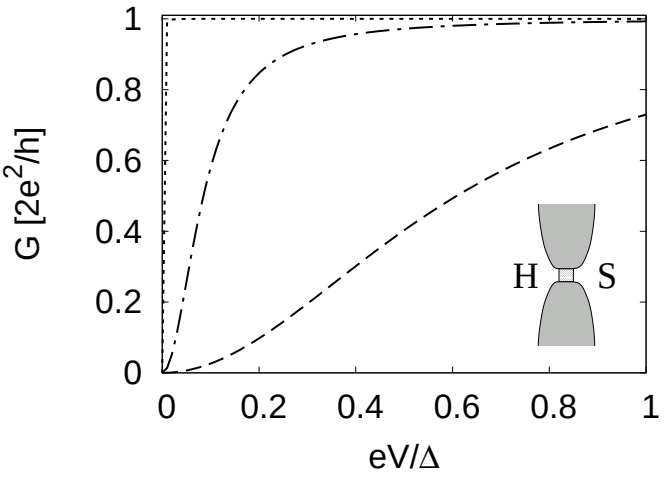

FIGURE 3.3: The subgap differential conductance G versus the applied voltage V for a ballistic single mode HS quantum point contact. The small grey rectangle in the contact represents a region with a different magnetization than in the half-metallic part. Physically such a region can be present due to a misaligned magnetization at the half-metal surface [14]. In our calculations this corresponds to the ferromagnetic spacer layer. The curves correspond to different values of the phase angles in the ferromagnetic spacer, $\theta = 0.8$ and $\rho = 0.9$ (dashed curve), $\theta = 1.4$ and $\rho = 1.2$, (dash-dotted curve), and $\theta = 1.56$ and $\rho = 1.53$ (dotted curve).

3.3.3 HS junction with half-metallic spacer

If the spacer layer between the half-metallic reservoir and the superconductor is not a ferromagnet, but a half metal, transmission through the minority channel is via evanescent modes, not propagating waves. The scattering matrix of the spacer layer, which was given by Eq. (3.13) for the case of a ferromagnetic spacer, now reads

$$S_{H'} = e^{-i\sigma_z\psi/2}e^{-i\sigma_y\theta/2}S'e^{i\sigma_y\theta/2}e^{i\sigma_z\psi/2}, \tag{3.17}$$

where

$$S'_{H'} = \begin{pmatrix} 0 & 0 & e^{i\nu_\uparrow} & 0 \\ 0 & -ie^{i\nu_\downarrow}\sqrt{1-\tau} & 0 & e^{i\nu_\downarrow}\sqrt{\tau} \\ e^{i\nu_\uparrow} & 0 & 0 & 0 \\ 0 & e^{i\nu_\downarrow}\sqrt{\tau} & 0 & -ie^{i\nu_\downarrow}\sqrt{1-\tau} \end{pmatrix}. \tag{3.18}$$

The (mode-dependent) phase shift $\nu_\downarrow$ and transmission coefficient τ for minority electrons are functions of the wavefunction decay rate q and effective mass $m_\downarrow$ of the evanescent minority electron wavefunctions, the velocity v of the majority electrons, and the thickness d of the half-metallic spacer layer. If $qd \gg 1$, the minority electron phase shift $\nu_\downarrow$ becomes independent of the layer thickness d,

$$-ie^{i\nu_\downarrow} = e^{i\beta} = \frac{v - i\hbar q/m_\downarrow}{v + i\hbar q/m_\downarrow}, \tag{3.19}$$

whereas the transmission coefficient $\tau \propto e^{-2qd}$ and $\nu_\uparrow = m_\uparrow v d/\hbar$, where $m_\uparrow$ is the effective mass of majority electrons. [The phase shift β is the reflection phase for minority electron reflection off a half-infinite half metal, see Eq. (3.14) above.]

With the definitions $\rho = \nu_\uparrow - \nu_\downarrow$ and $\eta = \nu_\uparrow + \nu_\downarrow$, we then find that the conductance of an HS junction with a half-metallic spacer is

$$G = \frac{2e^2}{h}\sum_\mu \frac{4\varepsilon^2\Delta^2\tau_\mu\left[\sin\rho_\mu + (1-\tau_\mu)^{1/2}\sin\eta_\mu\right]^2\sin^2\theta}{(B_0\Delta^2 - B_1\varepsilon^2)^2 + 4B_2^2\varepsilon^2(\Delta^2-\varepsilon^2)}, \tag{3.20}$$

where we abbreviated

$$\begin{aligned} B_0 &= [\sin\rho_\mu \cos\theta + (1-\tau_\mu)^{1/2} \sin\eta_\mu]^2 + [\cos\rho_\mu + (1-\tau_\mu)^{1/2} \cos\eta_\mu]^2, \\ B_1 &= 2 + \left(1 + \cos^2\theta\right)(1-\tau_\mu) + 2(1-\tau_\mu)^{1/2} \cos(\eta_\mu - \rho_\mu)(1+\cos\theta), \\ B_2 &= 1 + (1-\tau_\mu)^{1/2} \cos(\eta_\mu - \rho_\mu)(1+\cos\theta) + (1-\tau_\mu)\cos\theta, \end{aligned}$$

and restored the summation over the orbital modes μ. For τ_μ close to unity, this expression simplifies to the Andreev conductance for an HS junction with a ferromagnetic spacer, Eq. (3.16) above. For small energies one may neglect the terms proportional to ε^2 and ε^4 in the denominator, and we find that $G \propto \varepsilon^2\tau$. Since the transmission coefficients τ_μ are exponentially small if $q_\mu d \gg 1$, the conductance is dominated by the transverse mode μ with the lowest q_μ.

Similar to the case of ideal transmission, there is a special set of parameters at which the conductance becomes large, independent of transmission. This occurs when the coefficient $B_0 = 0$ in Eq. (3.20), so that the denominator in that equation vanishes at $\varepsilon = 0$. The condition $B_0 = 0$ translates to

$$\begin{aligned} \cos\rho_\mu &= -(1-\tau_\mu)^{1/2} \cos\eta_\mu, \\ \sin\rho_\mu \cos\theta &= -(1-\tau_\mu)^{1/2} \sin\eta_\mu. \end{aligned} \tag{3.21}$$

Solutions of Eq. (3.21) satisfy the relation $\sin^2\rho_\mu \sin^2\theta = \tau_\mu$, which generalizes the condition for resonance found for a ferromagnetic spacer layer (corresponding to $\tau_\mu = 1$). Since $\nu_{\downarrow\mu} = (\eta_\mu - \rho_\mu)/2$ is a material property if $q_\mu d \gg 1$, see Eq. (3.19) above, ρ_μ and η_μ are not independent in that limit. For a specific half metallic material and in the limiting case $q_\mu d \gg 1$, the relevant solution of Eq. (3.21) then becomes $(\rho_\mu + \eta_\mu)/2 = \nu_{\uparrow\mu} = \pi/2\,|\pi|$ and $\theta \to \pi$. Since $\nu_{\uparrow\mu}$ is a function of the thickness d of the spacer layer, not a material property, this condition can always be satisfied for special values of d. If a mode satisfies

the conditions (3.21), its contribution to the conductance is

$$G_{res,\mu} = \frac{2e^2}{\hbar} \frac{4\Delta^2\tau_\mu^2}{4\Delta^2\tau_\mu^2 + \varepsilon^2\left\{[1-\cos\theta+\tau_\mu(1+\cos\theta)]^2 - 4\tau_\mu^2\right\}}. \tag{3.22}$$

At zero energy, one finds perfect Andreev reflection irrespective of τ_μ. As before, the contribution of a single orbital mode in Eqs. (3.20), (3.22) describes the differential conductance of a single mode quantum point contact with a misaligned half metallic surface layer at the constriction, the analogue of the setup sketched in Fig. 3.3.

3.4 SHS junctions

We now contrast the transport current through an HS junction to the supercurrent through an SHS junction. As in the previous section, we consider the effect of a thin ferromagnetic layer between each superconductor and the adjacent half metal. (We do not consider the case of a thin half-metallic spacer layer in this section.) While, at zero temperature, the zero-bias conductance of a single single-channel HS junction vanishes (except at special choices of the parameters), the zero temperature Josephson current I is not zero. The reason is that, in contrast to the linear response conductance G, I is not a Fermi level property. Instead, it is determined by the full excitation spectrum.

In order to apply the theory of the previous sections, we consider the SHS junction as two opposing HS junctions, see Fig. 3.2. We refer to the opposing HS junction as S'H. Both junctions have intermediate ferromagnetic layers, which are denoted by F and F'. The two ferromagnets can have different magnetizations, parameterized by polar angles θ, ψ and θ', ψ', respectively. The superconductors S and S' are assumed to have equal superconducting gaps Δ, but the phases ϕ, ϕ' of the order parameters can differ.

Before turning to applications of our scattering theory, it is worthwhile to summarize

some general considerations. Because of the transformation property (3.11), the Josephson current I can depend on the superconducting phases ϕ and ϕ' and on the azimuthal angles ψ and ψ' through the single combination

$$\tilde{\phi} = \phi - \phi' - (\psi - \psi') \tag{3.23}$$

only. This observation was made previously in the context of the quasiclassical approach [10, 11, 14].

Under the operation of time reversal, the phases of the superconductors and the (position dependent) magnetization direction $\mathbf{m}$ transform as $\phi \to -\phi$, $\mathbf{m} \to -\mathbf{m}$. The supercurrent of the time reversed system is the opposite of the original, that is,

$$I(\phi - \phi', \mathbf{m}) = -I(\phi' - \phi, -\mathbf{m}). \tag{3.24}$$

The supercurrent is invariant under a position independent rotation of the magnetization. This, together with Eq. (3.24) results in $I(\tilde{\phi}) = -I(-\tilde{\phi})$.

For phase angles not close to the special point $\sin^2\theta = \sin^2\theta' = \sin^2\rho = \sin^2\rho' = 1$, the Andreev reflection probability at the SH interfaces is significantly smaller than unity [see Eq. (3.15) above]. As a consequence, the $\tilde{\phi}$-dependence of the supercurrent is nearly sinusoidal in this case. The detailed calculations of the next section show, however, that close to the special values of the phase angles the $\tilde{\phi}$-dependence becomes non-sinusoidal.

As an illustration of our scattering theory, we now consider the ballistic junctions addressed in the previous section. Our work on the Josephson effect in ballistic junctions complements that of Galaktionov *et al.*, who used a Green function approach [15].

3.4.1 SHS junction with ferromagnetic spacer

For the ballistic SHS junction different orbital modes are not mixed, so that the scattering problem is effectively one-dimensional. As before, we denote the difference of the (mode-dependent) phase shifts of majority and minority electrons transmitted through F by ρ, see Eq. (3.13); The corresponding quantity for F' is denoted by ρ'. We suppress the mode index μ, except in the final expressions. For the calculation of the supercurrent, it is necessary that phase shifts accumulated inside the half metal are included into the determinant in Eq. (3.3). For an orbital mode μ these phase shifts depend on the length L of the half-metallic segment and on the longitudinal component $k_\mu(\varepsilon) = k_\mu(0) + \varepsilon/(\hbar v_\mu)$ of the wave vector for that mode, where v_ν is the group velocity of the mode at $k_\mu(0)$. In order to include this into Eq. (3.3) we take the scattering matrix $\mathcal{R}'$ to include the scattering phase shifts accumulated inside the half metal,

$$\mathcal{R}' = \begin{pmatrix} e^{ik_\mu(\varepsilon)\mathrm{L}} & 0 \\ 0 & e^{-ik_\mu(-\varepsilon)\mathrm{L}} \end{pmatrix} \tilde{\mathcal{R}}' \begin{pmatrix} e^{ik_\mu(\varepsilon)\mathrm{L}} & 0 \\ 0 & e^{-ik_\mu(-\varepsilon)\mathrm{L}} \end{pmatrix}, \tag{3.25}$$

where $\tilde{\mathcal{R}}'$ is the reflection matrix for the S'H junction without the scattering phases from the half metal. This matrix is given in Eq. (3.15) of the previous section, but with θ, ψ, ϕ, and ρ replaced by θ', ψ', ϕ', and ρ', respectively.

Since there is a probability of normal reflection at each end of the SHS junction, for a given orbital mode, the contribution to the supercurrent contains terms that oscillate with the length L of the junction. For the total supercurrent, obtained by summing the contributions from different orbital modes, however, this results only in a small correction, provided that $k_\mu(0)\mathrm{L} \gg 1$, since in this case, the sum of the oscillating contributions averages out. Below, we calculate the non-oscillating contribution to the Josephson current for a given orbital mode, and restrict our discussion to the limiting cases of a "short

junction" ($L \ll \xi_S$) and a "long junction" ($L \gg \xi_S$). (In both cases, we assume that the ferromagnetic spacer layers are thin in comparison to the superconducting coherence length ξ_S. The same assumption was made in the previous section.)

For a short junction, one may neglect the energy-dependence of the wavenumber $k_\mu(\varepsilon)$ in the half metal. A closed-form expression valid for arbitrary temperatures could be obtained for the special case $\sin^2\theta = \sin^2\theta' = 1$ for a mode μ with $\sin^2\rho_\mu = \sin^2\rho'_\mu = 1$ only. The contribution I_μ to the supercurrent of such a mode is

$$I_\mu = -\frac{e\Delta}{2\hbar}\cos\frac{\tilde{\phi}+s_\mu\pi}{2}\tanh\left(\frac{\Delta}{2k_BT}\sin\frac{\tilde{\phi}+s_\mu\pi}{2}\right), \tag{3.26}$$

where s_μ is defined through the relation

$$(-1)^{s_\mu} = \sin\rho_\mu \sin\rho'_\mu. \tag{3.27}$$

The π shift in the current-phase relationship associated with s_μ originates in the properties of the interface reflection matrix (3.15): for this matrix, the transformation $\rho \to \rho + \pi$ is equivalent to $\phi \to \phi + \pi$.

In the limit of high temperatures $k_BT \gg \Delta$, one can find a closed-form expression for arbitrary values of θ, θ', ρ, and ρ'. Upon summation over all orbital modes, one has

$$I = -\sum_\mu \frac{e}{\hbar}\frac{\Delta^2}{8k_BT}\sin\tilde{\phi}\sin\rho_\mu\sin\rho'_\mu\sin\theta\sin\theta'. \tag{3.28}$$

Note that although the angles ρ_μ, ρ'_μ are mode dependent, for sufficiently thin spacer layers the mode dependence is weak enough that all modes contribute to the total Josephson current with the same sign. The supercurrent is reduced once the thickness of the spacer layers is large enough that $\rho_\mu, \rho'_\mu \gg 1$.

A numerical evaluation of the contributions to the zero-temperature supercurrent is shown in Fig. 3.4 for a few choices of the angles θ, θ', ρ, and ρ'. Although the discontinuity at $\tilde{\phi} = s\pi$ is smeared for generic values of the phase angles, the order of magnitude of

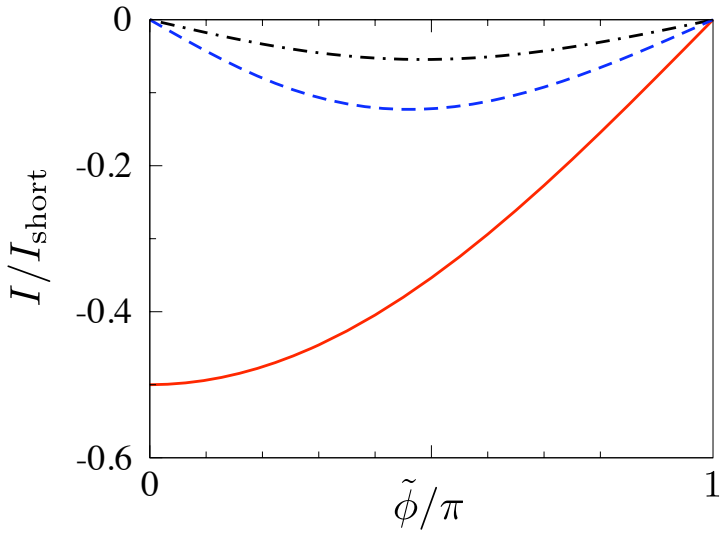

FIGURE 3.4: The contribution of a single transverse mode to the zero temperature supercurrent I of a short SHS junction, as a function of $\tilde{\phi}$, for ferromagnetic phase angles $\theta = \theta' = \rho = \rho' = \pi/2$ (solid), $\theta = \theta' = \rho = \rho' = \pi/4$ (dot-dash), and $\theta = \theta' = \pi/2$, $\rho = \rho' = \pi/4$ (dashed). The supercurrent is shown in units of $I_{short} = e\Delta/\hbar$.

the supercurrent is the same as at the special point $\sin^2\theta = \sin^2\theta' = \sin^2\rho = \sin^2\rho' = 1$. This is in contrast to the Fermi-level conductance of an HS junction, which was zero for generic phase angles and finite at the special point. As discussed above, the reason why the supercurrent has a different behavior is that it is not a Fermi-level property but, instead, depends on the entire excitation spectrum. For energies far away from the Fermi level, the Andreev conductance is not qualitatively different at the special point and elsewhere, see Fig. 3.3.

For a long SHS junction (but still with ferromagnetic spacer layers that are much thinner than ξ_S), again a compact expression at arbitrary temperatures could be obtained for the special case $\sin^2\theta = \sin^2\theta' = 1$, for the contribution I_μ of a mode μ with $\sin^2\rho_\mu = \sin^2\rho'_\mu = 1$ only. In this case one finds

$$I_\mu = -\frac{e}{\hbar} 2k_B T \sum_n \frac{\sin(\tilde{\phi} + s_\mu \pi)}{\cosh(2\omega_n L/\hbar v_\mu) - \cos(\tilde{\phi} + s_\mu \pi)}, \tag{3.29}$$

where s_μ was defined in Eq. (3.27). At zero temperature the summation can be replaced by an integration and one has

$$I_\mu = \frac{e v_\mu [\tilde{\phi} - (1 - s_\mu)\pi]}{2\pi L}, \quad 0 < \tilde{\phi} + s_\mu \pi < 2\pi. \tag{3.30}$$

In the limit of high temperatures, $T \gg \hbar v_\mu / L$, only the term with $n = 0$ contributes, so that

$$I_\mu = -\frac{e}{\hbar} 4k_B T e^{-2\pi k_B T L/\hbar v_\mu} \sin(\tilde{\phi} + s_\mu \pi). \tag{3.31}$$

The special point $\sin^2\theta = \sin^2\theta' = \sin^2\rho = \sin^2\rho' = 1$ is singular, however, and the supercurrent contributions have a qualitatively different dependence on temperature for generic θ, θ', ρ, and ρ'. In the high-temperature regime $\hbar v_\mu / L \ll k_B T \ll \Delta$, one finds

$$\begin{aligned} I = & -\frac{e}{\hbar} \frac{16\pi^2 k_B^3 T^3}{\Delta^2} \sum_\mu \sin\rho_\mu \sin\rho'_\mu \sin\theta \sin\theta' \sin\tilde{\phi} \\ & \times \frac{e^{-2\pi L k_B T/\hbar v_\mu}}{\left(1 - \sin^2\rho_\mu \sin^2\theta\right)\left(1 - \sin^2\rho'_\mu \sin^2\theta'\right)}, \end{aligned} \tag{3.32}$$

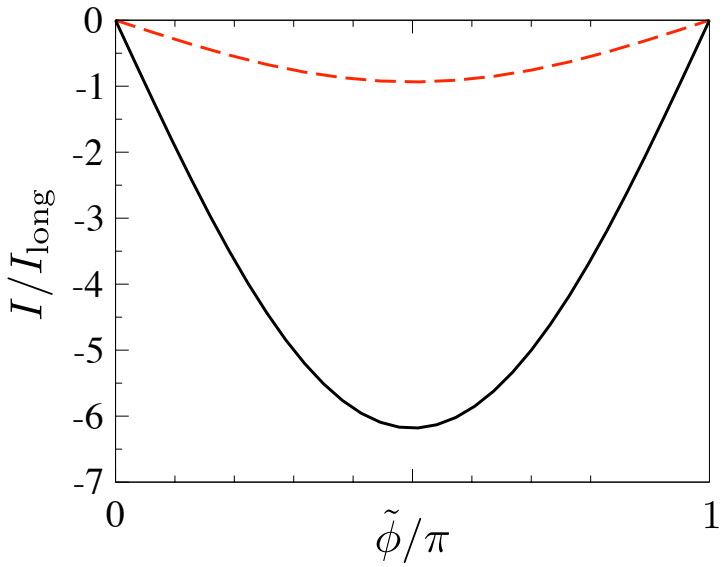

FIGURE 3.5: The contribution of a single transverse mode to the non-oscillating component of the zero temperature supercurrent I of a long SHS junction, as a function of $\tilde{\phi}$, for ferromagnetic phase angles $\theta = \theta' = \rho = \rho' = \pi/3$ (solid) and $\theta = \theta' = \rho = \rho' = \pi/4$ (dashed). The current is shown in units of $I_{long} = e\hbar^2 v_\mu^3/\pi L^3\Delta^2$, where v_μ is the mode-dependent longitudinal velocity.

This result is a factor $\sim (k_B T/\Delta)^2 \ll 1$ smaller (per orbital mode) than the contribution for the special choice of the angles θ, θ', ρ, and ρ' in Eq. (3.31). Whereas the supercurrent of a short Josephson junction depends on the full subgap excitation spectrum of the junction [25], the supercurrent in the long junction limit is determined by the junction's excitation spectrum up to the Thouless energy $\hbar v_F/L$ only [23]. In this range of the spectrum, the absence of Andreev reflection at the Fermi energy still strongly affects the magnitude of the supercurrent. For temperatures below the Thouless energy $\hbar v_F/L$ the suppression factor with which I_μ is reduced in comparison to the special case of Eq. (3.29) saturates around $(\hbar v_F/L\Delta)^2$. No closed-form expressions for I_μ at arbitrary temperatures could be obtained. Figure 3.5, shows I_μ versus $\tilde{\phi}$ at zero temperature, for two choices of the parameters θ, θ', ρ, and ρ'.

3.5 Conclusion

For the conventional proximity effect, the possibility of Andreev reflection of electrons at the Fermi level gives a nonzero linear conductance through a normal-metal–superconductor interface. In this article, we found that the situation is more delicate for the triplet proximity effect in half-metal–superconductor (HS) junctions. In the case that there is only one conducting channel at the HS interface, or that different orbital channels at the HS interface decouple, we found that Andreev reflection processes can be present only away from the Fermi level (except for special choices of the interface parameters). While this result, which is independent of the nature of the spin active spacer layer in the HS junction, leads to a vanishing linear conductance, it allows for a nonzero Josephson current through an effectively single-channel SHS junction. We have illustrated this statement on systems both in the quasiclassical and in the fully quantum mechanical regimes. In our calculations we have mainly concentrated on the case of ferromagnetic spin active

intermediate layers.

First, we have calculated the zero temperature differential Andreev conductance at finite bias for short HS junctions. This is the observable in which the present Andreev reflection processes manifest themselves in the most direct way. In addition to the calculation of the differential conductance for systems with ferromagnetic spacer layer, we also studied ballistic systems where the spacer is a thin half metallic layer.

Second, we calculated the zero bias Josephson current through SHS junctions. We have confirmed the observation, reported in earlier works [10, 11, 14], that the Josephson current depends on the superconducting phase through the single variable $\tilde{\phi} = \phi - \phi' - (\psi - \psi')$ only, which is the difference of the superconductor phase difference of two superconducting reservoirs and the azimuthal angle differences of the magnetization direction of the two ferromagnetic spacer layers in the SHS junction. In the framework of the scattering matrix approach, this observation follows directly from the fact that the phase of the superconductor and the azimuthal angle of the ferromagnetic spacer at an HS interface enter in identical ways in the calculation of the Andreev reflection amplitude. Further symmetry considerations showed that the supercurrent is an odd function of the variable $\tilde{\phi}$. Similarly to earlier works [10, 11, 14, 15], we also find that for symmetric ferromagnetic spacers, $\psi = \psi'$, $\rho = \rho'$, $\theta = \theta'$, the sign of the current is the opposite to the case of conventional SNS junctions (see Figs. 3.4 and 3.5). Consequently, the equilibrium phase difference corresponds to $\phi - \phi' = \pi$, i.e., a π-junction behavior is realized. For independent configurations in F and F', the equilibrium phase difference varies continuously as the function of interface parameters.

It is worthwhile to compare our results for the Josephson current in single channel SHS systems to the result for a single channel SNS systems. In the latter case, at zero temperature and in the absence of magnetic field, for a perfectly transparent normal re-

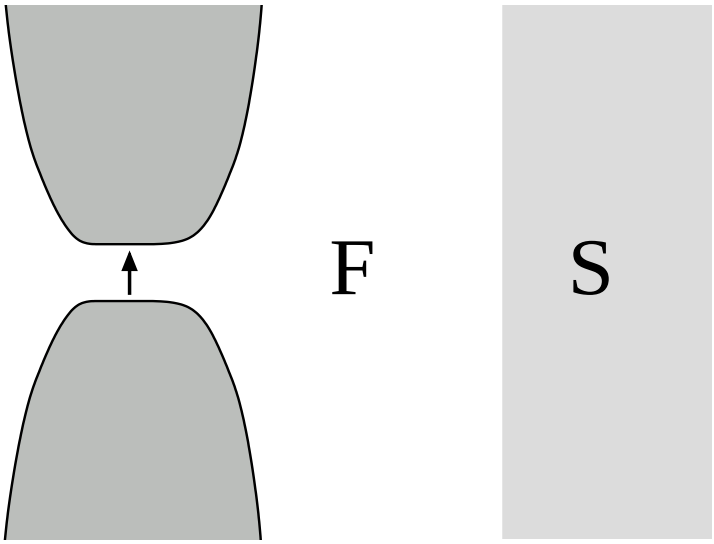

FIGURE 3.6: Sketch of a possible experimental setup for testing the vanishing Andreev reflection at the Fermi level: a single channel quantum point contact to an FS junction. The arrow in the quantum point contact indicates that the point contact transmits only one spin direction.

gion, the (per spin) Josephson current is given by [25] $I = (e\Delta/2\hbar)\sin(\phi/2)$, for short junctions and [26] $I = ev_F\phi/2\pi L$ for long junctions, where $|\phi| < \pi$. We found [see Eqs.(3.30) and (3.26)] that in the case of single channel SHS systems, in the special point $\sin^2\theta = \sin^2\theta' = \sin^2\rho = \sin^2\rho' = 1$, the current-phase relation is identical, apart from the phase shifts due to the azimuthal angles and s. Away from the special point, the current-phase relation becomes sinusoidal, similar (apart from the phase shifts) to the case of a normal region with low transparency. By adjusting the interface parameters, the single mode triplet Josephson current interpolates between the result for the conventional Josephson current through an ideal single mode channel and through a tunnel barrier. The key property that distinguishes the current phase relation in the triplet Josephson effect through single mode structures from the conventional Josephson effect is the magnetization dependent phase shift. This is a feature that is common between the fully quantum mechanical single channel limit and the multi mode case corresponding to the quasi-classics.

We end by relating our results about HS junctions to a possible experiment. One experimental setup could be the HS quantum point contact sketched in Fig. 3.3. Such a setup is somewhat subtle, as it relies on the presence of a surface magnetization in the point contact. The generality of our proof in the appendix suggests, however, that the main features of the single channel HS conductance, i.e., $G = 0$ at Fermi level and $G \neq 0$ for $0 < eV < \Delta$ could be tested in an experimentally more robust arrangement. Such a setup could be a single channel point contact to an FS junction, as sketched in Fig. 3.6. It is not necessary to have the system in the short junction limit, and there can be arbitrary number of modes at the ferromagnet-superconducting interface. The only important detail is that the junction ends in a single mode point contact through which only one spin direction can be transmitted. This can be achieved using a half metallic electrode or with a spin filtering quantum point contact [27].

APPENDIX

Absence of Andreev reflection for single-mode HS junctions

In this appendix we prove that, generically, the Andreev reflection amplitude $r_{\rm he}(0) = 0$ for a junction with $\mathrm{N} = 1$ orbital modes in the half metallic side. The number of modes on the superconducting side can be arbitrary. The starting point of the proof is the singular value decomposition of the scattering matrix S of the non-superconducting region between the half-metallic and superconducting reservoirs [18],

$$\mathrm{S} = \begin{pmatrix} \mathrm{V} & 0 \\ 0 & \mathrm{W} \end{pmatrix} \begin{pmatrix} \hat{\mathrm{R}} & \hat{\mathrm{T}}^{\mathrm{T}} \\ \hat{\mathrm{T}} & -\hat{\mathrm{R}}' \end{pmatrix} \begin{pmatrix} \mathrm{V}' & 0 \\ 0 & \mathrm{W}' \end{pmatrix}. \tag{3.33}$$

Here, V and V' are $\mathrm{N} \times \mathrm{N}$ unitary matrices, W and W' are unitary matrices of dimension $2\mathrm{N_S}$, $\mathrm{N_S}$ being the number of orbital channels at the normal-metal–superconductor interface, $\hat{\mathrm{T}}$ is an $2\mathrm{N_S} \times \mathrm{N}$ matrix with

$$\hat{\mathrm{T}}_{kl} = \delta_{kl}\sqrt{\tau_l}, \quad k = 1, \ldots, 2\mathrm{N_S}, \quad l = 1, \ldots, \mathrm{N}, \tag{3.34}$$

with τ_l the lth transmission eigenvalue, $l = 1, \ldots, \mathrm{N}$, and

$$\hat{\mathrm{R}} = \sqrt{1_{\mathrm{N}} - \hat{\mathrm{T}}^{\mathrm{T}}\hat{\mathrm{T}}}, \quad \hat{\mathrm{R}}' = \sqrt{1_{2\mathrm{N_S}} - \hat{\mathrm{T}}\hat{\mathrm{T}}^{\mathrm{T}}}. \tag{3.35}$$

Substituting the decomposition (3.33) in Eq. (3.8c), and assuming $\det(1_{2\mathrm{N_S}} + r'\sigma_2 r'^{*}\sigma_2) \neq 0$, one finds

$$r_{\rm he}(0) = -e^{-i\phi}\mathrm{V}^{*}\hat{\mathrm{T}}^{\mathrm{T}}\left(\mathrm{Z}^{\dagger} - \hat{\mathrm{R}}'\mathrm{Z}^{*}\hat{\mathrm{R}}'\right)^{-1}\hat{\mathrm{T}}\mathrm{V}' \tag{3.36}$$

with $\mathrm{Z} = \mathrm{W}'^{*}\sigma_2\mathrm{W}$. If $\mathrm{N} = 1$, the amplitude $r_{\rm he}(0)$ is proportional to the 11 element of the inverse in (3.36). Using the general result $\mathrm{A}^{-1} = (\det \mathrm{A})^{-1}\mathrm{adj}(\mathrm{A})$ for the matrix inverse, we find that this element is proportional to the determinant of an antisymmetric matrix of dimension $2\mathrm{N_S} - 1$, and is therefore zero. The case $r_{\rm he}(0) \neq 0$ is possible if

$\det(1_{2N_S} + r'\sigma_2 r'^{*}\sigma_2) = 0$, that is, if the system has an Andreev bound state at $\varepsilon = 0$ that is not coupled to the mode in the half metal. For the ballistic HS system in Sec. 3.3.2,

$$\det(1_{2N_S} + r'\sigma_2 r'^{*}\sigma_2) = 1 - \sin^2\rho \sin^2\theta, \tag{3.37}$$

resulting in $\sin^2\rho = \sin^2\theta = 1$ to be the only points where $r_{he}(0)$ can be nonzero.

BIBLIOGRAPHY

[1] R. S. Keizer, S. T. Goennenwein, T. M. Klapwijk, G. Miao, G. Xiao, and A. Gupta, Nature **439**, 825 (2006).

[2] R. A. de Groot, F. M. Mueller, P. G. van Engen, and K. H. J. Buschow, Phys. Rev. Lett. **50**, 2024 (1983).

[3] W. Pickett and J. Moodera, Physics Today **54**, (5) 39 (2001).

[4] J. Coey and M. Venkatesan, J. Appl. Phys. **91**, 8345 (2002).

[5] F. S. Bergeret, A. F. Volkov, and K. B. Efetov, Phys. Rev. Lett. **86**, 4096 (2001).

[6] A. Kadigrobov, R. I. Shekhter, and M. Jonson, Europhys. Lett. **54**, 394 (2001).

[7] F. S. Bergeret, A. F. Volkov, and K. B. Efetov, Phys. Rev. B **64**, 134506 (2001).

[8] M. Eschrig, J. Kopu, J. Cuevas, and G. Schön, Phys. Rev. Lett. **90**, 137003 (2003).

[9] F. S. Bergeret, A. F. Volkov, and K. B. Efetov, Rev. Mod. Phys. **77**, 1321 (2005).

[10] V. Braude and Y. V. Nazarov, Phys. Rev. Lett. **98**, 077003 (2007).

[11] M. Eschrig, T. Löfwander, T. Champel, J. Cuevas, J. Kopu, and G. Schön, J. Low Temp. Phys. **147**, 457 (2007).

[12] Y. Asano, Y. Tanaka, and A. A. Golubov, Phys. Rev. Lett. **98**, 107002 (2007).

[13] Y. Asano, Y. Sawa, Y. Tanaka, and A. A. Golubov, Phys. Rev. B **76**, 224525 (2007).

[14] M. Eschrig and T. Löfwander, Nature Physics **4**, 138 (2008).

[15] A. V. Galaktionov, M. S. Kalenkov, and A. D. Zaikin, Phys. Rev. B **77**, 094520 (2008).

[16] G. Eilenberger, Z. Phys. **214**, 195 (1968).

[17] A. I. Larkin and Y. N. Ovchinnikov, Sov. Phys. JETP **28**, 1200 (1969).

[18] C. W. J. Beenakker, Rev. Mod. Phys. **69**, 731 (1997).

[19] J. Yi-Qun, N. Zhi-Ping, F. Cui-Di, and X. Ding-Yu, Chin. Phys. Lett. **25**, 691 (2008).

[20] B. Béri, J. N. Kupferschmidt, C. W. J. Beenakker, and P. W. Brouwer, Phys. Rev. B **79**, 024517 (2009).

[21] G. E. Blonder, M. Tinkham, and T. M. Klapwijk, Phys. Rev. B **25**, 4515 (1982).

[22] Y. Takane and H. Ebisawa, J. Phys. Soc. Jpn. **61**, 1685 (1992).

[23] P. W. Brouwer and C. W. J. Beenakker, Chaos, Solitons and Fractals **8**, 1249 (1997).

[24] C. W. J. Beenakker, Phys. Rev. B **46**, 12841 (1992).

[25] C. W. J. Beenakker, in: Transport phenomena in Mesoscopic Systems, edited by H. Fukuyama and T. Ando (Springer, Berlin) p. 235 (1992), arXiv:cond-mat/0406127.

[26] C. Ishii, Progress of Theoretical Physics **44**, 1525 (1970).

[27] R. M. Potok, J. A. Folk, C. M. Marcus, and V. Umansky, Phys. Rev. Lett. **89**, 266602 (2002).

CHAPTER 4

ENHANCED TRIPLET ANDREEV REFLECTION OFF A DOMAIN WALL IN A LATERAL GEOMETRY

4.1 Introduction

A normal metal inherits superconducting properties if it is in electrical contact to a superconductor. This "superconductor proximity effect" is mediated by Andreev reflection [1], the process in which an electron incident from the normal metal is reflected as a hole at the normal-metal–superconductor interface. As phase coherence between the electron and the Andreev reflected hole is preserved over long distances $\sim \hbar v_{\mathrm{F}}/\mathrm{T}$, where v_{F} is the Fermi velocity and T the temperature, superconducting correlations extend deep into the normal metal.

At the interface between a ferromagnet and a superconductor, majority electrons (electrons with their spin parallel to the magnetization direction **m**) are Andreev reflected as minority holes and vice versa.[1] With the relative phase between majority electrons and minority holes now set by the exchange energy of the ferromagnet instead of the much smaller excitation energy of electron and hole, the proximity effect becomes effectively short-range in a ferromagnet. The situation is even more extreme in a half metal, a material in which only majority charge carriers exist. At a half-metal–superconductor interface Andreev reflection of majority electrons is strongly suppressed, simply because of the absence of minority holes.

It was realized by Bergeret *et al.* [2] (see also Ref. [3]) that the situation is entirely different if spin-rotation symmetry around the (mean) magnetization direction at the su-

[1] We here exclude interfaces between ferromagnets and superconductors with unconventional order parameters in which the Cooper pairs are not spin singlets.

perconductor interface is broken: In that case, majority electrons may be reflected as majority holes. The (odd-frequency) "triplet proximity effect" that results from such "spin-flip" Andreev reflection can penetrate ferromagnets or half metals the same distance as the standard proximity effect penetrates normal metals [4]. Various experiments have hinted at the existence of this effect [5–8], the most striking of which is the observation of a Josephson current through a μm long link of the half metal CrO_2 by Keizer *et al.* [6].

There have been various proposals for the origin of the broken spin-rotation symmetry needed for the existence of the long-range triplet proximity effect. One possibility is an artificial structure, in which there is a thin ferromagnetic or half-metallic spacer layer at the interface with a magnetization direction different from that of the bulk magnet, see Ref. [9] and Chapter 3. For this scenario the ferromagnetic spacer layer should be thin enough that the standard proximity effect has a range larger than its thickness. A second possibility is a magnetically disordered or "spin-active" interface [10, 11]. Finally, the triplet proximity effect can be caused by variations of the magnetization direction **m** associated with a domain wall, either perpendicular [12] or parallel to the superconductor interface [13].

In this chapter we focus on the triplet proximity effect in the presence of a domain wall in a half-metallic film. The case of a half metal is not only most relevant for the experiment of Ref. [6], it also allows for an unambiguous identification of the triplet proximity effect [10]: in the absence of minority carriers, spin-conserving Andreev reflection of majority electrons into minority holes is ruled out, and the "spin-flip" Andreev reflection associated with the triplet proximity effect is the only possible Andreev reflection process in a half metal.

Following the approach in the previous Chapter 3 we employ a scattering approach which allows the treatment of exchange fields of arbitrary strength, in particular the half

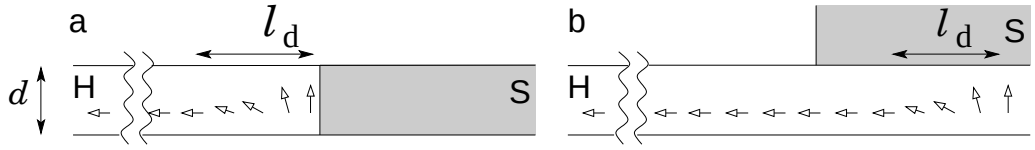

FIGURE 4.1: Superconductor–half-metal junction with a domain wall and serial (a) and lateral (b) contacts.

metallic case. While a distinction of odd- and even-frequency contributions to the triplet proximity effect is not immediate in the scattering approach, the method is well suited for the calculation of physical observables, such as the subgap-conductance and the Josephson current. Our work thus complements previous studies of the triplet proximity effect in the presence of domain walls in ferromagnets restricted to the limit of weak exchange fields [12–14].

Although domain walls occur generically in magnetic materials, at first sight they are an unlikely source of the triplet proximity effect in a half metal: The density of minority carriers decays exponentially away from the superconductor interface, so that only domain walls that happen to be adjacent to the interface can contribute to the triplet proximity effect and, of these, only a region of width comparable to the minority carrier decay length ξ_-. Typically ξ_- is comparable to the (majority) Fermi wavelength λ_F and much smaller than the domain wall width l_d. This severely restricts the magnitude of the triplet proximity effect mediated by domain walls in the contact geometry of Fig. 4.1(a), in which a half-metallic film and the superconductor are placed "in series" and the domain wall is parallel to the interface. As the previous Chapter 3 showed, an additional and not less important complication of the series geometry is that destructive interference between different reflection paths is found to completely suppress the Andreev reflection amplitude at the Fermi level $\varepsilon = 0$.

It is the goal of this chapter to show that these limitations are absent in a different con-

tact geometry, shown in Fig. 4.1(b), in which the superconductor is laterally coupled to a magnetic film over a distance much larger than the film thickness d. Although this lateral contact geometry has received almost no theoretical attention — most theoretical works deal with the serial geometry of Fig. 4.1(a) — it is the relevant one for the experiment of Ref. [6]. We find that for a lateral contact majority electrons have an amplitude r_{he} for Andreev reflection as majority holes that remains finite at the Fermi level and scales proportional to $\lambda_{\mathrm{F}}/\min(l_{\mathrm{d}}, d)$. Especially for thin half-metallic films ($d \ll l_{\mathrm{d}}$), the reflection amplitude for a lateral contact is significantly enhanced with respect to the serial geometry, for which $r_{\mathrm{he}} \propto \varepsilon\xi_{-}/l_{\mathrm{d}}\Delta$, Δ being the magnitude of the superconducting order parameter.

In Sec. 4.2 below we calculate the Andreev reflection amplitudes. Section 4.3 discusses two applications: the two-terminal subgap conductance between the half metal and the superconductor in the lateral geometry, and the Josephson effect in a superconductor–half-metal–superconductor junction. We conclude in Sec. 4.4.

4.2 Calculation of Andreev reflection amplitudes

In the lateral contact, the domain wall is perpendicular to the superconductor interface. We first calculate the Andreev reflection amplitude r_{he} in the presence of such a domain wall and then account for the combined effect of multiple Andreev reflections in a thin half-metallic film ($d \lesssim l_{\mathrm{d}}$). Quasiparticle excitations near the interface are described by the Bogoliubov-de Gennes equation

$$\begin{pmatrix} \hat{\mathrm{H}} & i\Delta e^{i\phi}\sigma_2 \\ -i\Delta e^{-i\phi}\sigma_2 & -\hat{\mathrm{H}}^* \end{pmatrix} \Psi = \varepsilon\Psi, \tag{4.1}$$

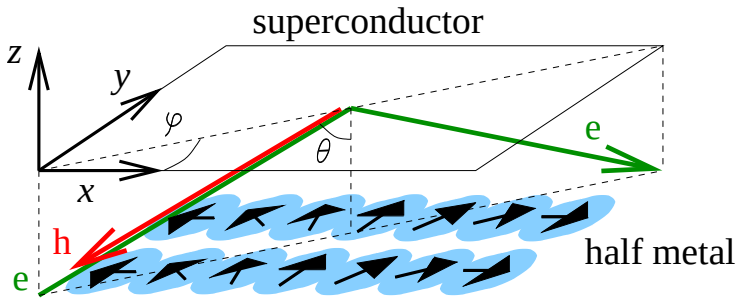

FIGURE 4.2: Half-metal–superconductor interface with a domain wall. An electron (e) incident on the interface is either normally reflected, or Andreev reflected as a hole (h). The Andreev reflection amplitude r_{he} for this situation given by Eq. (4.14) of the main text.

where Ψ is a four-component wavefunction with components for the electron/hole and spin degrees of freedom and and $\Delta e^{i\phi}$ is the superconducting order parameter. We choose coordinates such that the half-metal–superconductor interface is the plane $z = 0$ and the magnetization direction $\mathbf{m}$ in the half metal varies in the x direction, see Fig. 4.2. In the superconductor ($z > 0$), we take the Hamiltonian to be

$$\hat{H} = \hat{\mathbf{p}}\frac{1}{2m_S}\hat{\mathbf{p}} - \varepsilon_{F,S}, \tag{4.2}$$

where m_S and $\varepsilon_{F,S} = \hbar^2 k_S^2/2m_S$ are the effective mass and Fermi energy, respectively. In the half metal ($z < 0$) we set

$$\hat{H} = \sum_{\pm} \hat{\mathbf{p}}\frac{\hat{P}_{\pm}}{2m_{\pm}}\hat{\mathbf{p}} - \varepsilon_{F,\pm}\hat{P}_{\pm}, \tag{4.3}$$

where $m_{\pm}$ and $\varepsilon_{F,\pm} = \hbar^2 k_{\pm}^2/2m_{\pm}$ are the effective mass and the Fermi energy for majority (+) and minority (−) carriers in the half metal, and $\hat{P}_{\pm} = (1 \pm \mathbf{m}(x)\cdot\boldsymbol{\sigma})/2$ project onto the majority and minority components, respectively. We take the limit $\varepsilon_{F,-} \to -\infty$, so that there are no minority carriers in the half metal. We further assume that the interface has a normal-state transmission probability $\tau \ll 1$, which we model through the presence of a potential barrier $V\delta(z)$ at the interface.

We choose a right-handed set of unit vectors $\mathbf{e}_1$, $\mathbf{e}_2$, and $\mathbf{e}_3$ and consider a variation in

the magnetization direction $\mathbf{m}$ of the form

$$\mathbf{m}(x) = (\mathbf{e}_1 \cos\phi_\mathrm{m} + \mathbf{e}_2 \sin\phi_\mathrm{m}) \sin\theta_\mathrm{m}(x) + \mathbf{e}_3 \cos\theta_\mathrm{m}(x). \tag{4.4}$$

We then employ a gauge transformation that rotates $\mathbf{m}$ to the $\mathbf{e}_3$-direction

$$\Psi(x) \to \begin{pmatrix} \mathrm{U}^\dagger(x) & 0 \\ 0 & \mathrm{U}^\mathrm{T}(x) \end{pmatrix} \Psi(x), \tag{4.5}$$

with

$$\mathrm{U}(x) = e^{i\theta_\mathrm{m}(\mathbf{m}(x)\times\mathbf{e}_3)\cdot\sigma/2\sin\theta_\mathrm{m}}. \tag{4.6}$$

This gauge transformation adds a spin-dependent gauge potential

$$\mathbf{A} = i\hbar \mathrm{U}^\dagger \nabla \mathrm{U} \tag{4.7}$$

to the Hamiltonian $\hat{\mathrm{H}}$ [15], but it does not affect the singlet superconducting order parameter, $\mathrm{U}^\mathrm{T} i\sigma_2 \Delta \mathrm{U} = i\sigma_2\Delta$.

Since the domain wall width l_d is typically much larger than the Fermi wavelength, we may neglect spatial variations of $\mathbf{A}$. The wavefunction Ψ_e of an electronic quasiparticle in the half metal incident on the superconductor then reads as

$$\Psi_\mathrm{e}(\mathbf{r}) = \frac{1}{\sqrt{v_{+,z}}} e^{ik_x x + ik_y y} \begin{pmatrix} e^{ik_z z} + r_\mathrm{ee} e^{-ik_z z} \\ 0 \\ r_\mathrm{he} e^{ik_z z} \\ 0 \end{pmatrix}, \tag{4.8}$$

where r_ee and r_he are the amplitudes of normal reflection and Andreev reflection, respectively. Further $k_x = k_+ \cos\varphi \sin\theta$, $k_y = k_+ \sin\varphi \sin\theta$, and $k_z = k_+ \cos\theta = m_+ v_{+,z}/\hbar$, where the polar angles φ and θ parameterize the propagation direction of the electron with respect to the superconductor interface and the domain wall (see Fig. 4.2). We neglected the small difference of the wavenumbers of electrons and holes if the excitation energy ε is finite.

The Andreev reflection amplitude r_{he} can be found by matching Ψ_{e} to a linear combination of the four linearly independent wavefunctions in the superconductor,

$$\Psi_{\alpha,\beta}(\mathbf{r}) \propto e^{ik_x x + ik_y y + iq(\alpha,\beta)z} \begin{pmatrix} 1 \\ -i\alpha e^{i\phi_{\mathrm{m}}} \\ i\alpha e^{-i\eta(\beta)} \\ e^{-i\eta(\beta)-i\phi_{\mathrm{m}}} \end{pmatrix}, \tag{4.9}$$

where $\alpha, \beta = \pm 1$, $\eta(\beta) = \phi - \phi_{\mathrm{m}} + \beta \arccos(\varepsilon/\Delta)$ and $q(\alpha, \beta)$ is the solution of

$$q^2 \;=\; k_{\mathrm{S}}^2 - k_x^2 - k_y^2 + \frac{2im_{\mathrm{S}}\beta}{\hbar^2}\sqrt{\Delta^2 - \varepsilon^2} - \alpha k_x \frac{\partial \theta_{\mathrm{m}}}{\partial x} \tag{4.10}$$

with $\mathrm{Im}\, q > 0$. The matching conditions are on the wavefunction and its derivative at the superconductor interface at $z = 0$. The wavefunction Ψ is continuous

$$\Psi(z \downarrow 0) \;=\; \Psi(z \uparrow 0), \tag{4.11}$$

whereas its derivative satisfies the equation

$$\frac{\hbar^2}{2m_{\mathrm{S}}} \left.\frac{\partial \Psi}{\partial z}\right|_{z\downarrow 0} \;=\; \sum_{\pm} \frac{\hbar^2}{2m_{\pm}} \hat{\mathrm{P}}_{\pm} \left.\frac{\partial \Psi}{\partial z}\right|_{z\uparrow 0} + \mathrm{V}\Psi(z=0). \tag{4.12}$$

Since we are interested in the limit $\varepsilon_{\mathrm{F},-} \to -\infty$, for minority components we may replace the boundary conditions Eqs. (4.11) and (4.12) with

$$\hat{\mathrm{P}}_{-}\Psi_{\mathrm{S}}(z=0) \;=\; 0, \tag{4.13}$$

without a condition on the corresponding derivative. From the resulting six equations we can calculate the six unknowns: Two reflection amplitudes and four amplitudes for the wavefunction in the superconductor.

To lowest order in $\partial\theta_{\mathrm{m}}/\partial x$ and the transmission coefficient τ of the half-metal–superconductor interface we then find

$$r_{\mathrm{he}}(\theta, \varphi) = -\frac{\tau(\theta) k_+ \sin\theta \cos\varphi\, e^{-i(\phi-\phi_{\mathrm{m}})} \Delta}{4(k_{\mathrm{S}}^2 - k_+^2 \sin^2\theta)\sqrt{\Delta^2 - \varepsilon^2}} \frac{\partial \theta_{\mathrm{m}}}{\partial x}, \tag{4.14}$$

where we used the Andreev approximation (which is valid for all angles θ if $k_S^2 \gtrsim k_+^2 \gg \Delta m_S/\hbar^2$) and eliminated the potential barrier V at the interface in favor of the abovementioned transmission coefficient

$$\tau(\theta) = \frac{4\hbar^2 v_{S,z}(\theta) v_{+,z}(\theta)}{4V^2 + \hbar^2 [v_{S,z}(\theta) + v_{+,z}(\theta)]^2}, \tag{4.15}$$

with $m_S v_{S,z} = \hbar(k_S^2 - k_x^2 - k_y^2)^{1/2}$. The amplitude r_{eh} for Andreev reflection of a majority hole into a majority electron is

$$r_{eh} = r_{he}^*. \tag{4.16}$$

The presence of a finite triplet Andreev reflection amplitude at a domain wall is consistent with a previous quasiclassical analysis of the triplet proximity effect at a domain wall in ferromagnets in the limit of weak exchange fields [13]. [2]

We also note that $r_{he}^{\rm eff} \neq 0$ at the Fermi energy is not in contradiction with the observation of the previous Chapter 3 that $r_{he} = 0$ at $\varepsilon = 0$ in clean serial half-metal–superconductor junctions. For the serial geometry, the Andreev scattering problem may be described using a 2×2 scattering matrix. For the lateral geometry the scattering matrix is intrinsically four dimensional and the argument of of Chapter 3 does not apply.

The order of magnitude of the reflection amplitude (4.14) can be understood from the following argument: the amplitude that the incident majority electron is initially reflected into a hole of opposite spin is $\sim \tau(\theta) e^{-i\phi}$. Since the Andreev reflected hole exists up to a distance $\sim 1/k_S$ away from the position of the incident majority carrier [16], there is a finite overlap with majority hole states in the half metal. This overlap is proportional to $(\partial\theta_m/\partial x)/k_S$, hence the parameter dependence of Eq. (4.14).

[2] T. Champel and M. Eschrig, Phys. Rev. B **71**, 220506(R) (2005), observe that the triplet proximity effect is absent in a disordered ferromagnet if $\partial\theta_m/\partial x$ is constant. This observation is not inconsistent with Eq. (4.14), because r_{he} only enters through its angular average $\oint r_{he} \oint$ in a dirty ferromagnet and $\oint r_{he} \oint = 0$ if $\partial\theta_m/\partial x$ is spatially uniform.

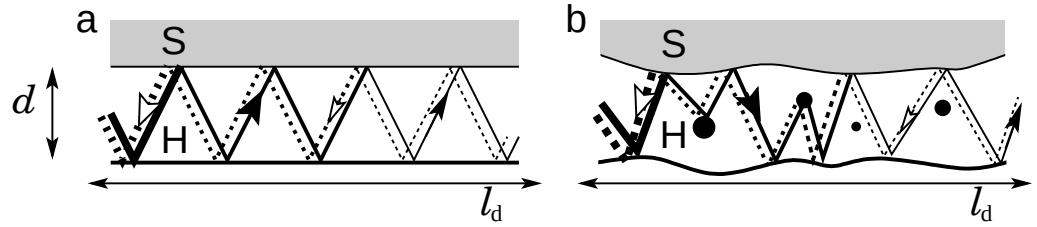

FIGURE 4.3: Ballistic (a) and disordered (b) half-metallic film of thickness d laterally coupled to a superconductor. The Andreev reflection amplitude in the presence of a slowly-varying magntization direction is enhanced by multiple scattering at the superconductor interface.

We now apply the above result to an extended half-metallic film of thickness $d \ll l_d$ laterally coupled to an s-wave superconductor, as in Fig. 4.1(b). In the thin film geometry electrons reflect repeatedly off the half-metal–superconductor interface, see Fig. 4.3(a). Since the wavefunctions of the incident electron and the Andreev reflected hole have the same dependence on the position $\mathbf{r}$, see Eq. (4.8), amplitudes for Andreev scattering from reflections at different positions at the interface add up coherently. This results in an enhancement of the Andreev reflection probability similar in origin to the "reflectionless tunneling effect" in disordered normal-metal–superconductor junctions [17].

We consider a domain wall whose length is shorter than the superconducting coherence length ($l_d \ll \hbar v_+/\Delta$) and for which the orientation of the magnetization varies along the x direction. We assume that the film is in the clean limit (mean free path $\gg l_d$). The scattering states in the film are then parameterized using polar angles θ and φ which set the magnitude of the (now quantized) momentum in the z direction and the propagation direction in the xy plane, respectively. Combining contributions from the entire width of the domain wall, we find that the effective reflection amplitude for Andreev reflection off the domain wall is

$$r_{he}^{\text{eff}}(\theta,\varphi) = -\frac{\tau(\theta)k_+\cos\theta e^{-i(\phi-\phi_m)}\Delta\delta\theta_m}{8(k_S^2 - k_+^2\sin^2\theta)d\sqrt{\Delta^2-\varepsilon^2}}\,\text{sign}\,(\cos\varphi), \tag{4.17}$$

where $\delta\theta_m = \theta_m(\infty) - \theta_m(-\infty)$ is the total angle by which the magnetization direc-

tion changes. The same result is found by directly solving the scattering problem in the thin-film geometry, which is done in the following Chapter 5. For thin films, this Andreev reflection amplitude is significantly larger than the single reflection amplitude of Eq. (4.14). As the final effective amplitude depends only on the total change in angle $\delta\theta_m$, r_{he}^{eff} remains finite in the adiabatic limit $l_d \to \infty$, despite the vanishing of the rate of change, $\partial\theta_m(x)/\partial x \approx \delta\theta_m/l_d \to 0$.

Equations (4.14) and (4.17) are the main results of this chapter. As advertised in Sec. 4.1, the Andreev reflection amplitude r_{he}^{eff} is independent of the location of the domain wall, as long as it is "under" the superconducting contact, and the angle of incidence φ. The absence of a dependence on φ implies that the Andreev reflection amplitude does not depend on the orientation of the domain wall. The appearance of the azimuthal angle ϕ_m in the scattering phase is consistent with the Andreev reflection amplitude found in Chapter 3 for the serial geometry (see also Ref. [18]).

4.3 Applications

With the reflection amplitudes obtained above we now consider the conductance G_{HS} of a lateral half-metal–superconductor junction [as in Fig. 4.1(b)] and the Josephson effect in a lateral superconductor–half-metal–superconductor junction (as in Fig. 4.4). As before, we consider the case that there is a domain wall somewhere below the superconducting contacts and that the transmission coefficient of the half-metal–superconductor interface $\tau \ll 1$. We also assume that the half metal is in the clean limit [3] that $k_+ d \gg 1$ (many transverse modes), and that $l_d \ll \hbar v_+/\Delta$ (domain wall is short in comparison to the superconducting coherence length). In order to simplify our final expressions, we set

[3] Normal reflection of majority carriers may occur at the "edge" of the lateral contacts, but this does not affect our result if the transparency τ of the half-metal–superconductor interface is small.

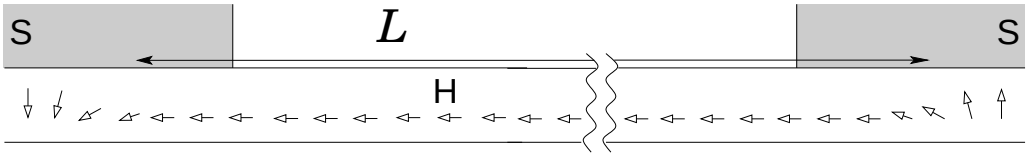

FIGURE 4.4: Superconductor–half-metal–superconductor junction with a domain walls and lateral contacts.

$k_S = k_+$. For the subgap conductance $G_{HS}(V) = \partial I/\partial V$ we then find

$$\begin{aligned} G_{HS}(V) &= \frac{2e^2}{h} \mathrm{tr}\, r_{he}^{\mathrm{eff}}(eV) r_{he}^{\mathrm{eff}}(eV)^\dagger \\ &= \frac{e^2 W}{hd} \frac{\langle \tau(\theta)^2 \rangle \Delta^2}{64\pi(\Delta^2 - e^2V^2)} (\delta\theta_m)^2, \end{aligned} \tag{4.18}$$

where W is the width of the half-metallic film and the brackets $\langle \ldots \rangle$ denote an angular average. This result is to be contrasted with the conductance of a half-metal–superconductor junction with a domain wall parallel to the interface in the serial geometry, which is proportional to

$$G_{HS}(V) \propto \frac{e^2 W d}{h l_d^2} \frac{e^2 V^2}{\Delta^2} (\delta\theta_m)^2 \tag{4.19}$$

if $eV \ll \Delta$, see Chapter 3.

When calculating the Josephson effect, we take the junction to be reflection symmetric, with a domain wall below each superconductor such that the azimuthal angles ϕ_m and the angle changes $\delta\theta_m$ are equal, see Fig. 4.4. We then calculate the zero-temperature supercurrent from the expression [19]

$$I = -\frac{2e}{\pi\hbar} \frac{\partial}{\partial\phi} \mathrm{Re} \int_0^\infty d\omega \mathrm{tr}\, \ln[1 + e^{-2\omega L/\hbar v} |r_{he}^{\mathrm{eff}}(i\omega)|^2 e^{i\phi}], \tag{4.20}$$

where v is the propagation velocity of a transverse mode, L the distance between the domain walls, and ϕ the phase difference between the superconducting order parameters. For short junctions, $L \ll \hbar v_+/\Delta$, we then find

$$eI = \pi G_{HS}(0) \Delta \sin\phi, \tag{4.21}$$

where $G_{HS}(0)$ is the Fermi level conductance of a single half-metal–superconductor interface given in Eq. (4.18) above. For a long junction, $L \gg \hbar v_+/\Delta$ one has

$$eI = \frac{8}{15} G_{HS}(0) \frac{\hbar v_+}{L} \sin\phi, \tag{4.22}$$

where $v_+ = \hbar k_+/m_+$. We note that the long-junction limit of the supercurrent (4.22) is parametrically larger than the supercurrent in a serial geometry, which according to Chapter 3 scales proportional to,

$$eI \propto \frac{\hbar^3 v_+^3}{L^3 \Delta^2}. \tag{4.23}$$

The junction becomes a "π-junction", with a supercurrent proportional to $-\sin\phi$, if the two domain walls have opposite $\delta\theta_m$. [4]

4.4 Conclusion

We expect that, although the calculations presented in this chapter are for ballistic half-metal–superconductor junctions, the enhanced tripled proximity effect in the lateral geometry also exists in the presence of disorder, in the same way as reflectionless tunneling exists both in clean and disordered junctions [17]. As long as the non-Andreev reflected electron is transmitted through the domain wall, as in Fig. 4.3(b), the coherent addition of amplitudes from multiple Andreev reflections is not affected by changes of the electron's propagation direction in a disordered half metallic film. We have thus identified a mechanism by which domain walls in a lateral geometry contribute to the long-range proximity effect irrespective of their position (as long as they are under the superconducting contact), their orientation, and their width.

This mechanism could be a microscopic explanation for the Josephson currents ob-

[4] The possibility to generate a π junction is a common feature of hybrid magnet-superconductor structures with the triplet proximity effect, see, *e.g.*, Refs. [9, 18] and Chapter 3 .

served in the experiment by Keizer *et al.*, which employed the lateral contact geometry analyzed here [6]. The magnitude of the Josephson current observed there showed hysteresis as a function of the applied in-plane magnetic field, a feature consistent with the dependence on large scale magnetic texture and/or domain walls implied by the mechanism we considered here.

BIBLIOGRAPHY

[1] A. F. Andreev, Zh. Eksp. Teor. Fiz **46**, 1823 (1964), [Sov. Phys. JETP **19**, 1228 (1964)].

[2] F. S. Bergeret, A. F. Volkov, and K. B. Efetov, Phys. Rev. Lett. **86**, 4096 (2001); F. S. Bergeret, A. F. Volkov, and K. B. Efetov, Phys. Rev. B **64**, 134506, (2001).

[3] A. Kadigrobov, R. Shekhter, and M. Jonson, Europhys. Lett. **54**, 394 (2001).

[4] F. S. Bergeret, A. F. Volkov, and K. B. Efetov, Rev. Mod. Phys. **77**, 1321 (2005).

[5] I. Sosnin, H. Cho, V. T. Petrashov, and A. F. Volkov, Phys. Rev. Lett. **96**, 157002 (2006).

[6] R. S. Keizer, S. T. B. Goennenwein, T. M. Klapwijk, G. X. Miao, G. Xiao, and A. Gupta, Nature **439**, 825 (2006).

[7] V. N. Krivoruchko, and V. Y. Tarenkov, Phys. Rev. B **75**, 214508 (2007).

[8] K. A. Yates, W. R. Branford, F. Magnus, Y. Miyoshi, B. Morris, L. F. Cohen, P. M. Sousa, O. Conde, and A. J. Silvestre, Appl. Phys. Lett. **91**, 172504 (2007).

[9] Y. Asano, Y. Sawa, Y. Tanaka, and A. A. Golubov, Phys. Rev. B **76**, 224525 (2007).

[10] M. Eschrig, J. Kopu, J. C. Cuevas, and G. Schön, Phys. Rev. Lett. **90**, 137003 (2003).

[11] M. Eschrig and T. Löfwander, Nat. Phys. **4**, 138 (2008).

[12] A. F. Volkov and K. B. Efetov, Phys. Rev. B **78**, 024519 (2008).

[13] A. F. Volkov, Y. V. Fominov, and K. B. Efetov, Phys. Rev. B **72**, 184504 (2005); Y. V. Fominov, A. F. Volkov, and K. B. Efetov, *ibid.* **75**, 104509 (2007)

[14] J. Linder, T. Yokoyama, and A. Sudbø, Phys. Rev. B **79**, 054523 (2009).

[15] G. E. Volovik, J. Phys. C **20**, L83 (1987).

[16] P. Recher, E. V. Sukhorukov, and D. Loss, Phys. Rev. B **63**, 165314 (2001); G. Falci, D. Feinberg, and F. W. J. Hekking, Europhys. Lett. **54**, 255 (2001).

[17] Y. V. Nazarov, Phys. Rev. Lett. **73**, 134 (1994).

[18] V. Braude and Y. V. Nazarov, Phys. Rev. Lett. **98**, 077003 (2007).

[19] P. W. Brouwer and C. W. J. Beenakker, Chaos, Solitons & Fractals **8**, 1249 (1997).

CHAPTER 5

SYMMETRIES IN DOMAIN WALL INDUCED TRIPLET ANDREEV REFLECTION INTO HALF-METALS

5.1 Introduction

Superconducting correlations in *s*-wave superconductors are of spin singlet symmetry. Half-metals only support quasiparticle excitations of one spin orientation. If superconducting correlations originating in *s*-wave superconductors are to extend into half-metals, despite the absence of quasiparticle excitations of both spin directions, a conversion mechanism is thus needed which changes the spin symmetry at the half-metal's interface with the superconductor. The breaking of azimuthal spin rotation symmetry around the magnetization direction of the half-metal provides such conversion of singlet pairing correlations into ones of triplet symmetry—in which case the spins of the two particles may be aligned [1, 2]. Breaking of this remaining symmetry gives rise to rotation of the spin's orientation and results in a "long range triplet proximity effect" which can penetrate ferromagnets over the same distance as normal metals, see Ref. [3] for a review.

Chapter 3 showed that this mechanism is more delicate for half-metals: In the single channel quantum limit, unitarity and electron-hole symmetry impose restrictions on the reflection processes at the interface with a superconductor which fully suppress Andreev reflection at the Fermi energy. Here we show that the same restrictions apply if the interface is invariant under translations as well as rotations by π about the interface normal. In these cases, even when spin rotation symmetry is fully broken, the subgap conductance through a half-metal–superconductor junction will be suppressed close to the Fermi energy, compared to normal-metal–superconductor junctions. Similarly the

magnitude of the Josephson current between two superconductors connected through a long half-metallic link will be strongly reduced in comparison to what it would have been in a normal metal link of equal length.

Experiments however have provided evidence that superconducting correlations can indeed extend into half-metallic systems [4–7], most dramatically a Josephson effect has been observed between two superconducting contacts deposited on a layer of the half-metal CrO_2 [5].

That spin rotation symmetry could be broken at the interface appears plausible. Magnetic anisotropy at the interface may differ from the bulk one, due *e.g.*, to strain at the interface, and finite interface roughness may reduce the coupling of spins at the interface to the bulk [8, 9]. This motivates that the interface's scattering matrix should include a "spin-flip" term at the interface. With the help of the boundary conditions given by the scattering matrix superconducting correlations induced in the half-metal can be investigated using quasiclassical Green functions [9–11]. Thin ferromagnetic or half-metallic spacer layers whose magnetization is misaligned with the bulk orientation similarly give rise to spin rotation at the interface and have been investigated in Refs. [12, 13] as well as in Chapter 3. All of these mechanisms for Andreev reflection are suppressed in the vicinity of the Fermi energy.

Domain walls, on the other hand, which are well known to induce long range triplet correlations in ferromagnets [14–16], have received relatively little attention. Only recently has it been shown for the extremely half-metallic limit that domain walls oriented normal to the superconductor's interface may indeed serve as a source of the triplet proximity effect in half-metallic systems. It was also found that Andreev reflection in this case is not suppressed at the Fermi energy. The present chapter aims to investigate further the role of domain walls inducing Andreev reflection in half-metallic systems. Employing a

perturbative approach different from the previous Chapter 4, we determine the dependence on orientation and geometry, allow for the presence of minority carriers in the half-metal, and investigate the symmetry of the Andreev reflection mechanisms.

This chapter is organized as follows. In Section 5.2 we consider the restrictions of symmetry on Andreev reflection and how they may be lifted. Following in Section 5.4 is a calculation of the Andreev reflection amplitudes for three ways of breaking azimuthal spin rotation symmetry: Domain walls oriented either along the interface or normal to it, and a "spin-active" interface for comparison. Orientation, it turns out, is crucially important. Section 5.5 considers a geometry appropriate for a laterally attached superconducting contact on a half-metallic film. Section 5.6 concludes. An appendix contains details of calculations presented in the main text.

5.2 Constraints imposed by unitarity and particle-hole degeneracy

At excitation energies ε below the superconducting gap Δ, quasiparticles incident on the half-metal–superconductor interface from the half-metallic side will be reflected back into the half metal. This reflection can be either normal reflection or Andreev reflection, for which electron-like quasiparticles are reflected as holes and vice versa. This scattering processes are illustrated in Fig. 5.1.

This reflection process is described by a scattering matrix $\mathcal{S}(\mathbf{k}'_\parallel, \mathbf{k}_\parallel; \varepsilon)$, which takes the form

$$\mathcal{S}(\mathbf{k}'_\parallel, \mathbf{k}_\parallel; \varepsilon) = \begin{pmatrix} r_{\mathrm{ee}}(\mathbf{k}'_\parallel, \mathbf{k}_\parallel; \varepsilon) & r_{\mathrm{eh}}(\mathbf{k}'_\parallel, \mathbf{k}_\parallel; \varepsilon) \\ r_{\mathrm{he}}(\mathbf{k}'_\parallel, \mathbf{k}_\parallel; \varepsilon) & r_{\mathrm{hh}}(\mathbf{k}'_\parallel, \mathbf{k}_\parallel; \varepsilon) \end{pmatrix}, \tag{5.1}$$

where $\mathbf{k}_\parallel$ and $\mathbf{k}'_\parallel$ are the wavevectors of the incoming and outgoing quasiparticle states, respectively, and the subscripts e and h refer to electron-like and hole-like states. The

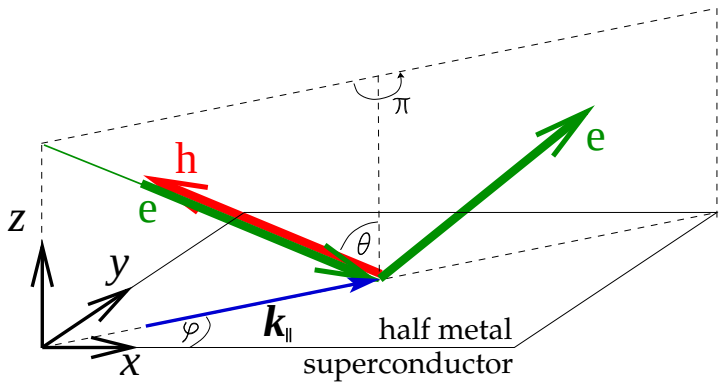

FIGURE 5.1: Along a translationally invariant interface a state with parallel wavevector $k_\parallel$ can only be scattered to a state with the same parallel wavevector. As electron and hole states with the same wavevector have opposite group velocities, the Andreev reflected hole traces out the path of the ingoing electron. If the interface is invariant under a rotation of π around the interface normal, Andreev reflection at the Fermi energy will be suppressed.

scattering amplitudes r_{eh} and r_{he} describe Andreev reflection processes.

The scattering matrix $\mathcal{S}(\mathbf{k}'_\parallel, \mathbf{k}_\parallel; \varepsilon)$ satisfies two constraints: Unitarity and particle-hole symmetry. The latter condition reads

$$\mathcal{S}(\mathbf{k}'_\parallel, \mathbf{k}_\parallel; \varepsilon) = \begin{pmatrix} 0 & 1 \\ 1 & 0 \end{pmatrix} \mathcal{S}(-\mathbf{k}'_\parallel, -\mathbf{k}_\parallel; -\varepsilon)^* \begin{pmatrix} 0 & 1 \\ 1 & 0 \end{pmatrix}. \tag{5.2}$$

The combination of unitarity and particle-hole degeneracy severely restricts the form of the scattering matrix if there is translation invariance along the interface, which implies

$$\mathcal{S}(\mathbf{k}'_\parallel, \mathbf{k}_\parallel; \varepsilon) = \mathcal{S}(\mathbf{k}_\parallel; \varepsilon)\delta_{\mathbf{k}'_\parallel, \mathbf{k}_\parallel}, \tag{5.3}$$

and if the scattering problem is invariant for a π rotation around the interface normal, which implies

$$\mathcal{S}(\mathbf{k}'_\parallel, \mathbf{k}_\parallel; \varepsilon) = \mathcal{S}(-\mathbf{k}'_\parallel, -\mathbf{k}_\parallel; \varepsilon). \tag{5.4}$$

If Eqs. (5.3) and (5.4) are both met, particle-hole symmetry implies

$$r_{\mathrm{ee}}(\mathbf{k}_\parallel; \varepsilon) = r_{\mathrm{hh}}(\mathbf{k}_\parallel; -\varepsilon)^*, \quad r_{\mathrm{eh}}(\mathbf{k}_\parallel; \varepsilon) = r_{\mathrm{he}}(\mathbf{k}_\parallel; -\varepsilon)^*. \tag{5.5}$$

In combination with the condition of unitarity, this results in the equality

$$r_{ee}(\mathbf{k}_{\parallel};0)r_{eh}(\mathbf{k}_{\parallel};0) = 0 \tag{5.6}$$

for the scattering matrix at the Fermi level $\varepsilon = 0$. Since $r_{ee} \neq 0$, except for a special choice of parameters, this implies that generically one must have

$$r_{eh}(\mathbf{k}_{\parallel};0) = 0. \tag{5.7}$$

Equation (5.7) poses a severe restriction on the magnitude and the spatial extension of the proximity effect in half metals that is absent in ferromagnet–superconductor junctions with otherwise comparable characteristics. A nonzero Andreev reflection amplitude for a half-metal–superconductor junction can be obtained only by fine-tuning device parameters such that the normal reflection amplitude becomes zero, or by invoking processes that break the symmetries leading to Eq. (5.7). The former scenario was discussed in Chapter 3 and will not be addressed here. Examples of symmetry-breaking processes that result in a nonzero Andreev reflection amplitude are: lifting of particle-hole degeneracy by a finite excitation energy ε, see Chapter 3, breaking of the rotation symmetry around the interface normal, Chapter 4, breaking of the translation symmetry along the interface, or the breaking of phase coherence [17]. A domain wall for which the magnetization direction varies in a direction parallel to the interface is an example of a perturbation that breaks the rotation symmetry, see Chapter 4. However, a domain wall for which the magnetization direction varies in a direction perpendicular to the interface does not lift the constraints leading to Eq. (5.7). The role of variations in the magnetization direction will be considered in more detail in Sec. 5.4 below.

A finite excitation energy ε lifts the particle-hole degeneracy, and the Andreev reflection amplitude r_{eh} becomes nonzero. The order of magnitude of the Andreev reflection

amplitudes at finite ε can be estimated as

$$|r_{\mathrm{eh}}(\varepsilon)| \sim \frac{|\varepsilon|}{\max(\Delta/\tau, E_\xi)} |r_{\mathrm{eh,\,FS}}|, \tag{5.8}$$

where E_ξ is the Thouless energy of the interface layer where the singlet-triplet conversion takes place, τ is the transparency of the superconductor interface, Δ the superconducting gap, and $r_{\mathrm{eh,\,FS}}$ the Andreev reflection amplitude of a ferromagnet–superconductor amplitude of otherwise comparable characteristics. The first term in the denominator comes about because electrons and holes scattering off a normal-metal–superconductor interface of transparency τ at finite excitation energy ε experience an additional phase difference $\sim \pm\varepsilon\tau/\Delta$, which lifts the electron-hole degeneracy [18]. The second term in the denominator appears from phase differences acquired in the interface layer. The typical thickness of this interface layer is of the order of minority decay length ξ, which implies that E_ξ is of the order of the Fermi energy. For tunneling interfaces one always has $|r_{\mathrm{eh}}(\varepsilon)| \ll |r_{\mathrm{eh,\,FS}}|$ and we conclude that the breaking of electron hole symmetry by finite excitation energies is not an efficient route towards sizeable Andreev reflection in that case. The suppression of Andreev reflection in half-metal–superconductor junctions (as compared to ferromagnet–superconductor junctions) is absent only for transparent interfaces and excitation energies of order Δ.

The ε-dependence of r_{eh} not only determines the conductance through the half-metal–superconductor interface at finite bias, it also sets the scale for the Josephson effect in a superconductor-half-metal–superconductor junction. If the Thouless energy E_L of the Josephson junction length is large in comparison to Δ ("short junction limit"), the Josephson current I is carried by quasiparticle states with energies up to Δ. In this limit, the symmetry considerations that suppressed Andreev reflection at $\varepsilon = 0$ do not affect the order of magnitude of I, and one concludes that otherwise comparable superconductor-half-metal–superconductor and superconductor–ferromagnet–superconductor junctions have comparable Josephson currents. If, however, $E_L \ll \Delta$

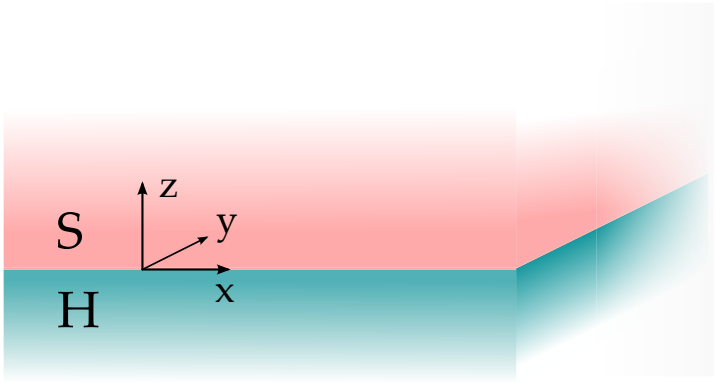

FIGURE 5.2: The half-metal (H) occupies the lower half space ($z < 0$) while the superconducting material (S) fills the upper one ($z > 0$).

("long junction limit"), only quasiparticle states with energy below E_L contribute to I, so that I is significantly suppressed below the Josephson currents in comparable superconductor–ferromagnet–superconductor junctions; see Chapter 3.

In the remainder of this article, we present explicit model calculations of the Andreev reflection amplitudes for the case that singlet-triplet conversion is mediated by a domain wall in the half metal.

5.3 Hamiltonian and Scattering states

5.3.1 Bogoliubov-de Gennes Hamiltonian

We choose coordinates such that the half-metal–superconductor interface is the plane $z = 0$, see Fig. 5.2. The half metal occupies the negative half-space ($z < 0$). The superconductor is taken to be of *s*-wave, spin-singlet type. Quasiparticle excitations near the

interface are described by the Bogoliubov-de Gennes equation

$$\mathcal{H}\Psi(\mathbf{r}) = \varepsilon\Psi(\mathbf{r}), \quad \mathcal{H} = \begin{pmatrix} \hat{\mathrm{H}} & i\Delta e^{i\phi}\sigma_2 \\ -i\Delta e^{-i\phi}\sigma_2 & -\hat{\mathrm{H}}^* \end{pmatrix}, \tag{5.9}$$

where the four-component spinor

$$\Psi(\mathbf{r}) = (u_\uparrow(\mathbf{r}), u_\downarrow(\mathbf{r}), v_\uparrow(\mathbf{r}), v_\downarrow(\mathbf{r}))^{\mathrm{T}} \tag{5.10}$$

consists of wavefunctions $u_\sigma(\mathbf{r})$ for the electron and $v_\sigma(\mathbf{r})$ for the hole degrees of freedom. The superconducting order parameter $\Delta(\mathbf{r})e^{i\phi}$ is nonzero only in the superconductor. We will take $\Delta(\mathbf{r}) = \Delta\Theta(z)$, where $\Theta(z) = 1$ if $z > 0$ and 0 otherwise. This step function model is appropriate for tunneling interfaces of *s*-wave superconductors [19].

For the single-particle Hamiltonian, we take the simplest model that contains the essential features of the half-metal–superconductor interface,

$$\hat{\mathrm{H}} = -\hbar^2\nabla\frac{1}{2m(z)}\nabla - \sum_{\sigma=\uparrow,\downarrow} \mathrm{V}_\sigma(z)\hat{\mathrm{P}}_\sigma(\mathbf{r}) + \hbar w\delta(z), \tag{5.11}$$

where

$$m(z) = \begin{cases} m_{\mathrm{H}} & \text{if } z < 0, \\ m_{\mathrm{S}} & \text{if } z > 0, \end{cases}, \tag{5.12}$$

with m_{H} and m_{S} being the effective masses for the half metal and the superconductor, respectively,

$$\mathrm{V}_\sigma(z) = \begin{cases} \mathrm{V}_{\mathrm{H},\sigma} & \text{if } z < 0, \\ \mathrm{V}_{\mathrm{S}} & \text{if } z > 0, \end{cases} \tag{5.13}$$

where $\sigma = \{\uparrow, \downarrow\}$ and the potentials $\mathrm{V}_{\mathrm{H},\uparrow}$, $\mathrm{V}_{\mathrm{H},\downarrow}$, and V_{S} represent the combined effect of the chemical potential and band offsets for the majority and minority electrons in the half metal and for the superconductor, respectively. w sets the strength of a delta-function potential barrier at the interface. The operators

$$\hat{\mathrm{P}}_\uparrow = \frac{1}{2} + \frac{1}{2}\mathbf{m}(\mathbf{r})\cdot\hat{\boldsymbol{\sigma}} \tag{5.14}$$

$$\hat{\mathrm{P}}_\downarrow = \frac{1}{2} - \frac{1}{2}\mathbf{m}(\mathbf{r})\cdot\hat{\boldsymbol{\sigma}} \tag{5.15}$$

project onto the majority and minority components, respectively, where $\mathbf{m}(\mathbf{r})$ is a unit vector pointing along the magnetization direction in the half metal.

The potentials $V_{H,\uparrow}$, $V_{H,\downarrow}$, and V_S are chosen such that $V_{H,\uparrow}$, $V_S > 0$, and $V_{H,\downarrow} < 0$. As a result, majority states in the half metal and in the normal state of the superconductor are propagating states, with Fermi wavenumbers

$$k_\uparrow = \frac{1}{\hbar}\sqrt{2m_H V_{H,\uparrow}}, \quad k_S = \frac{1}{\hbar}\sqrt{2m_S V_S}, \tag{5.16}$$

respectively. The corresponding Fermi velocities are $v_\uparrow = \hbar k_\uparrow/m_H$ and $v_S = \hbar k_S/m_S$, respectively. Minority states in the half metal are evanescent with wavefunction decay rate

$$\kappa_\downarrow = \frac{1}{\hbar}\sqrt{2m_H|V_{H,\downarrow}|}. \tag{5.17}$$

For a translationally invariant interface, solutions of the Bogoliubov-de Gennes equation (5.9) can be written as a product

$$\Psi(\mathbf{r}) = e^{i\mathbf{k}_\parallel\cdot\mathbf{r}}\psi_{\mathbf{k}_\parallel}(z), \tag{5.18}$$

where $\mathbf{k}_\parallel = (k_x, k_y, 0)^T$. For $z \ll 0$, the function $\psi_{\mathbf{k}_\parallel}(z)$ is of the form

$$\lim_{z\to-\infty}\psi_{\mathbf{k}_\parallel}(z) = \begin{pmatrix} \psi^e_{\mathbf{k}_\parallel\uparrow}(z) \\ 0 \\ \psi^h_{\mathbf{k}_\parallel\uparrow}(z) \\ 0 \end{pmatrix}. \tag{5.19}$$

5.3.2 Scattering states for $\Delta = 0$

We first consider solutions of the Bogoliubov-de Gennes equation (5.9) in the normal state (*i.e.*, with $\Delta = 0$), for a spatially uniform magnetization direction $\mathbf{m} = \mathbf{e}_3$, and at

$\varepsilon = 0$. In this case, solutions of the Bogoliubov-de Gennes equation (5.9) can be written as a product

$$\Psi(\mathbf{r}) = e^{i\mathbf{k}_\parallel \cdot \mathbf{r}} \Psi_{\mathbf{k}_\parallel}(z), \tag{5.20}$$

where $\mathbf{k}_\parallel = (k_x, k_y, 0)^{\mathrm{T}}$. For $z < 0$, the spinor wavefunction $\Psi_{\mathbf{k}_\parallel}$ has the general form

$$\Psi_{\mathbf{k}_\parallel}(z) = v_{+z}^{-1/2} \begin{pmatrix} c_{\mathrm{e}\uparrow} e^{ik_{\uparrow z} z} + c'_{\mathrm{e}\uparrow} e^{-ik_{\uparrow z} z} \\ 0 \\ c_{\mathrm{h}\uparrow} e^{-ik_{\uparrow z} z} + c'_{\mathrm{h}\uparrow} e^{ik_{\uparrow z} z} \\ 0 \end{pmatrix} + v_{\downarrow z}^{-1/2} \begin{pmatrix} 0 \\ c_{\mathrm{e}\downarrow} e^{\kappa_{\downarrow z} z} \\ 0 \\ c_{\mathrm{h}\downarrow} e^{\kappa_{\downarrow z} z} \end{pmatrix}, \tag{5.21}$$

where

$$k_{\uparrow z} = \sqrt{k_\uparrow^2 - |\mathbf{k}_\parallel|^2}, \quad \kappa_{\downarrow z} = \sqrt{\xi_\downarrow^2 + |\mathbf{k}_\parallel|^2}, \tag{5.22}$$

and

$$v_{\uparrow z} = \hbar k_{\uparrow z}/m_{\mathrm{H}}, \quad v_{\downarrow z} = \hbar \kappa_{\downarrow z}/m_{\mathrm{H}}. \tag{5.23}$$

For $z > 0$, the general form of the spinor wavefunction is

$$\Psi_{\mathbf{k}_\parallel}(z) = v_{\mathrm{S}z}^{-1/2} \begin{pmatrix} d_{\mathrm{e}\uparrow} e^{ik_{\mathrm{S}z} z} + d'_{\mathrm{e}\uparrow} e^{-ik_{\mathrm{S}z} z} \\ d_{\mathrm{e}\downarrow} e^{ik_{\mathrm{S}z} z} + d'_{\mathrm{e}\downarrow} e^{-ik_{\mathrm{S}z} z} \\ d_{\mathrm{h}\uparrow} e^{-ik_{\mathrm{S}z} z} + d'_{\mathrm{h}\uparrow} e^{ik_{\mathrm{S}z} z} \\ d_{\mathrm{h}\downarrow} e^{-ik_{\mathrm{S}z} z} + d'_{\mathrm{h}\downarrow} e^{ik_{\mathrm{S}z} z} \end{pmatrix}, \tag{5.24}$$

where

$$k_{\mathrm{S}z} = \sqrt{k_{\mathrm{S}}^2 - |\mathbf{k}_\parallel|^2}, \quad v_{\mathrm{S}z} = \hbar k_{\mathrm{S}z}/m_{\mathrm{S}}. \tag{5.25}$$

The amplitudes appearing in the above equations are related as

$$\begin{pmatrix} c'_{e\uparrow} \\ d'_{e\uparrow} \\ c'_{h\uparrow} \\ d'_{h\uparrow} \end{pmatrix} = \begin{pmatrix} r & t & 0 & 0 \\ t & r' & 0 & 0 \\ 0 & 0 & r^* & t^* \\ 0 & 0 & t^* & r'^* \end{pmatrix} \begin{pmatrix} c_{e\uparrow} \\ d_{e\uparrow} \\ c_{h\uparrow} \\ d_{h\uparrow} \end{pmatrix}, \tag{5.26}$$

$$\begin{pmatrix} c_{e\downarrow} \\ d'_{e\downarrow} \\ c_{h\downarrow} \\ d'_{h\downarrow} \end{pmatrix} = \begin{pmatrix} t_\downarrow & 0 \\ r'_\downarrow & 0 \\ 0 & t^*_\downarrow \\ 0 & r'^*_\downarrow \end{pmatrix} \begin{pmatrix} d_{e\downarrow} \\ d_{h\downarrow} \end{pmatrix}, \tag{5.27}$$

with

$$t = \frac{2(v_{\uparrow z} v_{Sz})^{1/2}}{2iw + v_{\uparrow z} + v_{Sz}}, \tag{5.28}$$

$$r = -1 + t v_{\uparrow z}^{1/2} v_{Sz}^{-1/2}, \tag{5.29}$$

$$r' = -1 + t v_{\uparrow z}^{-1/2} v_{Sz}^{1/2}, \tag{5.30}$$

$$r'_\downarrow = -1 + t_\downarrow v_{\downarrow z}^{-1/2} v_{Sz}^{1/2}, \tag{5.31}$$

$$t_\downarrow = \frac{2i(v_{\downarrow z} v_{Sz})^{1/2}}{2w + v_{\downarrow z} + i v_{Sz}}. \tag{5.32}$$

The amplitudes r, r', and t are majority electron reflection and transmission amplitudes of the half-metal–superconductor interface (with the superconductor in the normal state); the amplitude $r'_\downarrow$ is the minority electron reflection amplitude. The coefficient $t_\downarrow$ parameterizes the evanescent wave amplitude for minority electrons in the half metal.

5.3.3 Scattering states

We now use the notation established in the previous subsection to construct scattering states for the half-metal–superconductor interface at finite excitation energy ε. As before,

we consider a spatially uniform magnetization direction $\mathbf{m} = \mathbf{e}_3$.

The spinor wavefunction $\Psi_{\mathbf{k}_\parallel}(z)$ takes the general form

$$\Psi_{\mathbf{k}_\parallel}(z) = v_{\uparrow z}^{-1/2} \begin{pmatrix} c_{e\uparrow} e^{ik_{\uparrow z}(\varepsilon)z} + c'_{e\uparrow} e^{-ik_{\uparrow z}(\varepsilon)z} \\ 0 \\ c_{h\uparrow} e^{-ik_{\uparrow z}(-\varepsilon)z} + c'_{h\uparrow} e^{ik_{\uparrow z}(-\varepsilon)z} \\ 0 \end{pmatrix} + v_{\downarrow z}^{-1/2} \begin{pmatrix} 0 \\ c_{e\downarrow} e^{\kappa_{\downarrow z}(\varepsilon)z} \\ 0 \\ c_{h\downarrow} e^{\kappa_{\downarrow z}(-\varepsilon)z} \end{pmatrix}, \quad (5.33)$$

for $z < 0$, and

$$\Psi_{\mathbf{k}_\parallel}(z) = \frac{e^{ik_{Sz}z - \kappa_{Sz}(\varepsilon)z}}{\sqrt{v_{Sz}}} \begin{pmatrix} d'_\uparrow \\ d'_\downarrow \\ -d'_\downarrow e^{-i\eta(\varepsilon)-i\phi} \\ d'_\uparrow e^{-i\eta(\varepsilon)-i\phi} \end{pmatrix} + \frac{e^{-ik_{Sz}z - \kappa_{Sz}(\varepsilon)}}{\sqrt{v_{Sz}}} \begin{pmatrix} d_\uparrow \\ d_\downarrow \\ -d_\downarrow e^{+i\eta(\varepsilon)+i\phi} \\ d_\uparrow e^{+i\eta(\varepsilon)+i\phi} \end{pmatrix} \quad (5.34)$$

for $z > 0$. Here we defined

$$k_{\uparrow z}(\varepsilon) = k_{\uparrow z} + \varepsilon/\hbar v_{\uparrow z}, \quad (5.35)$$

$$\kappa_{\downarrow z}(\varepsilon) = \kappa_{\downarrow z} - \varepsilon/\hbar v_{\downarrow z}, \quad (5.36)$$

$$\eta(\varepsilon) = \arccos(\varepsilon/\Delta), \quad (5.37)$$

$$\kappa_{Sz}(\varepsilon) = (\Delta^2 - \varepsilon^2)^{1/2}/\hbar v_{Sz}. \quad (5.38)$$

Solution of the Bogoliubov-de Gennes equation (5.9) then gives the following relations

between the coefficients

$$\begin{aligned}
c'_{\mathrm{e}\uparrow} &= \left(r + \frac{t^2}{e^{2i\eta}r'_\downarrow - r'}\right) c_{\mathrm{e}\uparrow}, \\
c_{\mathrm{h}\downarrow} &= \frac{tt_\downarrow e^{i\eta - i\phi}}{e^{2i\eta}r'_\downarrow - r'} c_{\mathrm{e}\uparrow}, \\
d_\uparrow &= \frac{t}{e^{2i\eta}r'_\downarrow - r'} c_{\mathrm{e}\uparrow}, \\
d'_\uparrow &= \frac{tr'_\downarrow e^{2i\eta}}{e^{2i\eta}r'_\downarrow - r'} c_{\mathrm{e}\uparrow}, \\
c'_{\mathrm{h}\uparrow} &= \left(r^* + \frac{t^{*2}}{e^{2i\eta}r'^*_\downarrow - r'^*}\right) c_{\mathrm{h}\uparrow}, \\
c_{\mathrm{e}\downarrow} &= -\frac{t^* t^*_\downarrow e^{i\eta + i\phi}}{e^{2i\eta}r'^*_\downarrow - r'^*} c_{\mathrm{h}\uparrow}, \\
d_\downarrow &= -\frac{t^* r'^*_\downarrow e^{i\eta + \phi}}{e^{2i\eta}r'^*_\downarrow - r'^*} c_{\mathrm{h}\uparrow}, \\
d'_\downarrow &= -\frac{t^* e^{i\eta + i\phi}}{e^{2i\eta}r'^*_\downarrow - r'^*} c_{\mathrm{h}\uparrow}.
\end{aligned} \tag{5.39}$$

With the help of these wavefunctions, we construct the "retarded" scattering states $|\mathbf{k}_\parallel, \mathrm{e}\rangle^{\mathrm{R}}$ and $|\mathbf{k}_\parallel, \mathrm{h}\rangle^{\mathrm{R}}$ as the state with wavefunction

$$\begin{aligned}
\langle \mathbf{r} \, | \mathbf{k}_\parallel, \mathrm{e}\rangle^{\mathrm{R}} &= \Psi_{\mathbf{k}_\parallel, \mathrm{e}}(z) e^{i\mathbf{k}_\parallel \cdot \mathbf{r}}, \\
\langle \mathbf{r} \, | \mathbf{k}_\parallel, \mathrm{h}\rangle^{\mathrm{R}} &= \Psi_{\mathbf{k}_\parallel, \mathrm{h}}(z) e^{i\mathbf{k}_\parallel \cdot \mathbf{r}},
\end{aligned} \tag{5.40}$$

where the spinor wavefunction $\Psi_{\mathbf{k}_\parallel, \mathrm{e}}(z)$ is given by Eqs. (5.33) and (5.34) with $c_{\mathrm{e}\uparrow} = 1$, $c_{\mathrm{h}\uparrow} = 0$, all other coefficients being determined by Eqs. (5.39), whereas the spinor wavefunction $\Psi_{\mathbf{k}_\parallel, \mathrm{e}}(z)$ is given by Eqs. (5.33) and (5.34) with $c_{\mathrm{e}\uparrow} = 0$, $c_{\mathrm{h}\downarrow} = 1$. Similarly, the "advanced" scattering states $|\mathbf{k}_\parallel, \mathrm{e}\rangle^{\mathrm{A}}$ and $|\mathbf{k}_\parallel, \mathrm{h}\rangle^{\mathrm{A}}$ are then defined as the states for which $c'_{\mathrm{e}\uparrow} = 1$, $c'_{\mathrm{h}\uparrow} = 0$ and $c'_{\mathrm{e}\uparrow} = 0$, $c'_{\mathrm{h}\uparrow} = 1$, respectively, again with all other coefficients determined by Eqs. (5.39). These scattering states will be at the basis of the calculation of the Andreev reflection amplitudes in the presence of a non-uniform magnetization, which is described in the next section.

5.4 Andreev reflection in the presence of a non-uniform magnetization direction

5.4.1 Slow variations of the magnetization direction

A varying magnetization breaks the remaining symmetries in spin space and allows for Andreev reflection at the half-metal–superconductor interface. Here we consider a continuous variation of the the magnetization direction $\mathbf{m}(\mathbf{r})$ over a length l_d. An example of such a continuous change is a domain wall, for which the net change of the magnetization angle is π. However, smaller rotation angles are possible, *e.g.* induced by strain at the interface due to lattice mismatches [8]. Throughout our calculation we will assume that l_d is much larger than the microscopic length scales k_+^{-1}, k_S^{-1} and $\kappa_\downarrow^{-1}$.

To be specific, we choose a right-handed set of unit vectors $\mathbf{e}_1$, $\mathbf{e}_2$, and $\mathbf{e}_3$ and consider a variation of the magnetization direction $\mathbf{m}$ of the form

$$\mathbf{m}(\mathbf{r}) = (\mathbf{e}_1 \cos\phi_\mathrm{m} + \mathbf{e}_2 \sin\phi_\mathrm{m}) \sin\theta_\mathrm{m}(\mathbf{r}) + \mathbf{e}_3 \cos\theta_\mathrm{m}(\mathbf{r}). \tag{5.41}$$

(Such variations of the magnetization direction are sufficient to model domain walls, but they do not allow for certain continuous changes of the magnetization at a fixed polar angle, as it occurs in helical magnets. The full expressions in the presence of variations in both ϕ_m and θ_m are given in App. 5.6.) We then employ a gauge transformation that rotates $\mathbf{m}$ to the $\mathbf{e}_3$-direction,

$$\mathcal{H} \to \mathcal{U}(\mathbf{r})^\dagger \mathcal{H} \mathcal{U}(\mathbf{r}), \quad \mathcal{U}(\mathbf{r}) = \begin{pmatrix} \mathrm{U}(\mathbf{r}) & 0 \\ 0 & \mathrm{U}^*(\mathbf{r}) \end{pmatrix}, \tag{5.42}$$

with

$$\mathrm{U}(\mathbf{r}) = e^{i\theta_\mathrm{m}(\mathbf{m}(\mathbf{r})\times\mathbf{e}_3)\cdot\sigma/2\sin\theta_\mathrm{m}}. \tag{5.43}$$

This gauge transformation adds a spin-dependent gauge potential

$$\begin{aligned} \mathbf{A}(\mathbf{r}) &= i\hbar U^{\dagger}\nabla U \\ &= \frac{\hbar}{2}(\sigma_2 \cos\phi_m - \sigma_1 \sin\phi_m)\nabla\theta_m \end{aligned} \tag{5.44}$$

to the Hamiltonian $\hat{H}$ [20], but it does not affect the singlet superconducting order parameter, since $U^{T} i\sigma_2 \Delta U = i\sigma_2\Delta$. To lowest order in the rate of change of the angle θ_m we then find that the perturbation $\hat{V}$ to the Hamiltonian $\hat{H}$ reads

$$\hat{V} = i(\sigma_2 \cos\phi_m - \sigma_1 \sin\phi_m)\left(\nabla\theta \cdot \frac{\hbar^2}{2m}\nabla + \nabla\frac{\hbar^2}{2m}\cdot\nabla\theta\right). \tag{5.45}$$

Since we take the length scale l_d for variations of the magnetization angle θ_m to be large in comparison to the microscopic length scales k_+^{-1}, k_S^{-1} and $\kappa_\downarrow^{-1}$, we may neglect spatial variations of the perturbation $\hat{V}$ in the direction parallel to the interface. In this approximation translation symmetry along the interface is preserved and the scattering matrix $\mathcal{S}(\mathbf{k}'_\parallel, \mathbf{k}_\parallel; \varepsilon)$ remains diagonal, see Eq. (5.3). To lowest order in the rate of change of θ_m, the Andreev reflection amplitudes may then be calculated in perturbation theory. Using the scattering states defined in the previous section, one has

$$\begin{aligned} r_{he}(\mathbf{k}_\parallel, \varepsilon) &= -\frac{i}{\hbar}\langle \mathbf{k}_\parallel, h, \varepsilon | \mathcal{V} | \mathbf{k}_\parallel, e, \varepsilon \rangle, \\ r_{eh}(\mathbf{k}_\parallel, \varepsilon) &= -\frac{i}{\hbar}\langle \mathbf{k}_\parallel, e, \varepsilon | \mathcal{V} | \mathbf{k}_\parallel, h, \varepsilon \rangle, \end{aligned} \tag{5.46}$$

where

$$\mathcal{V} = \begin{pmatrix} \hat{V} & 0 \\ 0 & -\hat{V}^* \end{pmatrix}. \tag{5.47}$$

We now present calculations of the Andreev reflection amplitudes for two special cases: Variation of the angle θ_m in a direction perpendicular to the superconductor interface, Fig. 5.3(a), and variation of θ_m in a direction parallel to the superconductor interface, Fig. 5.3(b). These two cases differ with respect to the symmetries discussed in

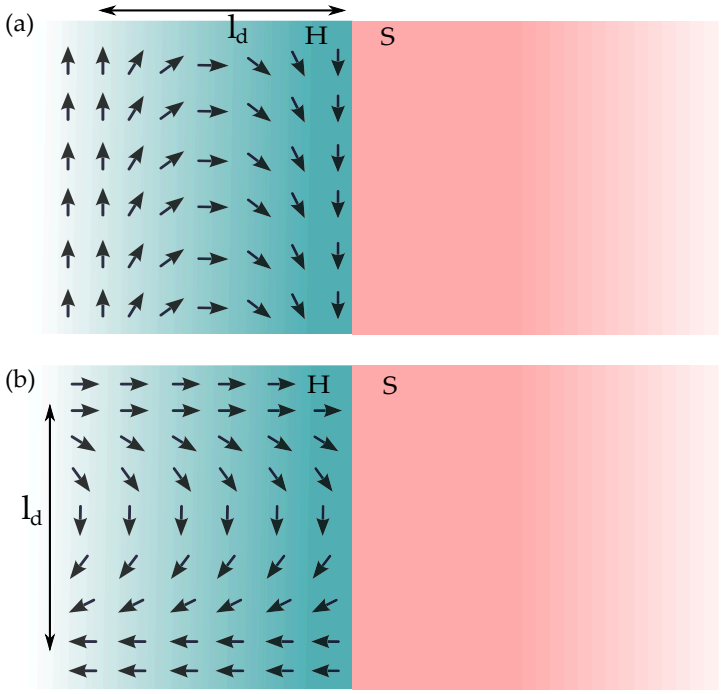

FIGURE 5.3: Domain walls of different orientation. In (a) the magnetization varies in a direction perpendicular to the interface, in (b) the variation is along a direction parallel to the interface. In (b) translational symmetry along the interface is broken whereas it is preserved in (a).

Sec. 5.2: The rotation symmetry around an axis normal to the interface is preserved in the former case, whereas it is broken in the latter case. We will see that this difference has profound consequences for the Andreev reflection amplitude.

For a domain wall of length l_d oriented in parallel to the interface we take

$$\theta_\mathrm{m}(z) = z/l_\mathrm{d} \tag{5.48}$$

if $z < 0$. The use of the gauge transformation (5.42) requires that θ_m is defined for $z > 0$, too. In our calculation, we have set $\theta_\mathrm{m} = 0$ for $z > 0$, although this choice does not affect our final result. Calculating the Andreev reflection amplitude, we then find

$$r_\mathrm{he}(\mathbf{k}_\parallel;\varepsilon) = -\frac{i\varepsilon e^{-i(\phi-\phi_\mathrm{m})}\Delta}{\kappa_{\downarrow z} l_\mathrm{d}\sqrt{\Delta^2-\varepsilon^2}}\left[\frac{|tt_\downarrow|^2}{8\sqrt{\Delta^2-\varepsilon^2}} - \mathrm{Re}\left(\frac{v_{\uparrow z}-iv_{\downarrow z}}{v_{\uparrow z}+iv_{\downarrow z}}\right)\frac{\mathrm{Re}\, tt_\downarrow}{\hbar(v_{\uparrow z}v_{\downarrow z})^{1/2}k_{\uparrow z}}\right]. \tag{5.49}$$

The amplitude for the conversion of holes into electrons is then given by

$$r_\mathrm{eh}(\mathbf{k}_\parallel;\varepsilon) = r_\mathrm{he}(\mathbf{k}_\parallel;-\varepsilon)^*. \tag{5.50}$$

The dependence of this result on the interface parameters agrees with what was derived in Sec. 5.2 using general considerations. Note that in the limit $1/\kappa_\downarrow \to 0$, in which the minority carriers are completely expelled from the half metal, the Andreev reflection amplitude r_he vanishes.

A variation of the magnetization direction in which $\nabla\theta_\mathrm{m}$ is parallel to the superconductor interface breaks the rotation symmetry, thus allowing, in principle, for a nonzero Andreev reflection amplitude at the Fermi level $\varepsilon = 0$. Here we elaborate on our previous calculation of this effect and generalize the results of the previous Chapter 4 to the case of a finite minority wavefunction decay rate $\kappa_\downarrow$ in the half metal. Calculating the Andreev reflection amplitude according to Eq. (5.46), we then find

$$\begin{aligned} r_\mathrm{he}(\mathbf{k}_\parallel;\varepsilon) &= -r_\mathrm{eh}(\mathbf{k}_\parallel;-\varepsilon)^* \\ &= -\frac{e^{-i(\phi-\phi_\mathrm{m})}\Delta\nabla\theta_\mathrm{m}}{\sqrt{\Delta^2-\varepsilon^2}}\cdot\left[\frac{\mathbf{v}_{\mathrm{S}\parallel}|t|^2}{4k_{\mathrm{S}z}v_{\mathrm{S}z}} + \frac{\mathbf{v}_{\uparrow\parallel}v_{\uparrow z}^{1/2}\mathrm{Re}\, tt_\downarrow}{(k_{\uparrow z}v_{\uparrow z}+\kappa_{\downarrow z}v_{\downarrow z})v_{\downarrow z}^{1/2}}\right], \end{aligned} \tag{5.51}$$

where

$$\mathbf{v}_{\uparrow\parallel} = \hbar\mathbf{k}_\parallel/m_{\mathrm{H}}, \quad \mathbf{v}_{\mathrm{S}\parallel} = \hbar\mathbf{k}_\parallel/m_{\mathrm{S}}. \tag{5.52}$$

The first term in Eq. (5.51) comes from the overlap integral in Eq. (5.46) inside the superconductor, whereas the second term comes from the overlap integral in the half metal. The existence of a finite contribution to r_{he} from inside the superconductor is reponsible for the fact that r_{he} remains nonzero in the limit $\kappa_\downarrow \to \infty$ if θ_{m} varies parallel to the interface.

We note that the presence of Andreev reflection at the Fermi energy for a domain wall with $\nabla\theta_{\mathrm{m}}$ parallel to the interface is accompanied by a nontrivial angle dependence of the Andreev reflection amplitudes r_{eh} and r_{he}: If $\nabla\theta_{\mathrm{m}}$ is parallel to the interface, r_{he} and r_{eh} are even functions of ε, but odd functions of $\mathbf{k}_\parallel$. On the other hand, if $\nabla\theta_{\mathrm{m}}$ is normal to the interface, r_{he} and r_{eh} are odd functions of ε, but even functions of $\mathbf{k}_\parallel$. Similar behavior has been noticed previously on the level of the quasiclassical Green functions [9, 21].

5.4.2 Spin-active interfaces

As a second example of a spatially varying magnetization direction, we now investigate a simplified model of a thin ferromagnetic or half-metallic layer located at the interface, whose magnetization is misaligned with respect to the bulk of the half-metal. In this model of a "spin-active interface", we take the magnetization direction to be the unit vector $\mathbf{e}_3$ in the entire half metal and consider a perturbation to the Hamitonian $\hat{\mathrm{H}}$ of the form

$$\hat{\mathrm{V}} = \tilde{h}\tilde{\mathbf{m}}\cdot\hat{\boldsymbol{\sigma}}\delta(z), \tag{5.53}$$

where

$$\tilde{\mathbf{m}} = (\mathbf{e}_1\cos\phi_{\mathrm{m}} + \mathbf{e}_2\sin\phi_{\mathrm{m}})\sin\theta_{\mathrm{m}} + \mathbf{e}_3\cos\theta_{\mathrm{m}}. \tag{5.54}$$

Triplet Andreev reflection at such "spin-active" interfaces has been considered previously in Refs. [9, 11] and in Chapter 3. Using Eq. (5.46) to calculate the Andreev reflection Andreev amplitude to first order in $\tilde{h}$ and taking the limit of a tunneling interface, $|tt_\downarrow|^2 \ll 1$, we then find

$$r_{\mathrm{he}}(\mathbf{k}_\parallel;\varepsilon) = r_{\mathrm{eh}}(\mathbf{k}_\parallel;-\mathbf{e})^* = -\frac{i\tilde{h}|tt_\downarrow|^2 \sin(\theta_{\mathrm{m}}) e^{-i(\phi-\phi_{\mathrm{m}})}}{2\hbar v_{\downarrow z}} \frac{\varepsilon\Delta}{\Delta^2-\varepsilon^2}. \tag{5.55}$$

The proportionality to the square of the tunneling probability is in agreement with the general considerations of Sec. 5.2. The opposite limit of an ideal interface ($|t| = 1$) was considered in Chapter 3.

5.5 Lateral geometry

A modification of the scattering problem arises in a lateral geometry, in which the half metal has a finite thickness d and we consider the scattering of quasiparticles that move parallel to the superconductor interface.

The geometry we consider is shown in detail in Fig. 5.4. As before, the half-metal–superconductor interface is the plane $z = 0$. The superconductor occupies the half space $z > 0$, whereas the half metallic film is in the region $-d < z < 0$. The system has a finite width W in the y direction. Hard-wall boundary conditions are applied at $z = -d$, $y = 0$, and $y = \mathrm{W}$.

We first solve for the scattering states in the presence of a uniform magnetization direction. The scattering states are normalized to unit flux in the x direction. There are electron-like and hole-like scattering states $|n_y n_z s;\mathrm{e}\rangle$ and $|n_y n_z s;\mathrm{h}\rangle$, each labeled by integers n_y, n_z, and s, where n_y and n_z represent the quantized transverse modes in the y and z directions, respectively, and $s = \pm 1$ for scattering states propagating in the positive

and negative x direction, respectively. In the limit $d \gg \xi_-$ the hard-wall boundary conditions at $z = -d$ are inconsequential for the minority carriers, and the corresponding wavefunctions read

$$\Psi_{n_y,n_z,s,\mathrm{e}}(\mathbf{r}) = \sqrt{\frac{v_{\uparrow z}}{4v_{\uparrow x}\mathrm{W}d}}\Psi_{\mathbf{k}_\parallel,\mathrm{e}}(z)\sin(k_y y)e^{ik_x(\varepsilon)sx}, \tag{5.56}$$

$$\Psi_{n_y,n_z,s,\mathrm{h}}(\mathbf{r}) = \sqrt{\frac{v_{\uparrow z}}{4v_{\uparrow x}\mathrm{W}d}}\Psi_{\mathbf{k}_\parallel,\mathrm{h}}(z)\sin(k_y y)e^{ik_x(-\varepsilon)sx}, \tag{5.57}$$

where $\Psi_{\mathbf{k}_\parallel,\mathrm{e}}(z)$ and $\Psi_{\mathbf{k}_\parallel,\mathrm{e}}(z)$ are given in Eq. (5.40) and

$$k_y = n_y\pi/\mathrm{W}, \quad n_y = 1, 2, \ldots \tag{5.58}$$

$$k_x(\varepsilon) = \sqrt{k_\uparrow^2 - k_{\uparrow z}^2 - k_y^2} + \varepsilon/\hbar v_{\uparrow x}, \tag{5.59}$$

and the allowed wavenumbers $k_{\uparrow z}$ are determined from the condition that the wavefunctions vanish at $z = -d$, which, in the limit of a tunneling interface, implies the condition

$$2k_{\uparrow z,\mathrm{e}}d + \pi - \arg\left(r + \frac{t^2}{e^{2i\eta}r'_\downarrow - r_\downarrow}\right) = 2\pi n_z, \qquad n_z = 1, 2, \ldots \tag{5.60}$$

for electron like states, and analogously for hole like states

$$2k_{\uparrow z,\mathrm{h}}d + \pi - \arg\left(r^* + \frac{t^{*2}}{e^{2i\eta}r'^*_\downarrow - r^*_\downarrow}\right) = 2\pi n_z, \qquad n_z = 1, 2, \ldots. \tag{5.61}$$

In the limit of a tunneling interface the wavenumbers will be

$$k_{\uparrow z} = \frac{\pi n_z}{d} + O(t), \quad n_z = 1, 2, \ldots, \tag{5.62}$$

yet for the purposes of our calculation higher order terms need to be kept in order to find a finite overlap among the different states.

We now consider the effect of a region in which the magnetization direction is not spatially uniform. In this case, scattering between the electron-like and hole-like quasiparticle states is possible. In contrast to the serial geometry, in the lateral geometry, normal reflection of electrons or holes at the interface does not come with a reversal of the propagation direction. This situation is shown schematically in Fig. 5.4.

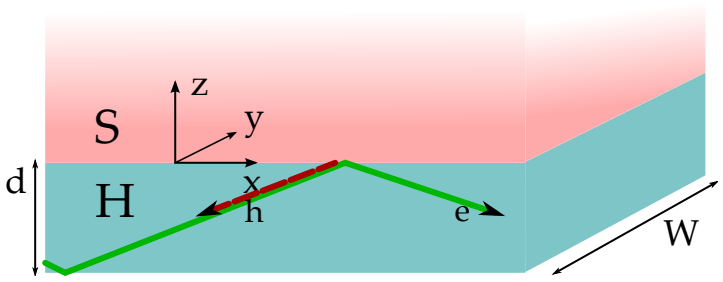

FIGURE 5.4: A lateral superconducting contact giving rise to a waveguide geometry. Quasiparticles which are not Andreev reflected in the region of inhomogeneous magnetization under the superconductor will emergy on the other side of the contact.

To lowest order in the rate of change of the magnetization direction, the Andreev reflection amplitude $r_{\rm he}^{\rm xy}$ and $r_{\rm eh}^{\rm xy}$ for a quasiparticle incident on a region of nonuniform magnetization, *e.g.*, under a superconducting contact, can be calculated in perturbation theory as

$$\begin{aligned} r_{\rm he}^{\rm xy}(n_y' n_z' s'; n_y n_z s) &= -\frac{i}{\hbar}\langle n_y' n_z' s'; {\rm h}|\mathcal{V}|n_y n_z s; {\rm e}\rangle, \\ r_{\rm eh}^{\rm xy}(n_y' n_z' s'; n_y n_z s) &= -\frac{i}{\hbar}\langle n_y' n_z' s'; {\rm e}|\mathcal{V}|n_y n_z s; {\rm h}\rangle, \end{aligned} \tag{5.63}$$

where $\mathcal{V}$ is given in Eq. (5.47) above. With these equations, the problem of calculating Andreev reflection coefficients is brought into a form similar to that of the previous section.

As an example, we consider the case that the magnetization direction $\mathbf{m}$ has the spatial dependence (5.41) with $\theta_{\rm m}$ a function of x only and that the thickness d of the half metal film is small in comparison to the superconducting coherence length $\xi_{\rm S}$. In that case the Andreev reflection matrix $r_{\rm he}^{\rm xy}(n_y' n_z' s'; n_y n_z s)$ is diagonal in the mode indices n_y, n_y' and n_z, n_z' and one finds

$$r_{\rm he}^{\rm xy}(n_y', n_z', s'; n_y, n_z, s) = \delta_{n_y', n_y}\delta_{n_z, n_z'}\frac{v_{\uparrow z}}{2v_{\uparrow x}d}\int dx r_{\rm he}(x;\mathbf{k}_\parallel)e^{2i\epsilon x/\hbar v_{+x}}, \tag{5.64}$$

where $r_{\rm he}(x, y; \mathbf{k}_\parallel)$ is the Andreev reflection amplitude of Eq. (5.51), evaluated with the derivative $d\theta_{\rm m}/dx$ at position x. The prefactor $v_{\uparrow z}/2v_{\uparrow x}d$ in Eq. (5.64) expresses the geometric enhancement of the reflection amplitude from the coherent superposition of multiple reflections at the half-metal–superconductor interface, see Chapter 4. The complex exponential factor accounts for the phase differences acquired by electrons and holes between these reflections.

If the region in which the magnetization direction varies has a size smaller than the superconducting coherence length, the x dependence of the complex exponential $e^{2i\varepsilon x/\hbar v_{+x}}$ in Eq. (5.64) can be neglected. Since $r_{\rm he}(x; \mathbf{k}_\parallel)$ is proportional to $d\theta_{\rm m}/dx$, the integral over x gives the total change $\delta\theta_{\rm m}$ of the magnetization angle $\theta_{\rm m}$. One finds with Eq. (5.51), and in agreement with the previous result in Chapter 4,

$$r_{\rm he}^{\rm xy}(n_y', n_z', s'; n_y, n_z, s) = -\delta_{n_y', n_y}\delta_{n_z, n_z'}\frac{v_{\uparrow z}}{2v_{+x}d}\frac{e^{-i(\phi-\phi_{\rm m})}\Delta\delta\theta_{\rm m}}{\sqrt{\Delta^2-\varepsilon^2}}\left[\frac{v_{{\rm S}x}|t|^2}{4k_{{\rm S}z}v_{{\rm S}z}} + \frac{v_{\uparrow\parallel}v_{\uparrow z}^{1/2}\,{\rm Re}\,tt_\downarrow}{(k_{\uparrow z}v_{\uparrow z}+\kappa_{\downarrow z}v_{\downarrow z})v_{\downarrow z}^{1/2}}\right], \tag{5.65}$$

In this limit, the Andreev reflection amplitude no longer depends on the size $l_{\rm d}$ of the domain wall, nor on the precise x dependence of the magnetization angle $\theta_{\rm m}$. In the opposite limit that the domain wall size $l_{\rm d}$ is large in comparison to the superconducting coherence length, the reflection amplitude at $\varepsilon = 0$ is still given by Eq. (5.65) above, but Andreev reflection is suppressed for excitation energies ε above the Thouless energy $\hbar v_{+x}/l_{\rm d}$ of the domain wall. A common domain wall profile is [22]

$$\theta_{\rm m}(x) = \arctan\left[\sinh(\pi x/l_{\rm d})\right]. \tag{5.66}$$

In this case the suppression at finite bias is by a factor $\mathrm{sech}(e{\rm V}l_{\rm d}/\hbar v_{\uparrow x})$.

Similar to Eq. (5.64) above where the magnetization varies along the x-direction, one finds the same result for variation of the magnetization along the direction normal

to the superconducting interface, as well as for a spin active interface. In these cases, $r_{\mathrm{he}}(x, y; \mathbf{k}_{\parallel})$ in Eq. (5.64) is the Andreev reflection amplitude of Eq. (5.49) and Eq. (5.55), respectively.

When the variation of the magnetic structure is a property of the interface, due *e.g.* to the interplay of the different lattice constants or the screening properties of the superconductor, one will find that the integration is extended along the whole interface. As before the condition for applicability of this simple correspondence is $\kappa_{\downarrow} d \ll 1$.

When the film thickness exceeds the superconducting coherence length Andreev reflection is no longer diagonal in the mode indices. One finds instead that the transition to modes which are close in lateral wavenumber, $k_x - k'_x \lessapprox 2\pi/l_{\mathrm{d}}$, becomes possible. Such non-diagonal Andreev reflection will contribute to the subgap conductance of a half-metal–superconductor junction, but not to the Josephson current between two superconductors linked by a half-metal.

5.6 Conclusion

In this chapter we have investigated the symmetry properties of triplet Andreev reflection into half-metals. The suppression of Andreev reflection in the single channel quantum limit identified in Chapter 3 was shown to also apply to generic clean systems which satisfy translation and point inversion symmetry. It was demonstrated that the orientation of domain walls has crucial consequences insofar as it may lift the latter symmetry, enabling Andreev reflection at the Fermi energy.

Using a perturbative approach we were able to obtain the Andreev reflection amplitude for half-metals in which minority carriers are not entirely absent but only evanes-

cently present. Crucially, their presence allows for finite Andreev reflection where a domain wall is oriented parallel to the interface or where there is a "spin-active" interface.

It was also identified that the Thouless energy associated with the length of the domain wall adds an additional energy scale to the problem. Where this Thouless energy is lower than the gap the subgap conductance will be suppressed with increasing bias voltage.

Worth noting is that very recently half-metal superconducting hybrid systems have garnered attention as possible candidates for allowing Majorana fermion excitations which are considered potentially promising candidates to implement topological quantum computing. While the system considered here is not a direct candidate, the ingredients present here—spin-flip scattering, half-metallicity, and *s*-wave superconducting order—are precisely the same as those in the first proposal by Sau *et al.* [23].

APPENDIX

Explicit calculation of the gaugetransformation

We have written the states in the half-metal as spinors with majority and minority spin components respectively. When the magnetization orientation changes it will induce transitions between these two. We perform a gauge transformation which rotates the basis in spin space such that the quantization axis is always aligned with the $\hat{e}_3$ axis. Doing so will induce a gaugepotential.

After the gauge transformation the normal electron part of the Hamiltonian in the half-metal reads

$$\hat{\mathrm{H}}' = (\hat{\mathbf{p}} - \hat{\mathbf{A}}) \frac{1}{2m(z)} (\hat{\mathbf{p}} - \hat{\mathbf{A}}) - \mathrm{V}_{\uparrow}(z) \frac{1+\sigma_z}{2} - \mathrm{V}_{\downarrow}(z) \frac{1-\sigma_z}{2} + \hbar\omega\delta(z) \tag{5.67}$$

where $\mathrm{U}\mathrm{U}^{\dagger} = 1$ and $\mathrm{U}^{\dagger}\mathbf{m}(\mathbf{x}) \cdot \boldsymbol{\sigma}\mathrm{U} = \sigma_z$ have been used. A posteriori, this form justifies our choice of states above: When $\hat{\mathrm{A}} \to 0$ majority and minority carriers are indeed decoupled. Note that it is not advisable to employ the gauge transformation only in the half-metal. Doing so would result in a discontinuous change in U at the interface to the superconductor, in turn giving rise to δ-functions.

Treating the gaugepotential $\hat{\mathbf{A}}$ as a perturbation, to first order the resulting perturbation $\hat{\mathrm{V}}$ to the single particle Hamiltonian $\hat{\mathrm{H}}$ of Eq. (5.11) is

$$\hat{\mathrm{V}} = -\frac{1}{2m} \left([\hat{\mathbf{p}}, \hat{\mathbf{A}}]_- + 2\hat{\mathbf{A}} \cdot \mathbf{p} \right), \tag{5.68}$$

where the commutator may be nonzero as the gaugepotential need not be constant. With $\hat{\mathbf{A}}^* = \hat{\mathbf{A}}^{\mathrm{T}}$ and $\hat{\mathbf{p}}^* = -\hat{\mathbf{p}}$ the contribution in the hole space follows

$$-\hat{\mathrm{V}}^* = -\frac{1}{2m} \left([\hat{\mathbf{p}}, \hat{\mathbf{A}}^{\mathrm{T}}]_- + 2\hat{\mathbf{A}}^{\mathrm{T}} \cdot \mathbf{p} \right). \tag{5.69}$$

The same result is obtained from directly considering the gaugepotential due to the gauge sector transformation of the Bogoliubov de Gennes Hamiltonian, see Eq. (5.42),

$$-\mathrm{H}'^{*} = -\mathrm{U}^{\mathrm{T}}\mathrm{H}^{*}\mathrm{U}^{*}. \tag{5.70}$$

The gauge potential naturally depends on changes both in the azimuthal angle ϕ_{m} as well as the polar angle θ_{m}. For the transformation given in Eq. (5.43),

$$\mathrm{U}(x) = e^{i\theta_{\mathrm{m}}(\mathbf{m}(x)\times\mathbf{e}_3)\cdot\sigma/2\sin\theta_{\mathrm{m}}},$$

the gaugepotential is found to be

$$\hat{\mathrm{A}}_i = -\frac{\hbar}{2}\left[\begin{pmatrix}\cos\phi\sin\theta\\ \sin\phi\sin\theta\\ 1-\cos\theta\end{pmatrix}\partial_i\phi(\mathbf{r}) + \begin{pmatrix}\sin\phi\\ -\cos\phi\\ 0\end{pmatrix}\partial_i\theta(\mathbf{r})\right]\cdot\hat{\boldsymbol{\sigma}}. \tag{5.71}$$

In the main text we have focussed on a variation in the polar angle. Setting $\phi = \phi_{\mathrm{m}}$ a constant one arrives at Eq. (5.44) of the main text. Using Eq. (5.68) the explicit form following in Eq. (5.45) is found.

BIBLIOGRAPHY

[1] F. S. Bergeret, A. F. Volkov, and K. B. Efetov, Phys. Rev. Lett. **86**, 4096 (2001).

[2] M. Eschrig, J. Kopu, J. C. Cuevas, and G. Schön, Phys. Rev. Lett. **90**, 137003 (2003).

[3] F. Bergeret, A. Volkov, and K. Efetov, Rev. Mod. Phys. **77**, 1321 (2005).

[4] I. Sosnin, H. Cho, V. T. Petrashov, and A. F. Volkov, Phys. Rev. Lett. **96**, 157002 (2006).

[5] R. S. Keizer, S. T. B. Goennenwein, T. M. Klapwijk, G. X. Miao, G. Xiao, and A. Gupta, Nature **439**, 825 (2006).

[6] V. N. Krivoruchko and V. Y. Tarenkov, Phys. Rev. B **78**, 054522 (2008).

[7] K. A. Yates, W. R. Branford, F. Magnus, Y. Miyoshi, B. Morris, L. F. Cohen, P. M. Sousa, O. Conde, and A. J. Silvestre, Appl. Phys. Lett. **91**, 172504 (2007).

[8] G. Miao, G. Xiao, and A. Gupta, Phys. Rev. B **71**, 094418 (2005).

[9] M. Eschrig and T. Löfwander, Nat. Phys. **4**, 138 (2008).

[10] M. Eschrig, Phys. Rev. B **80**, 134511 (2009).

[11] A. V. Galaktionov, M. S. Kalenkov, and A. D. Zaikin, Phys. Rev. B **77**, 094520 (2008).

[12] Y. Asano, Y. Tanaka, and A. A. Golubov, Phys. Rev. Lett. **98**, 107002 (2007).

[13] Y. Asano, Y. Sawa, Y. Tanaka, and A. A. Golubov, Phys. Rev. B **76**, 224525 (2007).

[14] A. F. Volkov, Phys. Rev. B **77**, 064521 (2008).

[15] A. F. Volkov, Y. V. Fominov, and K. B. Efetov, Phys. Rev. B **72**, 184504 (2005).

[16] Y. V. Fominov, A. F. Volkov, and K. B. Efetov, Phys. Rev. B **75**, 104509 (2007).

[17] B. Béri, Phys. Rev. B **79**, 245315 (2009).

[18] G. E. Blonder, M. Tinkham, and T. M. Klapwijk, Phys. Rev. B **25**, 4515 (1982).

[19] K. K. Likharev, Rev. Mod. Phys. **51**, 101 (1979).

[20] G. E. Volovik, J. Phys. C: Solid State Phys. **20**, L83 (1987).

[21] M. Eschrig, T. Lofwander, T. Champel, J. C. Cuevas, J. Kopu, and G. Schon, J. Low Temp. Phys. **147**, 457 (2007).

[22] R. C. O'Handley, *Modern Magnetic Materials* (Wiley (New York), 2000).

[23] J. D. Sau, R. M. Lutchyn, S. Tewari, and S. Das Sarma, Phys. Rev. Lett. **104**, 040502 (2010).